SOURCE- AND AGE-RESOLVED MECHANISTIC AIR QUALITY MODELS: MODEL DEVELOPMENT AND APPLICATION IN SOUTHEAST TEXAS

A Dissertation

by

HONGLIANG ZHANG

Submitted to the Office of Graduate Studies of
Texas A&M University
in partial fulfillment of the requirements for the degree of

DOCTOR OF PHILOSOPHY

May 2012

Major Subject: Civil Engineering

Source- and Age-Resolved Mechanistic Air Quality Models:

Model Development and Application in Southeast Texas

SOURCE- AND AGE-RESOLVED MECHANISTIC AIR QUALITY MODELS:

MODEL DEVELOPMENT AND APPLICATION IN SOUTHEAST TEXAS

A Dissertation

by

HONGLIANG ZHANG

Submitted to the Office of Graduate Studies of
Texas A&M University
in partial fulfillment of the requirements for the degree of

DOCTOR OF PHILOSOPHY

Approved by:

Chair of Committee,	Qi Ying
Committee Members,	Bill Batchelor
	Bryan Boulanger
	Renyi Zhang
Head of Department,	Mark Burris

May 2012

Major Subject: Civil Engineering

ABSTRACT

Source- and Age-Resolved Mechanistic Air Quality Models: Model Development and Application in Southeast Texas. (May 2012)

Hongliang Zhang, B.S.; M.S., Tsinghua University

Chair of Advisory Committee: Dr. Qi Ying

Ozone (O_3) and particulate matter (PM) existing in the atmosphere have adverse effects to human and environment. Southeast Texas experiences high O_3 and PM events due to special meteorological conditions and high emission rates of volatile organic compounds (VOCs) and nitrogen oxides (NO_x). Quantitative knowledge of the contributions of different emissions sources to O_3 and PM is helpful to better understand their formation mechanisms and develop effective control strategies. Tagged reactive tracer techniques are developed and coupled into two chemical transport models (UCD/CIT model and CMAQ) to conduct source apportionment of O_3, primary PM, secondary inorganic PM, and secondary organic aerosol (SOA) and aging distribution of elemental carbon (EC) and organic carbon (OC).

Models successfully reproduce the concentrations of gas phase and PM phase species. Vehicles, natural gas, industries, and coal combustion are important O_3 sources. Upwind sources have non-negligible influences (20-50%) on daytime O_3, indicating that regional NO_x emission controls are necessary to reduce O_3 in Southeast Texas. EC is mainly from diesel engines while majority of primary OC is from internal combustion

engines and industrial sources. Open burning, road dust, internal combustion engines and industries are the major sources of primary $PM_{2.5}$. Wildfire dominates primary PM near fire locations. Over 80% of sulfate is produced in upwind areas and coal combustion contributes most. Ammonium ion is mainly from agriculture sources.

The SOA peak values can be better predicted when the emissions are adjusted by a factor of 2. 20% of the total SOA is due to anthropogenic sources. Solvent and gasoline engines are the major sources. Oligomers from biogenic SOA account for 30-58% of the total SOA, indicating that long range transport is important. PAHs from anthropogenic sources can produce 4% of total anthropogenic SOA. Wild fire, vehicles, solvent and industries are the major sources.

EC and OC emitted within 0-3 hours contribute approximately 70-90% in urban Houston and about 20-40% in rural areas. Significant diurnal variations in the relative contributions to EC are predicted. Fresh particles concentrations are high at morning and early evening. The concentrations of EC and OC that spend more than 9 hours in the air are low over land but almost accounts for 100% of the total EC and OC over the ocean.

ACKNOWLEDGEMENTS

I would like to extend heartfelt thanks to my advisor Dr. Qi Ying without whose guidance and help I would never finish this dissertation. I am grateful to my committee members, Dr. Bill Batchelor, Dr. Bryan Boulanger, and Dr. Renyi Zhang, for their support throughout the course of this research. Thanks also go to my friends and colleagues and the department faculty and staff for making my time at Texas A&M University a great experience.

Finally, I want to thank my family. Thanks to my parents for their countless encouragement and support since I was born, thanks to my wife for her patience and love, and thanks to my baby girl Elena Yiran Zhang for bringing me endless joy.

TABLE OF CONTENTS

Page

LIST OF FIGURES

Page

LIST OF TABLES

1. INTRODUCTION

Ground-level ozone (O_3) has severe adverse effects on both human health [1] and ecosystems [2, 3]. Airborne particulate matter (PM) has also been shown to significantly affect regional air quality, global climate and human health [4-6]. Southeast Texas is well known for the high density of industrial facilities located in the Houston-Galveston Bay (HGB) and Beaumont-Port Arthur (BPA) areas. Houston is the fourth-largest city in the United States with a population over 2.2 million. Because of the immense emissions of gas phase species, primary PM and precursors of secondary PM from both industrial and urban sources and the meteorology conditions characterized by high temperatures and intensive solar radiation as well as a land-sea breeze circulation that confines pollutants in Southeast Texas [7, 8], HGB and BPA are in violation of the national ambient air quality standards for ozone [9] and $PM_{2.5}$ concentrations exceed the NAAQS have been observed [10-12]. Quantitative knowledge of physical and chemical processes that form O_3 and $PM_{2.5}$, and the contributions of different emissions sources to their concentrations are crucial to the development of effective emission control strategies to reduce the adverse effects caused by O_3 and $PM_{2.5}$ in HGB and BPA areas.

O_3 is formed by photochemical reactions of nitrogen oxides (NO_x) and volatile organic compounds (VOCs). In the O_3 formation process, the major role of the VOCs is to form peroxy radicals (RO_2) that convert nitrogen monoxide (NO) back to nitrogen

---

This dissertation follows the style of *Environmental Science & Technology*.

dioxide (NO_2) without consuming O_3 and regenerate hydroxyl radical (OH) to allow sustained net O_3 formation [13, 14]. The ability of different VOCs in producing O_3 varies due to difference in their reaction rates with oxidants and intermediate reaction products. Thus, in the formation of O_3, it is different for areas that the O_3 is limited by NO_x or VOCs. A long-term trends analysis showed that the summertime O_3 over the contiguous United States is NO_x-limited except in some metropolitan areas where it is partly VOCs-limited [15]. To design efficient control strategies, it is necessary to quantitatively apportion the O_3 concentration to various types of local NO_x and VOC emission sources. Major NO_x sources are mobile vehicles, industries and coal combustion. Important VOCs sources include biogenic, vehicles, solvent utilization, and petroleum industries.

Particles in the air can be either primary (directly emitted) or secondary (formed from gas-to-particle conversion of semi-volatile gas phase vapors). Emitted particles will go through various physical and chemical processes that affect their overall mass concentrations as well as their physical properties and chemical composition. Organic particulate matter is typically 20-60% of the total PM in the continental mid-latitudes and up to 90% in tropical forested areas [16, 17]. SOA accounts for 20-80% of the total organic PM [17-19]. SOA can be formed from both anthropogenic and biogenic precursor VOCs emissions. On global and continental scales, biogenic emissions are estimated to contribute much more significantly than anthropogenic sources to the overall SOA [20, 21]. Most of the SOA formed from biogenic sources are believed due to isoprene [22, 23] and monoterpenes emissions [24, 25] because of their high emission

rates from various vegetated surfaces. Anthropogenic sources are believed to account for a significant fraction of the SOA [26, 27] especially in urban areas. Most of the anthropogenic SOA is formed from the oxidation of higher alkanes and aromatic compounds [26, 28-30].

Different techniques have been developed to study the source and region contributions to O_3. Traditional brute-force (BF) method is a sensitivity method that evaluates the contributions from sources by zeroing-out the emissions and the difference between the zero-out sensitivity runs and the base case simulation is the taken as the source contribution [31]. First-order and high-order sensitivities obtained by the decoupled direct method (DDM) can also be used to determine the relative importance of the emission from different sources [32, 33]. However, these two methods are more suitable to estimate the change of O_3 concentrations under proposed emission reductions [34, 35]. Due to the non-linearity of the O_3 formation chemistry, the sum of the individual sensitivity of each source based on DDM or BF methods does not add up to the overall sensitivity [35]. Another set of methods used is the tracer-based techniques using reactive or non-reactive tracers to track O_3 or its precursors from different source or source regions [35]. This technique is useful for diagnostic evaluation to identify which sources or source regions contribute to O_3 concentrations. Two different approaches have been attempted to split O_3 production to NO_x and/or VOCs. One is based on the production rates of hydro peroxide to nitric acid and the other is based on the local sensitivity predicted by DDM. These results are most useful for culpability

analysis of different NO_x and VOC sources to O_3 formation but it does not provide all the information needed to design effective emission control strategies.

Techniques that account for the contributions of NO_x and VOCs to O_3 concentrations separately with consideration of non-linear chemistry are needed. Recently, Ying and Krishnan [36] attributed net O_3 formation to responsible VOC sources based on the contributions of the VOCs and their intermediate oxidation products to the NO to NO_2 conversion process. The sources of the directly emitted VOCs, the reactive intermediates and radicals formed by their oxidation were tracked in the chemistry, transport and removal processes by introducing additional chemical species to represent the contribution from a given source in the gas phase photochemical mechanism. However, NO_x sources to O_3 concentrations have not been determined in that study.

The receptor-oriented chemical mass balance (CMB) and positive matrix factorization (PMF) models are widely used tools to quantify source contributions to PM. The total concentrations of each chemical species in ambient samples measured at receptor locations are reconstructed from a linear combination of emission source profiles [37]. The CMB and PMF receptor models have been applied in many studies to determine the source contributions to PM in various parts of the country [38-42]. In the HGB area, diesel and gasoline vehicles, road dusts, meat cooking operations and wood combustion have been identified as the main sources to primary $PM_{2.5}$ [10, 11]. While the receptor models are robust and relatively easy to apply, they do not provide all the information needed to design effective control strategies. The fundamental non-reactive

assumption in the model formulations limits their applications mainly to primary pollutants and they cannot be used to evaluate the effectiveness of different emissions control strategies. Because of the requirement of accurate PM chemical composition, they can only be used in locations where such detailed measurements are available. As an alternative method, source-oriented modeling approaches track emissions from different source categories and their physical and chemical transformations in mechanistic air quality models [43-45]. The model results are then processed to generate source contribution estimations that cover the entire model domain. These models can also be used to evaluate different emissions control strategies.

SOA is a major component of PM and the sources of SOA, especially in urban areas, are not fully understood. Source-oriented models can be used but their ability is limited by the fact that SOA is universally under-predicted in all current air quality models [46]. Several explanations have been suggested to account for the discrepancy between model predictions and observations. Firstly, not all important SOA precursors are treated in the PM modules of existing air quality models, such as SOA from the oxidation of polycyclic aromatic hydrocarbons (PAHs) [47, 48]. Secondly, the mechanism of SOA formation may be incomplete or inappropriate in the current models. The Odum-type absorption/partitioning mechanism [49] used in most predictive models (for example, see [26, 28, 50]) are based on fitting the SOA yield data from chamber experiments that lasted less than a day and cannot represent the second and third generations of semi-volatile oxidation products which may be important under real atmospheric conditions [51]. Oxidation and interaction of condensed semi-volatile

organics in the aerosol-phase [52-54] and aqueous-phase [55, 56] may lead to further gas-to-particle partitioning of the semi-volatile organics. However, these processes are largely neglected in current models because of the experimental data regarding these processes are still scarce. Only very simplified and empirical treatments are included in some recent models [57]. Thirdly, previous studies demonstrated that under-estimation of VOC emissions in the inventory could also lead to lower SOA estimations [58].

Potential large contributions to SOA from PAH species have been recently proposed by several research groups. Chan et al. [47]found that the SOA yield of PAHs may be higher than previously estimated and could potentially be a significant contributor to atmospheric SOA. Shakya and Griffin [48] studied the SOA formation from the photo-oxidation of five PAH species in chamber and reported high SOA yields of naphthalene, methylnaphthalene, acenaphthylene, and acenaphthene. They estimated that SOA production from oxidation of PAHs emitted from mobile sources in Houston could account for more than 10% of the SOA formed from emissions from mobile sources in this region. This number, however, is simply based on the estimated yield and the estimated emission rates of PAHs. No photochemical modeling is used to support their suggestions. Kleeman et al. [29] have studied the source apportionment of SOA during a severe photochemical smog episode in Central California using a 3D air quality model. Lumped PAH species was used and results show that SOA formed from PAHs is about 4% to the total SOA. However, the lumped PAH species may not accurately account for SOA formation from different PAH species and the SOA formation condition in California during the simulation (a wintertime pollution episode with

limited photochemical activity) is very different with that of Texas in hot summer days. Thus, it is still unclear about the sources of PAHs in the Southeast Texas and their contributions to the overall SOA prediction.

The effects of the particles to human health and the climate are determined not only by their mass concentrations and source-origins but also by their physical properties and chemical compositions. While the chemical composition affects their potential health impacts, the physical properties affect their ability to absorb/reflect solar radiation and to form clouds, which will directly and indirectly affect the climate system. When the aerosols "age" in the atmosphere, their physical and chemical properties change due to various atmospheric processes such as absorption, condensation/evaporation, coagulation, homogeneous and heterogeneous reactions [59, 60]. Aged particles are more complex in chemical composition, have different morphology and more internally mixed [61] and thus their impacts on human health and climate are different from freshly emitted particles.

The aging time scales change significantly when the dominating aging processes switch [62, 63]. During the day, the absorption and condensation of secondary pollutants are the most important processes and the time scales are from a few minutes to less than 10 hours. At night, coagulation dominates the aging process due to decreasing of secondary pollutants formation and the time scales are about 10-50 hours. Moffet and Prather [60] show that in the Mexico city, fresh soot particles account for the majority of the absorption coefficient in the early morning and at night because of the absence of photochemistry, while aged soot particles are responsible for the majority of the midday

absorption when the solar irradiance is the highest, which promotes the formation of secondary semi-volatile vapors that can condense onto existing particles. However, in different locations or different days, the patterns may vary. For example, in remote areas where there are less direct emissions than those in the urban areas or during the winter days when the photochemistry is slower, the particles will exhibit different diurnal cycles in their overall optical properties. Correct spatial and temporal distributions of the particle and their aging status are needed to evaluate the impact of air quality on climate or regional or global scale. This information is might be available in the future directly with satellite-based retrieval methods but no remote sensing techniques have been reported so far. Advanced air quality models could provide this information but no modeling studies have been reported that determine the distribution of particle aging statues in regional/global scales.

The first objective of the research is to develop source-resolved 3D chemical transport models (the Community Multiscale Air Quality Model (CMAQ) and the UCD/CIT air quality model) for the source apportionment of O_3 and PM species. Tagged reactive tracer techniques will be used to trace the contributions of targeted pollutants from different emissions sources. The models will be applied to model a summer air quality episode in Texas to help understand the importance of each source type and/or upwind region to O_3 and PM. This will provide information for policy makers to design more effective emission control strategies. The models and the inputs developed during this study will be used as a starting point for the next two research objectives.

The second objective of the research is to study the potential of SOA formation from the photo-oxidation products of PAHs. SOA formation from the photo-oxidation products of PAHs will be added to the SOA modeling framework of the most recent version of the CMAQ model to determine the regional distribution of SOA products from PAHs in Southeast Texas during the Texas Air Quality Study 2006. A source-oriented modeling framework will be adopted to determine the major sources of the SOA from PAHs by tracking the emitted PAHs and their oxidation products in the gas and aerosol phases from different sources separately. This study will give a better understanding of the amount of SOA from PAHs and may improve the SOA underestimation problem in air quality models. The results from this study will also be useful in designing emission control strategies.

The third objective of the research is to enhance a source-resolved air quality model with age-resolved particle representation so that it is not only possible to determine the temporal and spatial variations of the particles and their source-origins but also their "aging" status (chemical compositions, optical properties) in regional scales. The UCD/CIT model will be used as a base model in this study. This model development will improve the understanding of properties variation of particles and will eventually lead to an increase in the ability of climate models to better predict the feedback of particles on weather and climate.

To conclude, this study will determine the source contributions to O_3 and PM from major sources in Texas and it helps to design efficient control strategies to reduction the adverse effects to human and the environment. The development of new

SOA formation pathway will increase the understanding of organic PM. The capability to predict the spatial and temporal distribution of fresh and aged aerosols will provide better understanding on how PM properties change during the atmospheric processes and help the global and regional models to more accurately predict the effects of PM on weather and climate.

2. CONTRIBUTIONS OF LOCAL AND REGIONAL SOURCES OF NO_X TO OZONE CONCENTRATIONS[*]

The Community Multi-scale Air Quality (CMAQ) model with a modified SAPRC-99 photochemical mechanism was used to investigate the contributions of local and upwind NO_x sources to O_3 concentrations in Southeast Texas during the 2000 Texas Air Quality Study (TexAQS 2000) from August 25 to September 5, 2000. Contributions from eight different local NO_x source types and eight different source regions to the 8-hour average daytime O_3 concentrations from 1100 to 1800 CST (referred to as AD O_3 hereafter) are determined. Both diesel engines and highway gasoline vehicles account for 25 ppb of AD O_3 in the urban Houston area. NO_x from natural gas combustion produces 35 ppb of AD O_3 in the industrial area of Houston. Contributions from industrial sources and coal combustion to AD O_3 have comparatively less broad spatial distribution with maximum values of 14 ppb and 20 ppb, respectively. Although the local sources are the most important sources, upwind sources have non-negligible influences (20-50%) on AD O_3 in the entire domain, with a maximum of 50 ppb in rural and coastal areas and 20 ppb in urban and industrial areas. To probe the origins of upwind sources contributions, NO_x emissions in the entire eastern United States are divided into eight different regions and their contributions to O_3 concentrations in the

---

Houston-Galveston-Brazoria (HGB) and Beaumont-Port Arthur (BPA) areas are determined. Among the various NO_x source regions resolved in this study, other Texas counties near the HGB and BPA areas and southeastern states are the most important non-local sources of O_3. Under favorable transport conditions, emissions from neighbor states and northeastern states could also contribute to non-negligible O_3 concentrations (7-15%) in the HGB and BPA areas. This indicates that in addition to reduce local emissions, regional NO_x emission controls, especially from the neighbor counties and states, are also necessary to improve O_3 air quality in Southeast Texas.

2.1 Introduction

Ground-level ozone (O_3), formed by photochemical reactions of nitrogen oxides (NO_x) and volatile organic compounds (VOCs), has severe adverse effects on both human health [1] and ecosystems [2, 3]. These human and environmental health concerns prompted the U.S. Environmental Protection Agency (EPA) to plan to further lower the current National Ambient Air Quality Standard (NAAQS) of daily 8-hour maximum O_3 from 75 ppb [64] to a level within the range of 60-70 ppb [65]. Although the exact value of the new standard has yet to be released, it is expected that more regions will fall into the non-attainment category.

The Houston-Galveston-Brazoria (HGB) and Beaumont-Port Arthur (BPA) areas in Southeast Texas have long been in violation of the NAAQS for O_3 [9] due to the mesoscale land-sea breeze circulation [7, 66], high temperatures and intense solar radiation, as well as the high emission rates of VOCs and NO_x from dense urban and industrial activities [36, 67]. Previous studies show that the concentrations of O_3 in this

area are affected by not only local sources but also the long-range transport of O_3 and its precursors [68-70]. Nielsen-Gammon et al. [68] used the lowest 8-hour O_3 concentration observed at a subset of monitoring stations that surround the metropolitan area as the background (i.e. non-local) O_3 concentration, and determined the local contribution as the difference between total O_3 concentration and the background value. Although the method can provide information on the relative importance of upwind sources on O_3 concentrations, biases can arise as the O_3 concentrations at the background stations could be affected by local sources due to recirculation patterns common in this area. Langford et al. [69] determined that nearly 84% of the variance in daily maximum 8-hour O_3 concentrations among thirty sites in the Houston area can be attributed to changes in the regional background due to long range transport. Pierce et al. [70] quantified the contributions of background O_3 production on Houston and Dallas air quality using ensemble Lagrangian trajectories and showed that the majority of the periods of high O_3 concentrations in Houston were associated with periods of enhanced background O_3 production. Xiao et al. [71] tested the nonlinear responses of O_3 formation to emissions from different source regions in the HGB area using photochemical model with high-order sensitivity analysis and stated the importance of the accuracy of emission inventories to improve the predictions of O_3 response to emission reductions. These studies are helpful to understand the relative importance of regional and local sources to O_3 formation, but the contributions from different local sources or geographical regions are not quantified.

Different techniques have been developed to study the contributions of precursors from various sources or source regions to O_3 concentrations at receptor locations. Traditional brute-force (BF) method is a sensitivity method that evaluates the contributions from sources by zeroing-out the emissions. The difference between the zero-out sensitivity runs and the base case simulation is taken as the source contribution [31]. First-order and high-order sensitivities obtained by the decoupled direct method (DDM) can also be used to determine the relative importance of the emission from different sources [32, 33]. However, similar to the brute-force method, DDM results are more suitable to estimate the change of O_3 concentrations under proposed emission reductions [34, 35]. Due to the non-linearity of the O_3 formation chemistry, the sum of the individual sensitivity of each source based on DDM or BF methods oftentimes does not add up to the overall sensitivity [35]. Kim et al. [72] used a Community Multi-scale Air Quality (CMAQ) model with higher-order DDM and determined that O_3 concentrations in the Dallas-Fort Worth (DFW) area are sensitive to NO_x emissions from local sources as well as neighboring states and Texas areas outside DFW, but are not sensitive to non-DFW VOC emissions. Such analysis has not been performed for the HGB and BPA areas.

Another set of O_3 source apportionment method used in 3D chemical transport air quality models is the tracer-based techniques that track O_3 or its precursors from different sources or source regions. Models based on these techniques are useful diagnostic evaluation tools to identify which sources or source regions contribute to O_3 concentrations. In the GEOS-Chem model, O_x (O_3+NO_2) formed in different

geographical regions can be assigned to different tagged O_x species so that contributions of long range transport to local O_x concentration can be determined directly (for example, see [73]). In the CAMx/OSAT model non-reactive tracers are used to track the amount of O_3 formed by NO_x and VOC from different sources or source regions. Two different approaches have been attempted to attribute O_3 production to NO_x or VOCs. One is based on the production rates of hydroperoxide to nitric acid and the other is based on the local sensitivity predicted by DDM. The CAMx/OSAT results are most useful for culpability analysis [74] but it does not provide all the information needed to design effective emission control strategies. For example, in some areas where O_3 is limited by VOCs, simultaneous reductions of NO_x emissions with VOCs can be more effective in reducing O_3. However, the relative importance of different NO_x sources to O_3 concentrations will not be properly accounted for by the CAMx/OSAT model in areas and times when NO_x is not the major limiting precursor.

Evaluating the source contributions of NO_x and VOCs to O_3 concentrations separately with consideration of non-linear chemistry can provide useful information to help design further emission control strategies. Recently, Ying and Krishnan [36] attributed net O_3 formation to responsible VOC sources in the HGB and BPA areas. Contributions of NO_x sources to O_3 concentrations in the HGB and BPA areas have not been determined in previous studies. The objective of this study is to further develop and apply a tagged reactive tracer technique to determine the contributions of local (sources in the HGB and BPA areas) and regional NO_x sources to the predicted O_3 concentrations

and also to provide insights into the long range transport of O_3 and its precursors to Southeast Texas during a two-week summer O_3 episode.

2.2 Methodology

NO_x is responsible for O_3 formation because photolysis of NO_2 generates O(3P) radical, which rapidly reacts with O_2 to generate O_3. Thus, by directly tracking the sources of NO_x and O(3P) in the photochemical mechanism, the contributions of NO_x to O_3 can be determined. In this study, the SAPRC-99 photochemical mechanism [75] was expanded to track the contributions of different NO_x sources or source regions to O_3 concentrations using a reactive tagged species method [36, 45]. A brief summary of the method is described in the following.

In the expanded SAPRC mechanism, tagged species are introduced to track the emission source categories or source regions of nitrogen containing species (We use the term "sources" in the following for simplicity). In addition, tagged O_3 species are also included to explicitly determine the contributions of different NO_x sources to O_3 concentration. For example, reaction set (R2-1) shows expanded reactions from the two reactions directly responsible for O_3 production:

$$\begin{aligned} &NO_2^{Xn} + h\nu \rightarrow NO^{Xn} + O(3P)^{Xn} \\ &O(3P)^{Xn} + O_2 \rightarrow O_3^{Xn} \end{aligned} \quad , n=1, 2, \ldots, N \quad (R2\text{-}1)$$

where N is the number of sources and superscript Xn is used to denote species from source n. The source type of the resulting NO_3 from the $NO_2 + O_3$ reaction follows their nitrogen containing precursors. When NO_2 reacts with NO_3 from different sources,

the resulting N_2O_5 is a double tagged species to keep the source information of NO_2 and NO_3 concurrently. Reaction set (R2-2) summarizes the above discussion:

$$NO_2^{Xn} + O_3^{Xm} \rightarrow NO_3^{Xn}$$
$$NO_2^{Xn} + NO_3^{Xm} \rightarrow N_2O_5^{Xn\_m}, \text{ n and m = 1, 2, …, N} \quad \text{(R2-2)}$$

This technique can also be used to determine the amount of background (upwind of the model domain) and locally formed O_3. In reality, the background O_3 can be further divided into two subgroups: O_3 formed through photolysis reactions of upwind NO_x and O_3 directly transported into the domain as O_3 molecules. To differentiate these two different subgroups of background O_3, the species used to represent the O_3 from boundary conditions and O_3 formed in the domain are separated using different tagged species. For example, O_3B_n (n=1,2,…,N is source index) are used to represent O_3 directly from boundary conditions (which is formed in the upwind areas due to NO_x source type n). The O_3B_n species will go through the same chemical reactions as the O_3X_n species. This allows a direct determination of the relative importance of long range transport of O_3 and NO_x to the predicted O_3 concentrations at receptor locations.

Attention should be paid to the scenarios when O_3 formed in one NO_x source region is transported overnight to another NO_x source region. When photochemical reaction starts the next day, the source attribution of the O_3 will likely be biased towards local sources based on the current treatment of the null cycle of NO_x. For example, consider the reactions of the null cycle of NO_x (reaction set R2-3) when O_3 formed in source region A is transported to source region B, based on the current method:

$$O_3^A + NO_B \rightarrow NO_2^B + O_2$$
$$NO_2^B + h\nu \rightarrow NO_B + O(3P)^B \quad \text{(R2-3)}$$
$$O(3P)^B + O_2 \rightarrow O_3^B$$

Although there is no net effect on the overall O_3 concentration due to these reactions, the attribution of O_3 is changed from source A to source B. The other limitation of this source tracking technique is that although it attributes the predicted O_3 concentrations to different NO_x sources, it does not imply that removing the NO_x emissions from a source entirely will lead to the reduction of the amount of O_3 predicted to be associated with that source. This technique is intended to give the contributions of different NO_x sources in the O_3 formation chemistry based on the current level of emissions. It is also important to understand how the O_3 concentration in the target region will respond to NO_x and VOC reductions in order to develop effective emission control strategies.

The impact on the computation time due to increased number of species and reactions is generally small. In this study, emissions of eight sources are simultaneously tracked. The computation time is increased by approximately 50%, although the number of gas-phase reactions increases from 224 in the original SAPRC99 mechanism to 1680 in the current model. The source code can be easily modified if additional explicit sources or source regions need to be tracked. The code is also universally applicable so that no further modification to the CMAQ code is needed when apply the model for other modeling domains. The only preparation work will be generating separate emissions for each source type or source region.

2.3 Model application

In this study, the CMAQ model with expanded SAPRC-99 photochemical mechanisms is applied to quantify the contributions of NO_x to O_3 in Southeast Texas from August 25 to September 5, 2000 during the Texas Air Quality Study (TexAQS) due to different emission sources and source regions. The simulation starts from August 16, 2000 and the first 9 days of simulation results were not used in the analysis as the model performance of O_3 during August 16 – August 24 has been shown to be not as good as the remaining days. This also ensures that initial conditions are dissipated and do not affect the source apportionment results. Details of the modeling episode and model inputs can be found in Ying and Krishnan [36] and are briefly summarized below. A three-level nested domain is used in this study. The horizontal grid resolutions of the nested domains are 36 km, 12 km and 4 km, respectively. The 36-km horizontal resolution parent domain covers the eastern US, the 12km domain covers the east Texas and neighbor states and the 4-km domain covers the HGB and BPA areas as shown in Figure 2-1. The largest domain is the 36-km resolution domain covers the East US. The pink box shows the 12-km domain focusing on East Texas and the green box shows the 4-km domain which contains the HGB and BPA areas. Different levels of shadings in the map show different regions: (1) Houston-Galveston-Bay (HGB) and Beaumont-Port Arthur (BPA) areas, (2) Dallas-Fort Worth area, (3) Other counties in Texas, (4) Neighbor states, (5) Midwestern states, (6) Southeastern states, and (7) Northeastern states. In additional, all the other areas in the domain, including Mexico, Canada, the Atlantic Ocean, and Great Lakes are grouped to "other" regions. A detailed map of the

4-km domain with the names of counties and the locations of the observation stations in the HGB and BPA areas is shown in Figure 2-2. The vertical domain is divided into 14 layers with 8 layers below 2000 m AGL. The initial and boundary conditions for the 36 km domain are generated based on the default CMAQ profile.

The meteorology fields were generated using the Meteorology-Chemistry Interface Processor (MCIP) from the PSU/NCAR mesoscale model (MM5) outputs provided by the Texas Commission of Environmental Quality (TCEQ). The MM5 results have been evaluated by TCEQ staff and used in the 2004 Mid-Course review of the December 2002 O_3 SIP revision. Three distinctive day time wind patterns were identified through back-trajectory analysis in a previous study [76]. In summary, between August 25 and 29, southerly wind dominates during the day. Between August 30 and September 3, westerly wind dominates. Northerly wind dominates during September 4 and 5. The difference in the dominant wind directions during the day puts different sources in the upwind direction of the receptors and greatly affects the concentrations and source apportionment results of secondary pollutants such as O_3 and secondary organic aerosol (SOA).

The emissions were generated based on EPA's 2001 Clean Air Interstate Rules (CAIR) emission inventory and emissions of alkenes from industrial sources in the HGB and BPA areas were adjusted to account for the potential missing sources [36]. To determine the contribution of regional transport to O_3 concentrations in Southeast Texas, NOx emissions were grouped into 8 regions. The region designations are shown in Figure 2-1. The contributions from the 36 km boundary conditions are also lumped into

the "other" category. To determine the contributions from major emission sources, the NO_x emissions in the 4-km Southeast Texas domain were grouped into 8 source categories: biogenic sources, diesel engines, highway gasoline, off-highway gasoline, industries, coal combustion, natural gas combustion and other sources. The natural gas combustion source includes industrial processes that use natural gas as fuel and does not include natural gas production processes. Natural gas combustion is the largest NO source followed by diesel engines and highway gasoline vehicles in Southeast Texas.

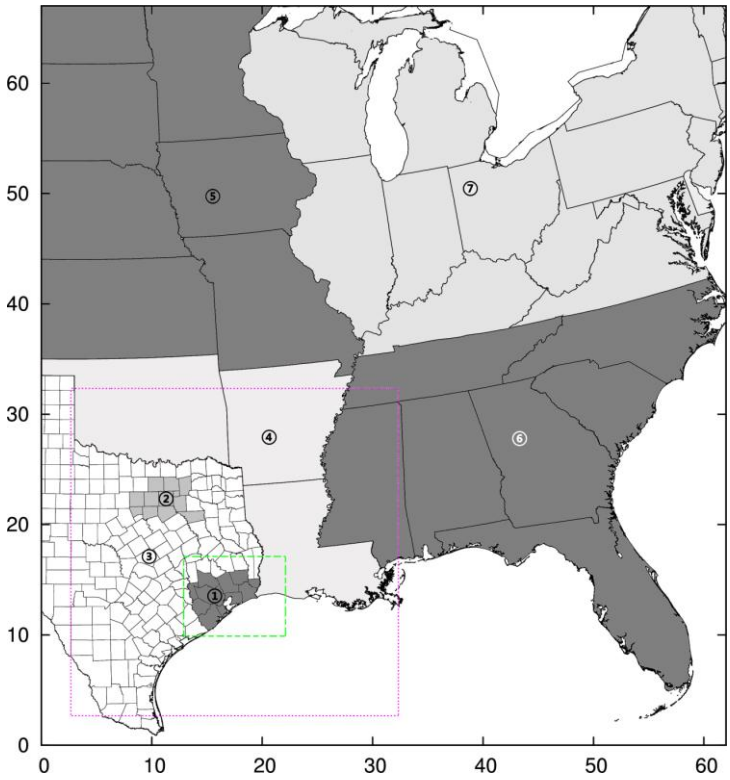

Figure 2-1. The nested domains used in the study and the designation of different source regions.

Two sets of simulations were conducted to resolve the source contributions and source region contributions to O_3 in the 4-km domain. The first set of simulations for the 36-, 12- and 4-km domains tracks the NO_x and O_3 formed from different source regions

using source region resolved NO_x emissions. The 36-km and 12-km simulations provide source region resolved boundary conditions for the 12- and 4-km simulations, respectively. In the 4-km domain simulation, the amount of O_3 directly transported into the domain from the boundary conditions and formed in the domain due to NO_x from different source regions are determined using the method described in section 2. The second set of simulations uses non-tagged emissions for the 36- and 12-km domain. For the 4 km domain simulation, O_3 formed from NO_x emitted from different sources within the 4-km domain and from upwind sources are determined. This set of simulation determines the contributions of different emission sources of NO_x in the 4-km domain to O_3 and the total amount of O_3 from upwind sources (i.e. boundary conditions, which include directly transported as O_3 as well as O_3 formed through upwind NO_x).

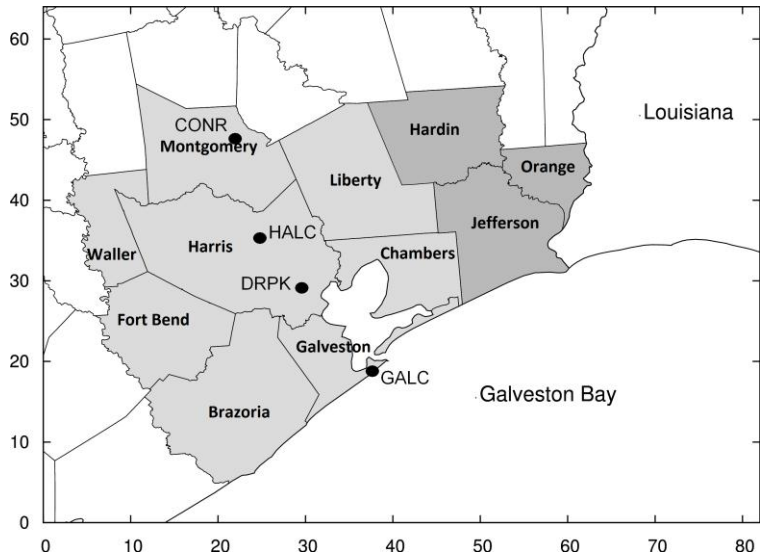

Figure 2-2. The 4-km model domain which covers Southeast Texas. Counties within HGB area (light grey) and BP area (dark grey) are listed.

2.4 Results and discussion

2.4.1Model performance

The same model domain and emission inventory have been used in previous studies of O_3 and SOA formation, and model performance on O_3, NOx, CO, VOCs species and particulate matter in the 4 km domain has been discussed in greater details [36, 76]. Since this study includes discussions of regional transport of O_3, the model performance of O_3 at all the regions is examined by comparing hourly O_3 concentrations with all available observations in EPA's AQS (Air Quality System) database. Mean normalized bias (MNB), as defined in equation (E2-1), is used as a statistical measure for the analysis. C_m represents the model-predicted concentration, C_o represents the observed concentration, and N equals the number of prediction-observation pairs from all the available monitoring stations.

$$\text{MNB}=\frac{1}{N}\sum_{i=1}^{N}\frac{C_o - C_m}{C_o} \quad \text{(E2-1)}$$

Figure 2-3 shows the box-and-whisker plot of calculated MNB for O_3 for all the days during the episode in different model domains. At each station, the fractional biases based on hourly O_3 are averaged to obtain the MNB for that station. The MNB values of all the available stations of a given day are ranked to give the distribution of daily MNB as shown in Figure 2-3. The box represents the 25th and 75th quantiles and the bar in the middle of box represents the median value. The 91st and 9th quantiles are shown by upper and lower whiskers. The cut point used for the MNB calculation is 60 ppb [77]. Figure 2-3(a) shows the distribution of MNB of O_3 based on the 594 stations included in

36-km domain but not in 12-km domain. The middle 50% of the data are in the range from -0.1 to 0.3, indicating a general under-prediction of the O_3 concentrations. In Figure 2-3(b), MNB of O_3 at the 38 stations included in 12-km domain but not included in 4-km domain are mostly in the range of ± 0.15 except for August 27 and September 1 and 2. The middle 50% of the MNB at the 60 stations in 4-km domain are generally within the range of -0.1 to 0.2, although there are a few days with larger positive MNB values. This under-prediction of O_3 has also been reported by other researchers and is generally attributed to missing reactive VOC emissions from the industrial sources in this area. The overall MNB averaged over the entire episode for the 36-, 12- and 4-km domains are 0.035, -0.007 and 0.024, suggesting that overall the model performance during this episode is acceptable. This provides confidence in the results of the following O_3 source apportionment calculations.

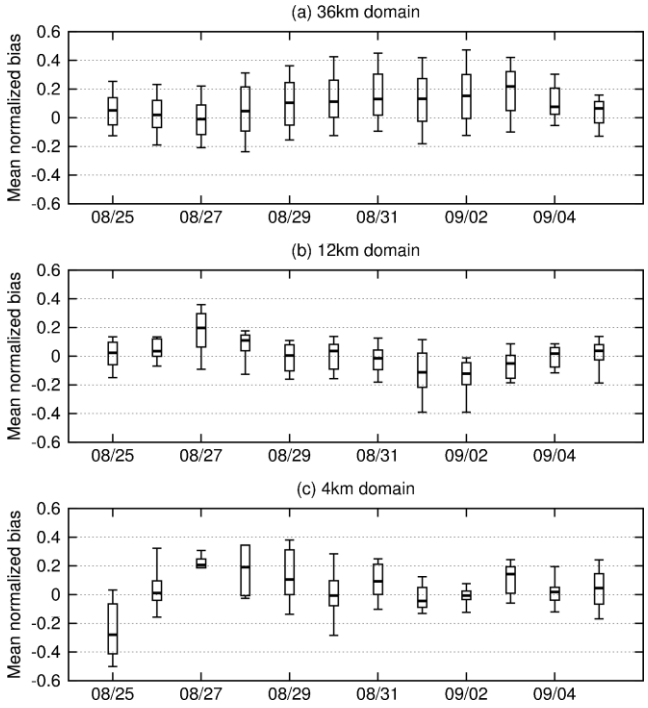

Figure 2-3. Box–whisker plot of mean fractional bias calculated using all available observations and the predicted concentrations for all domains.

2.4.2 Contribution of NO_x sources to O_3 concentrations

Figure 2-4 shows the predicted contributions from each NO_x emission source in the 4 km domain to O_3 concentrations and the observed O_3 concentrations at four sites. Conroe (CONR) is a suburban site north of Houston and Galveston Airport (GALC) is a remote coastal site. The Houston Deer Park (DRPK) is under influence of industrial emissions from Houston Ship Channel (HSC) and Aldine (HALC) is an urban site surrounded by commercial and residential activities. Figure 2-4(a) shows the source apportionment results at the suburban site CONR. On August 25-29, diesel engines, highway gasoline vehicles and natural gas are the three main sources of NOx to form high O_3 concentrations and each of them contributes to about 30 ppb of total O_3. This is due to the significant transport of emissions from downwind urban and industrial areas.

From August 30 to September 3, wind during the day is mostly coming from the west, and the contributions of upwind sources increase to account for more than 50% of the peak O_3 concentrations. On September 4 and 5, 60-70 ppb of peak hour O_3 is due to upwind sources. Contributions of diesel engines and highway gasoline vehicles decreases to less than 20 ppb and contribution of natural gas becomes very small. Other sources all have minor influences. The panel also shows that the predicted O_3 concentrations well capture the episode trend and peak values of observations on most of the days.

Figure 2-4(b) illustrates that diesel engines and highway-gasoline vehicles are the two largest sources of O_3 at the urban site (HALC) for most days and they can both contribute to as much as 60 ppb of O_3. From August 30 to the end of the episode, concentrations due to upwind sources increase from 20 ppb to 60 ppb gradually and upwind sources become the most important sources for the last two days due to significant northerly winds during the peak O_3 hours. Natural gas has large influence on the first two days (about 30 ppb), but becomes less important on the rest days of August and increases again in September days (about 10-20 ppb), suggesting that the natural gas sources are located to the south and north of the site but not as much in the west side. Except for the under-prediction of peak O_3 concentrations in the first two days, the model predicted O_3 concentrations generally match the observations.

Figure 2-4(c) shows that natural gas is the most important source at industrial site DRPK. NO_x from natural gas can produce as high as 60 ppb O_3 especially at noon time. The contributions from diesel engines and highway gasoline vehicles are similar

throughout the episode. During the southerly and northerly wind periods their contributions are generally less than 5 ppb, but during the westerly wind days their contributions are about 20 ppb. The contributions from industrial sources have about 5-10 ppb contributions to O_3 concentrations. Upwind sources also significantly affect O_3 concentrations at DRPK and contribute to 10-20 ppb on August and early September days and 20-30 ppb on September 3-4. The predicted peak O3 concentrations agree well with observation on 9 out of the 12 days.

Figure 2-4(d) shows that upwind sources dominate the O_3 concentrations at GALC. From August 25 to 29, the O_3 concentrations are low and are completely dominated by upwind sources. From August 30 to September 3, contributions from upwind sources remain high while the remaining sources show non-negligible contribution. Their contributions become more important in the last two days when natural gas contributes a maximum contribution of 40 ppb. Coal combustion contributes about 10 ppb O_3 concentrations on August 30 and 31when the plumes from a coal-fired power plant passed through the monitoring site. Diesel engines, highway gasoline vehicles, industries and other all contribute less than 5 ppb during the entire episode.

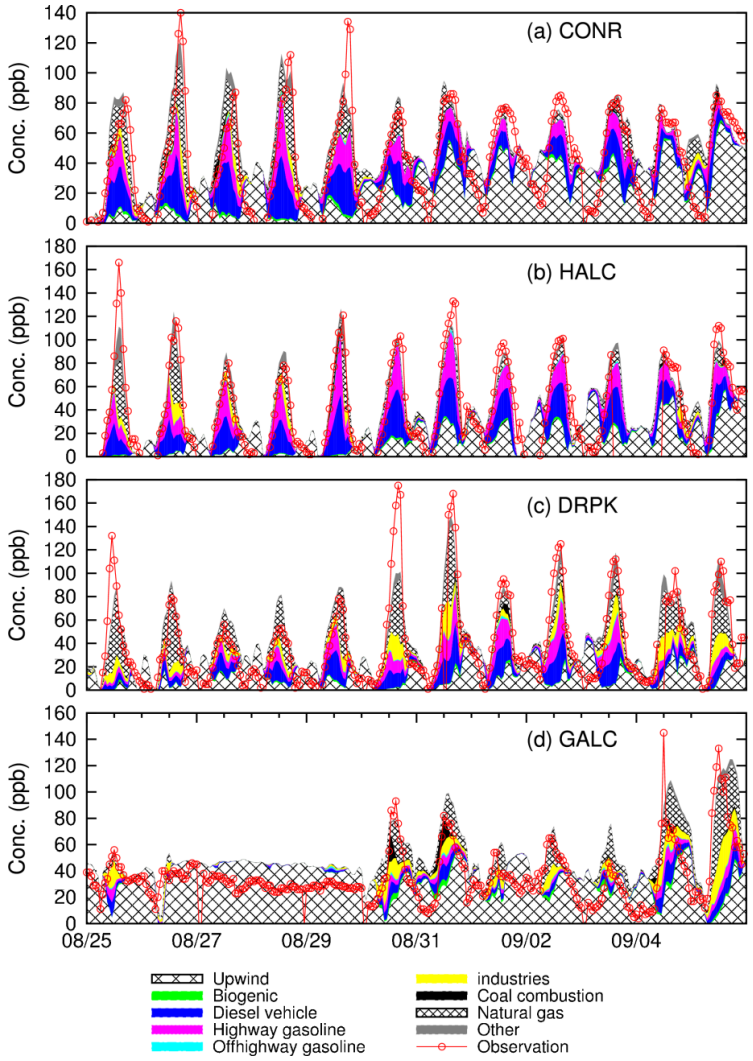

Figure 2-4. Contribution from each NOx source type to O_3 concentrations and observed O_3 concentrations at (a) CONR, (b) HALC, (c) DRPK, and (d) GALC.

Figure 2-5 shows the regional distribution of each NO_x source contributing to episode averaged daytime O_3 concentrations during the 8 hours from 1100-1800 CST, when the O_3 concentrations are generally the highest during the day. Figure 2-5(a) shows that contributions from biogenic sources are highest in the west boundary of the 4-km domain with a maximum of 3 ppb. Figure 2-5(b) shows that locally emitted NO_x from diesel engines account for 25 ppb O_3 in the metropolitan Houston and 10-15 ppb O_3 in

the area around Houston and the BPA area. Highway gasoline vehicles also contribute about 25 ppb O_3 in urban Houston with a more limited regional distribution compared to diesel engines as shown in Figure 2-5 (c). Figure 2-5(d) shows that the off-highway gasoline vehicles contribute to the O_3 concentrations with a maximum of approximately 1.5-2 ppb in urban Houston. Contributions from industries in both the HGB and BPA areas have a highest value of about 14 ppb as illustrated in Figure 2-5(e). Figure 2-5(f) shows that high contributions from coal combustion are located near the locations where NO_x is emitted and have a maximum value of 20 ppb. The plumes from three major coal-fired power plants can be clearly seen on the plot. Figure 2-5(g) shows that the influence of natural gas reaches highest in urban Houston and Ship Channel area with a maximum of about 30 ppb. Figure 2-5(h) shows the contributions from "other" sources can be as high as 14ppb near the urban and industrial areas.

Figure 2-5(i) shows that episode averaged 8 hour daytime O_3 concentrations due to O_3 or O_3 precursors entering 4-km domain from upwind sources as boundary conditions are ubiquitous with a maximum greater than 50 ppb. In the urban Houston and Ship Channel area, upwind sources are the fourth largest source following diesel engines, highway gasoline vehicles and natural gas. Except in the very core region of urban Houston and the HSC area, upwind sources become the dominant source of O_3. Thus, to better understand the high O_3 scenarios, it is necessary to further understand which source regions are responsible for the upwind O_3.

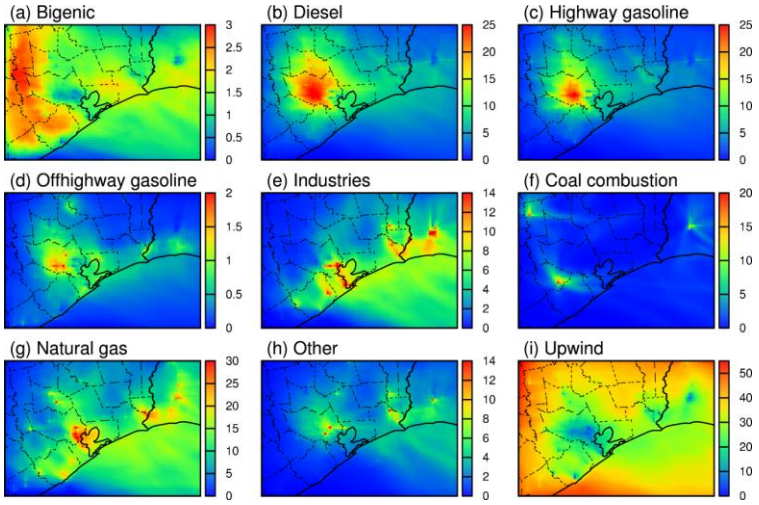

Figure 2-5. Episode-averaged contributions from each NO_x source type during high O_3 concentrations hours (1100-1800 CST). Units are ppb.

A set of brute-force (BF) simulations was made to illustrate the difference between the sensitivity analysis results with the current source apportionment results with reactive tracers. In each BF simulation, NO_x emissions from one source were removed entirely from the simulation. Since the O_3 formation in the urban Houston areas and part of the downwind regions is VOC-limited, reducing NO_x emissions from each source increases O_3 concentrations in these areas. This agrees with a previous analysis by Fiore et al. [15], which shows that summertime O_3 over the contiguous United States is NO_x limited except in some metropolitan areas where it is partly VOC limited, and the recent study of Xiao et al. [71] which shows that responses of daytime O_3 to NO_x reduction can be negative in part of the urban Houston area. In the remaining areas of the domain, the contribution of each NO_x source to O_3 concentrations based on the BF sensitivity results show similar spatial distributions as the results of this study, although the BF method predicts lower contributions by a factor of 3-5 than the reactive tracer

method used in this study. This clearly demonstrates that the method developed in this study determines the contributions of different NO_x sources in the O_3 formation chemistry based on the current level of NO_x and VOC concentrations and the non-linearity in O_3 response to emission change.

2.4.3 Contribution of NO_x source regions to O_3 concentrations

Figure 2-6 shows the predicted hourly-averaged relative source contributions to O_3 due to NO_x from different source regions during the study period at four sites in the HGB area. Figure 2-6(a) shows that on the first 5 days the HGB-BPA area is the dominant source region of NO_x for the daytime O_3 at CONR while NO_x blown from southeastern states and "other" regions contributes to approximately 50% and 30% of the nighttime O_3, respectively. From August 30 to September 3, the contributions from local NO_x to O_3 concentrations are reduced to approximately 50% and NO_x from other counties in Texas and neighbor states contributes to 20-50% and 10-20%, respectively. On September 4-5, the contributions of northeastern states increase to a maximum of approximately 30% and contributions from "other" regions reduce to less than 10%.

Figure 2-6(b) shows the O_3 contributions of different regions at HALC. Local source dominate the daytime source contributions of NO_x to O_3 and southeastern states are the largest nighttime sources for the first 5 days. NO_x emitted from other counties in Texas accounts for 20-30% for daytime O_3 and up to 60% for the nighttime O_3 during August 29-September 3 while contributions from local sources of NO_x to O_3 decrease to approximately 70% during the day and 10% at night. Contributions from "other" regions

gradually increase to as high as 30-40% at night on September 3, and reduce to less than 10% the dominant wind direction changes to the north on September 4 and 5.

Figure 2-6(c) shows that at DRPK, the local sources of NO_x dominate the daytime O_3 concentrations during the whole episode. Before August 30, the nighttime O_3 concentrations are dominated by NO_x from southeastern states and "other" regions. On the days of August 30 to September 3, the contributions of southeastern states decrease to very small, and the contributions of other counties in Texas increase to as high as 50%. The effect of NO_x from neighbor states also increases. On September 4 and 5, the contributions of northeastern increases and reach a maximum of 30% at night.

As shown in Figure 2-6(d), southeastern states are the dominant contributors of NO_x to O_3 concentrations and "other" regions account for 20-40% throughout the days between August 25 and August 29 due to southerly wind. From August 30 to September 3, contributions of southeastern states decrease while contributions of "other" regions increase. On September 4 and 5, the strong winds from north blow the emissions from the Houston area to Galveston (GALC) and make it the main source region of NO_x to the O_3 concentrations.

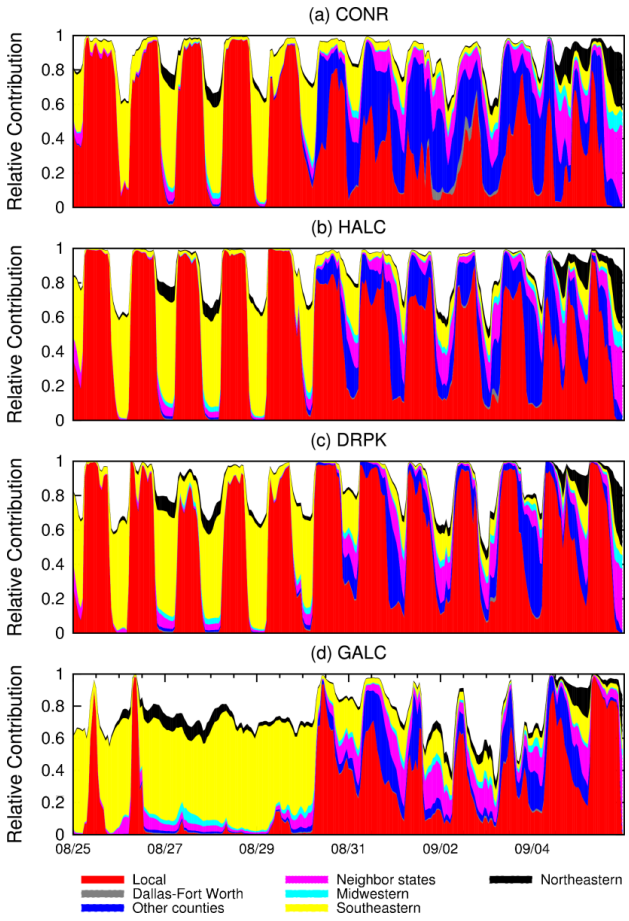

Figure 2-6. Relative contribution from each NOx source region to O_3 concentrations at (a) CONR, (b) HALC, (c) DRPK and (d) GALC. The white space represents the relative contribution of the "other" region.

Figure 2-7 shows the regional NO_x source contributions to episode averaged daytime 8-hour O_3 concentrations. As shown in Figure 2-7(a), the highest O_3 concentrations occur in the urban and industrial areas of Houston and have a maximum value of approximately 80-90 ppb and majority of the areas in the domain have O_3 concentrations greater than 60 ppb. The HGB and BPA areas have largest NO_x contributions to O_3 in the urban Houston area, which can be as high as 70 ppb as shown in Figure 2-7(b). Pollutants from the Dallas-Fort Worth area are rarely transported to

Southeast Texas during this modeling episode and have very little effect on O_3 concentration in the HGB area (see Figure 2-7(c)). NO_x from other counties in Texas (mostly counties in the 4 km domain) can contribute to 10-20 ppb of O_3 concentrations in urban Houston (see Figure 2-7(d)). Figure 2-7(e) shows that the NO_x emitted from neighbor states and Midwestern states have very small effect on Southeast Texas. NO_x from southeastern states contributes to up to 16 ppb of O_3 in the coastal areas and the Gulf of Mexico as shown in Figure 2-7(g). Figure 2-7(h) illustrates that the NO_x from northeastern contributes less than 4 ppb to the O_3 concentrations in the BPA area and less than 2 ppb in the HGB area. Figure 2-7(i) shows that O_3 concentrations due to NO_x from "other" regions are highest near the southern boundary of the domain. The point sources of NO_x from off-shore drilling platforms over the Gulf of Mexico produce about 16 ppb of O_3 and have some influence further inland.

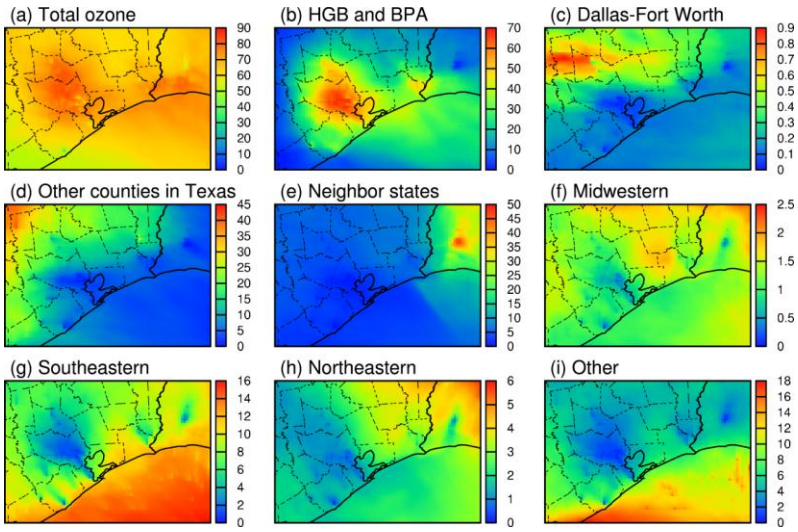

Figure 2-7. Episode-averaged contributions from each NO_x region to O_3 concentrations during high O_3 hours (1100-1800 CST). Units are ppb.

Table 2-1 shows the contributions of each NO_x source region to 8-hour average daytime O_3 concentrations for counties in the HGB and BPA areas. Local NO_x sources are the largest sources to all the counties except Waller County, which is more affected by emissions from other Texas counties. Harris County includes the urban area of Houston and has the highest O_3 concentrations (75 ppb), of which local contributions account for 70.8%. The contributions of Dallas-Fort Worth area to all the counties in the HGB and BPA area are less than 1%. Other counties in Texas are the second largest NO_x source region and contribute to 7.0-36.0% of O_3 concentrations to the HGB and BPA counties. Neighbor states have higher contributions in BPA counties than in the HGB counties since Louisiana is closer to the BPA area. The Midwestern states account for approximately 2% with a maximum of 2.6% in Hardin County of the BPA area. Southeastern states have higher contributions in the coastal counties (10-15%) than inland counties (for example, 4.3% in Harris County). Episode averaged contributions from the northeastern states are less than 6%. Other region contributes to slightly more than 10% in Galveston and Brazoria Counties.

Table 2-1. Percentage contributions of each NO_x region (RG) to averaged 8-hour daytime O_3 concentrations in different counties in the HGB and BPA (three shadowed rows) areas.

Counties	Total O_3 (ppb)	RG1	RG2	RG3	RG4	RG5	RG6	RG7	RG8
		Percentage (%)							
Brazoria	60.8	46.9	0.2	15.6	5.6	1.5	15.2	2.4	12.6
Chambers	71.0	61.8	0.2	7.0	5.8	1.7	12.7	3.3	7.5
Fort Bend	65.1	47.0	0.3	22.7	6.8	1.8	10.6	2.2	8.5
Galveston	66.6	58.4	0.2	8.6	4.5	1.4	14.2	2.3	10.5
Harris	75.0	70.8	0.3	13.4	5.0	1.2	4.3	1.6	3.5
Montgomery	73.8	53.0	0.8	25.3	7.2	1.5	5.7	1.8	4.7
Liberty	69.1	48.8	0.6	19.1	9.3	2.1	9.9	3.9	6.2
Waller	64.7	31.6	0.6	36.0	8.7	2.0	10.5	2.1	8.5
Hardin	62.1	33.4	0.8	23.6	12.1	2.6	13.8	5.7	7.9
Jefferson	68.8	50.8	0.4	9.6	9.6	2.1	14.8	4.2	8.4
Orange	67.4	50.9	0.4	13.0	12.9	1.9	10.6	4.7	5.7

The results shown in Figure 2-7 indicate the importance of each region to daytime O_3 concentration averaged over the entire episode. Figure 2-4 and Figure 2-6 show that contributions from non-local sources could be much more important under specific meteorology conditions. To show the potential maximum contributions of NO_x from each region to O_3 concentrations, 1 hour maximum contributions from 6 regions are shown in Figure 2-8. Figure 2-8(a) shows the O_3 contributions due to local NO_x sources could be as high as 120 ppb around HGB area and along the coast. Figure 2-8(b) shows that the NO_x from other counties in Texas contributes to O_3 concentrations as high as 60 ppb in the HGB and BPA areas but contributes to much less O_3 concentrations (about 10-30 ppb) in the urban Houston and Ship Channel due to rapid titration of O_3 by NO_x emitted combustion sources. High O_3 due to NO_x emissions from the neighbor states (mostly from Louisiana) passes through the 4-km domain at midnight of September 5 with concentrations as high as 30 ppb (see Figure 2-8(c)). Figure 2-8(d)

shows that O_3 formed by NO_x from southeastern states could be transported to Southeast Texas and contributes to as high as 35 ppb. The amount of O_3 reaches HGB and BPA from that source region is 15-20 ppb and 20-30 ppb, respectively. Largest contribution from Northeastern states happens at the nighttime of September 5 due to long range transport of pollutants when the wind blows NO_x and O_3 from the northeast. As shown in Figure 2-8(e), the O_3 concentrations arriving HGB and BPA area from the Northeastern states could be as high as 15-20 ppb.

Figure 2-8(f) shows that maximum contribution from "other" region happens at early morning of September 4 and enters the 4-km domain from the southwest boundary. The highest concentration from the "other" sources is approximately 15 ppb and 10 ppb in HGB and BPA areas, respectively. The "other" region includes emissions from part of Mexico that borders with Texas, part of Canada, the off-shore drilling platforms, the ocean-going vessels as well as O_3 and NO_x enter the 4-km domain from the 36-km domain boundary condition. O_3 due to Canada/Mexico and off-shore drilling platforms and ocean-going vessels over the ocean have small contributions to O_3 in the HGB area. Most of the O_3 due to "other" source region is in fact from the 36-km boundary conditions. This suggests that future simulations should move the western and southern boundary further away from the HGB and BPA area to reduce the effect of boundary conditions.

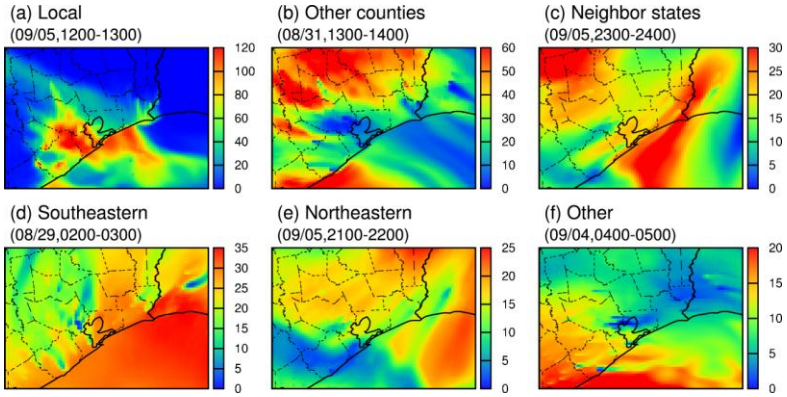

Figure 2-8. Potential highest contributions from each NO_x region to 1-hour O_3 concentrations. Units are ppb.

2.4.4 Regional O_3 transport mechanism: Upwind direct vs. upwind secondary formation

Section 2.4.2 demonstrates how much O_3 in the 4 km domain is due to upwind transport of O_3 and its NO_x precursors. However, whether the predicted upwind O_3 is due to direct transport of O_3 or due to secondary formation by upwind NO_x precursors is still unclear. To determine the relative importance of the two different mechanisms, the boundary conditions for 4-km domain simulation were modified to separately track the sources of O_3 species and its precursors, as described in Section 2.2.2. The upwind O_3 enters the 4 km domain as boundary conditions of O_3 is termed upwind direct O_3 (UWD) while the O_3 forms in the 4 km domain through photolysis reactions of upwind NOx from the boundary conditions is termed upwind secondary O_3 (UWS). Figure 2-9 shows the episode average contributions of UWD and UWS O_3 during high O_3 hours (1100-1800 CST) and low O_3 hours (1900-1000 CST). Figure 2-9(a) shows that the UWD O_3 during high O_3 hours is highest near the boundary of the 4-km domain with a concentration of over 50 ppb but has small contributions to the O_3 concentrations in the HGB and BPA areas from 11:00 to 18:00 CST. This is because a large fraction of the O_3

is reacted with NO_x before reaching the HGB and BPA areas. Figure 2-9(b) shows that the maximum of UWS O_3 near the west boundary of the domain can be as high as 45 ppb. In most part of the domain, the UWS O_3 is approximately 25 ppb. In the urban Houston area, it is less than 10 ppb due to the competition of boundary NO_x with locally emitted NO_x. During the nighttime and early morning, the UWD O_3 can be transported farther inland than during high O_3 hours, as shown in Figure 2-9(c). This is due to reduced urban emissions of NO_x at nighttime hours. The highest UWD O_3 is from the south boundary of domain and has a maximum of 35 ppb. Figure 2-9(d) shows that the UWS O_3 has a maximum of 12 ppb over the northeastern part of the domain. This UWS O_3 is in fact the remaining of the UWS formed in the 4 km domain during daytime as there is no photochemical formation of O_3 at night. The UWD O_3 is more important than UWS O_3 during nighttime hours, indicating a continuous regional transport of O_3 from upwind sources at night. At nighttime and early morning hours, the lifetime of O_3 is longer and both UWD and UWS O_3 can be transported further into the center part of the domain.

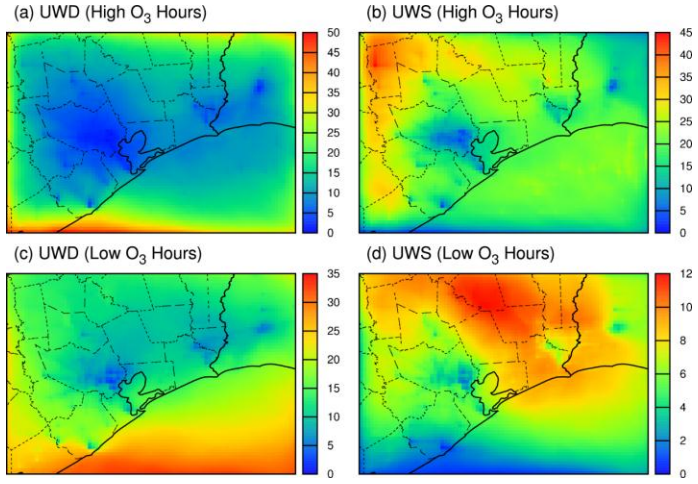

Figure 2-9. Episode average contributions of upwind direct O_3 (UWD) and upwind secondary O_3 (UWS) during high O_3 hours (1100-1800 CST) and low O_3 hours (1900-1000 CST).

2.5 Conclusions

Source apportionment technique developed in this study allows a direct and quantitative determination of the relative importance of different NOx sources and source regions to O_3 concentration using 3D mechanistic air quality models. In Southeast Texas, diesel engines and highway gasoline vehicles have the largest contributions to the average daytime O_3 in the urban Houston area and natural gas combustion plays the most important role in the industrial areas. In additional to O_3 formed from local NOx sources, this study shows that O_3 from upwind sources (sources outside the 4 km Southeast Texas domain) can account for more than 20-50% of the overall average daytime O_3 concentration in HGB and BPA areas. During daytime high O_3 hours, most of the upwind O_3 is formed locally (i.e., in the 4 km Southeast Texas domain) from NO_x emitted in upwind regions. Among the various NO_x source regions resolved in this study, other Texas counties near HGB and BPA areas and southeastern states are important

non-local sources of O_3. Under favorable transport conditions, neighbor states and even northeastern states could also have 20-25 ppb contributions to average daytime O_3 concentrations in the HGB and BPA areas. These results suggest that in addition to local emission controls, regional NO_x emission controls, especially from nearby counties and states, may be necessary to further improve O_3 air quality in Southeast Texas.

Since the simulations are based on a short two-week episode in 2000 that does not represent all summer meteorology conditions in Southeast Texas, and the O_3 concentrations and precursor emissions have decreased significantly since then, the conclusions drawn from this study may not be representative of current or climatological conditions in Southeast Texas. The limitation of this source tracking technique is that it does not imply that removing the NO_x emissions from a source entirely will lead to the reduction of the amount of O_3 predicted to be associated with that source. This technique is intended to give the contributions of different NO_x sources in the O_3 formation chemistry based on the current level of emissions.

3. SOURCE APPORTIONMENT OF PRIMARY AND SECONDARY INORGANIC AIRBORNE PARTICULATE MATTER*

A nested version of the source-oriented externally mixed UCD/CIT model was developed to study the source contributions to airborne particulate matter (PM) during a two-week long air quality episode during the Texas 2000 Air Quality Study (TexAQS 2000). Contributions to primary PM and secondary ammonium sulfate were determined within the 4 km resolution domain that covers the Houston-Galveston Bay (HGB) and Beaumont-Port Arthur (BPA) areas.

The predicted 24-hour elemental carbon (EC), organic compounds (OC), sulfate, ammonium ion and primary $PM_{2.5}$ mass are in good agreement with filter-based observations. Predicted hourly sulfate, ammonium ion, and primary OC from diesel and gasoline engines at the La Porte agree well with measurements from an Aerodyne Aerosol Mass Spectrometer (AMS). The predicted contributions to biomass burning OC is also in general agreement with BBOA resolved by the AMS. The comparison between predicted source contributions to primary OC and $PM_{2.5}$ and a chemical mass balance (CMB) model suggests that, based on current emission inventory, PM emissions from industrial sources account for a significant fraction of primary OC and $PM_{2.5}$. This implies that further investigations on the industrial PM emissions are necessary.

EC is mainly from diesel engines and majority of the primary OC is from internal combustion engines and industrial sources. Open burning contributes large fractions of EC, OC and primary $PM_{2.5}$ mass. Road dust, internal combustion engines and industrial sources are the major sources of primary $PM_{2.5}$. Wildfire dominates the contributions to all primary PM components in areas near the fires. Secondary ammonium sulfate accounts for majority of the secondary inorganic PM. Over 80% of the secondary sulfate in the 4 km domain is produced in upwind areas. Coal combustion is the largest source of sulfate. Ammonium ion is mainly from agriculture sources and contributions from gasoline vehicles are significant in urban areas.

3.1 Introduction

Southeast Texas is well known for the high density of industrial facilities located in the Houston-Galveston Bay (HGB) and Beaumont-Port Arthur (BPA) areas. Houston is the forth-largest city in the United States with a population over 2.2 million. Based on the National Emissions Inventory (NEI) developed by the U.S. EPA, the emission rates of nitrogen oxides (NO_x), volatile organic compounds (VOCs) and fine particulate matter with aerodynamic diameter less than 2.5 μm ($PM_{2.5}$) from the HGB area are 27.4, 23.6 and 4.2metric tons km-2 year-1 in 2000, which exceed those from the Los Angeles County in California (23.6, 21.4 and 3.0 tons km-2 year-1, respectively).Because of the immense emissions of primary PM and precursors of secondary PM from both industrial and urban sources and the meteorology conditions characterized by high temperatures and intensive solar radiation as well as a land-sea breeze circulation that confines pollutants in Southeast Texas [7, 8], HGB and BPA have possible difficulties meeting

the national ambient air quality standards for $PM_{2.5}$ [10, 12, 78]. Quantitative knowledge of the contributions of different emissions sources to $PM_{2.5}$ concentrations is helpful to better understand $PM_{2.5}$formation mechanisms and is crucial to the development of effective emission control strategies to reduce the adverse effects caused by $PM_{2.5}$ in HGB and BPA areas.

The receptor-oriented chemical mass balance (CMB) and positive matrix factorization (PMF) models are widely used tools to quantify source contributions to air pollutants. The total concentrations of each chemical species in ambient samples measured at receptor locations are reconstructed from a linear combination of emission source profiles [37]. The CMB and PMF receptor models have been applied in many studies to determine the source contributions to PM in various parts of the country [38-40, 42].In the HGB area, diesel and gasoline vehicles, road dusts, meat cooking operations and wood combustion have been identified as the main sources to primary $PM_{2.5}$ [11, 78]. While the receptor models are robust and relatively easy to apply, they do not provide all the information needed to design effective control strategies. The fundamental non-reactive assumption in the model formulations limits their applications mainly to primary pollutants and they cannot be used to evaluate the effectiveness of different emissions control strategies. Because of the requirement of accurate PM chemical composition, they can only be used in locations where such detailed measurements are available. As an alternative method, source-oriented modeling approaches track emissions from different source categories and their physical and chemical transformations in mechanistic air quality models [43-45]. The model results

are then processed to generate source contribution estimations that cover the entire model domain. These models can also be used to evaluate different emissions control strategies.

TexAQS 2000 is a comprehensive campaign to improve understanding of the factors that control the formation and transport of air pollutants in the Southeastern Texas. Previous regional modeling studies for the TexAQS 2000 episode were mainly focused on understanding high ozone formation [79-81] and only a few studies have been devoted to study PM [12]. The regional source contributions to PM during this episode have not been determined.

In this study, the one-way nested source-oriented UCD/CIT air quality model was used to describe the emissions, transport, physical and chemical transformation and removal of airborne PM in southeast Texas during TexAQS 2000. The purpose of this study is to evaluate the performance of the UCD/CIT model in describing key gases and aerosol-phase pollutants and to determine the major sources that contribute to primary PM as well as secondary ammonium sulfate in the HGB and BPA areas during this episode. This work is a continuation of the development and application of the source-oriented UCD/CIT model and represents the first application of the model in a geographical region outside California. Source contributions to secondary organic aerosol are not considered and will be evaluated in a separate study.

3.2 Model description

The UCD/CIT source-oriented air quality model has been applied and evaluated in several previous studies on source apportionment of PM and visibility impairment in

the South Coast Air Basin and the Central Valley of California(for example, see [26, 45, 82, 83]).Details of the model development history and underlying principles have been described elsewhere ([84, 85] and the references therein), so only a brief summary is given below along with descriptions of recent updates to the model.

The UCD/CIT model can be used to directly determine the source contributions to both primary and secondary PM. The gas phase mechanism was expanded to predict the formation as well as the source origin of semi-volatile compounds by tracking the emission and transformation reactive precursors and intermediate products from different sources. In this study, emissions of NO_x, sulfur dioxide (SO_2) and ammonia (NH_3) from different sources and their reaction products (for example, N_2O_5, HNO_3, H_2SO_4, etc.) are independently simulated in the model by attaching source tags to species from different sources. To determine the contributions to secondary PM, the representation of particle species is expanded to allow direct tracking of the gas-to-particle partitioning of the tagged precursor gases from different sources. This enables the model to determine the source contributions to nitrate (NO_3^-), ammonium (NH_4^+), and sulfate (SO_4^{2-}) in this study. The UCD/CIT model can be configured as to use an externally mixed particle representation to directly determine the source contributions to primary PM [27]. In this study, the particles are represented as internally mixed aerosols and an artificial tracer approach is used to determine source contributions to primary PM [85].

The original source-oriented UCD/CIT model is revised to include a one-way nested domain capability that allows the nested domains to use tagged boundary

conditions for each emission source category based on source contribution results from a parent domain. This modification allows a more complete source attribution of PM by directly resolving the contributions from different upwind sources to concentrations in the nested domain. This is especially important when the contributions from upwind sources are significant comparing to the sources within the nested domain. The original chemical mechanism used in the UCD/CIT model was a revised version of the SAPRC-90 mechanism [86]. The SAPRC mechanism in this version of the UCD/CIT model is updated to a revised SAPRC-99 mechanism. An automatic mechanism generator was developed to create source-oriented SAPRC chemical mechanism that treats the reactions of species from different sources separately. The particle dry deposition scheme is updated in this version of the UCD/CIT model so that dry deposition velocities of particles are land cover and season dependent [87, 88].

3.3 Model application

3.3.1 Domain setup and meteorology inputs

In this study, the nested version of the UCD/CIT model is applied to simulate the air quality in eastern Texas during a two-week long (August 24, 2000 to September 5, 2000) air quality episode in the TexAQS 2000 study. The horizontal grid size for the three nested domains are 36km, 12km and 4km, respectively. The number of horizontal grid cells for these domains are 62×67, 89×89, and 83×65, respectively. 14 vertical layers that reach approximately 15km above surface are used. The first layer height is approximately 42 m. All three domains use the same vertical layer setup.

In this study, the meteorology fields were generated using the PSU/NCR mesoscale model (MM5) by the Texas Commission of Environmental Quality (TCEQ) and were converted into the data format required by the UCD/CIT model using a preprocessing program. The reaction rate constants for photolysis reactions were calculated off-line with the JPROC preprocessing program distributed with the Community Multiscale Air Quality (CMAQ) model version 4.6 [89]. Adjustments of the photolysis rate due to cloud cover are calculated based on algorithm described in Byun and Chin [90].

3.3.2 Emission inputs

Emissions of gaseous and particulate matter for the source-oriented UCD/CIT model were based on the 2001 Clean Air Interstate Rule (CAIR) emission inventory. Emissions of wildfire during the modeling episode were based on the data provided from the Center for Energy and Environmental Resources at the University of Texas at Austin. Continuous Emission Monitoring (CEM) data were used to replace annual emission data for electricity generation utilities. The revised emission inventory was processed using a revised SMOKE (Sparse Matrix Operator Kernel Emissions) model version 2.4. Biogenic emissions were generated using the Biogenic Emissions Inventory System, Version 3 (BEIS3) included in the SMOKE distribution. The 1-km resolution BELD3 land cover data with 230 different cover types [91] were used to estimate emissions from vegetation and soil.

Modifications were made to the original SMOKE program to generate emissions for each emission category using a sub-set of the emission inventory data determined by

a list of Source Classification Codes (SCCs) for that emission source category. An SCC filter is added to the SMOKE program so that the program only processes the emission inventory data listed in SCC code list. Nine primary PM emission categories (mobile gasoline engines, mobile diesel engines, high sulfur fuel (boilers, engines and industrial processes using oil or natural gas), wild fire, open burning (including household cooking, waste disposal and agriculture burning), road dust, agriculture dust, sea salt and other sources) and eight gas emission categories (diesel engines, gasoline engines, oil and gas production, high sulfur fuel, coal combustion, fire (including wildfire and open burning), biogenic, and other sources) were used in generating the emissions.

Table 3-1 lists the daily emission rates of gas phase precursors of secondary inorganic aerosol for all the emission source categories for August 31, 2000, a typical weekday with significant wildfire activities. Coal combustion accounts for the majority of the SO_2 emissions. Table 3-2 lists the daily emission rates of $PM_{2.5}$ elemental carbon (EC), organic compounds (OC), nitrate, sulfate and other components. Diesel vehicles and open burning are the two largest anthropogenic sources of EC. Approximately 47% of primary OC and 40% primary $PM_{2.5}$ mass (less wildfire) is emitted from the "other" sources, while diesel and gasoline engines combined only account for 16.7% and 11.1% of primary OC and $PM_{2.5}$ mass, respectively. Analysis of the emission inventory shows that approximately 60% of the primary $PM_{2.5}$ in the "other" source category is from industrial point sources (mainly catalyst cracking, process heaters and furnace electrode manufacture) and 40% is from area sources (mainly road construction and commercial charbroiling).

Table 3-1. Daily emission rates of gas phase precursors for each source on August 31, 2000 in the 4 km model domain. (Units: kmol day^{-1})

Source Types	NO	NO_2	SO_2	NH_3
Diesel	1224.7	64.4	73.1	4.0
Gasoline	693.7	36.4	19.4	139.7
Oil/gas Production	184.0	9.7	0.4	0.0
High Sulfur Fuel	8665.6	455.8	951.1	90.0
Coal Combustion	2197.1	115.6	4231.8	1.3
Open Burning and Wildfire	709.2	37.4	1.1*	327.2
Other	4429.8	233.0	4156.6	1648.8
Biogenics	1083.6	0.0	0.0	0.0
Total	19187.3	952.2	9433.1	2210.8

*Emissions of SO_2 from wildfire were not considered in this study.

The UCD/CIT uses sectional representation of particle size distributions with 15 size bins that cover the size range of 0.001 to 10 μm for the primary emitted particles. Modifications were made to the SMOKE program to generate size resolved PM emissions. The $PM_{2.5}$ speciation profiles included in the auxiliary data of the 2001 CAIR emission inventory were expanded to generate size- and composition- resolved source profiles using particle size and composition distribution information collected from various data sources described below. Detailed particulate emission size distributions measurements of mass and major chemical components are available for diesel and gasoline engines [92],residential wood burning, meat cooking and cigarette smoking [93] and open burning of agriculture mass [94]. Several data sources contain of particle size distribution of mass but not chemical components so it is assumed that all chemical species will have the same size distribution as the reported mass distribution. These profiles include feedlot dust [95], road dust [96], tire wear [97] and locomotive emissions [98]. For other sources without explicit size resolved measurements, rough estimation of the size distributions were made based on the 3-sizebin data from Taback

et al. [99]. Sea salt emissions from wave breaking were generated based on the algorithm described in Zhang et al. [100] and Lewis and Schwartz [101].

3.4 Results and discussion

3.4.1 Model performance evaluation

The predicted concentrations of gaseous and PM species in the 4 km domain were compared with surface observation data. In general, predicted concentrations of O_3, NOx and CO agree well with observations.SO_2 concentrations at industrial sites are slightly over-predicted. Peak O_3 concentrations are under-predicted at several stations due to underestimation of the high reactive VOC emissions from industrial sources [36, 80, 81]. This underestimation of O_3 does not affect the primary PM source apportionment results but may lead to some under-estimation of local secondary sulfate concentrations. The following analyses are focused on evaluating the overall model performance on PM predictions.

Figure 3-1 shows the mean fraction bias (MFB) and mean fractional error (MFE) for $PM_{2.5}$ EC, OC, sulfate, ammonium ion and mass based on the daily averaged species concentrations across different stations. The definitions of MFB and MFE are shown in equations (E3-1) and (E3-2):

$$\mathrm{MFB} = \frac{1}{N}\sum_{i=1}^{N}\frac{C_m - C_o}{(C_m + C_o)/2} \quad \text{(E3-1)}$$

$$\mathrm{MFE} = \frac{1}{N}\sum_{i=1}^{N}\frac{|C_m - C_o|}{(C_m + C_o)/2} \quad \text{(E3-2)}$$

in which C_m is the model-predicted concentration at station i, C_o is the observed concentration at station i, and N equals the number of prediction-observation pairs drawn

from all monitoring stations. The lines on the figure show the suggested performance goals (solid lines) and criteria (dash lines) as a function of observed concentration. Performance "goals" are the level of accuracy that is close to the best a model can be expected to achieve and performance "criteria" are the level of accuracy that is acceptable for standard modeling applications, more information can be found in Boylan and Russell's paper [102]. The observation data used in the calculation were from 6 stations that cover urban, industrial and suburban locations (BAYP, CONR, DRPK, GALC, HALC and JEFC). The analysis includes 13 days of data from August 24, 2000 to September 5, 2000. Most species meet their individual performance criteria. Sulfate ion meets the criteria for 11 out of 13 days for both MFB and MFE. The total primary $PM_{2.5}$ meets the criteria for 11 out of 12 days for both MFB and MFE (one data having concentration larger than $20\mu gm^{-3}$ was excluded).All EC and OC predictions are within the model performance criteria. Over 50% of the data points are within the model performance goal.

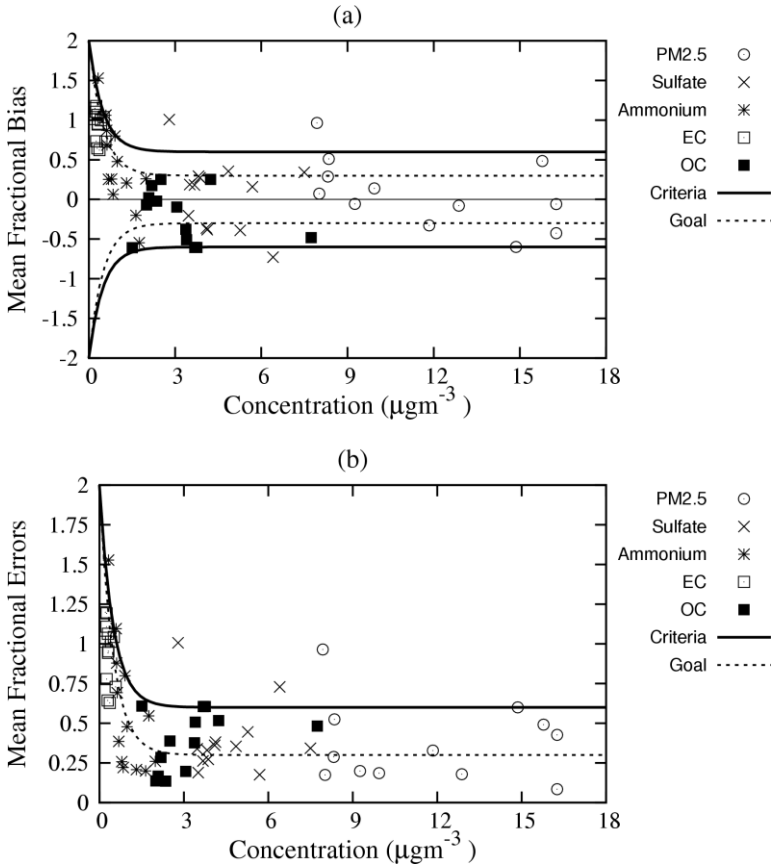

Figure 3-1. Mean fractional bias (a) and errors (b) for $PM_{2.5}$ mass, sulfate, ammonium, EC and OC along with the proposed performance goals and criteria.

Figure 3-2 shows the comparison of predicted $PM_{2.5}$ sulfate, nitrate and primary OC concentrations and the observed concentrations by an Aerodyne Aerosol Mass Spectrometer (AMS) at La Porte (LAPT).The AMS results were provided in 15-min time resolution and were averaged to 1-hour to compare with the model predictions. More details about the AMS measurements at LAPT can be found in Wood et al. [103] and the references therein. The predicted and observed sulfate concentrations are on the same order of magnitude as the AMS, and the predicted diurnal and episode trends show general good agreement with the observations. Predicted low nitrate concentrations of approximately 0.5 μgm^{-3} at LAPT are at same level as the AMS measurements although

the diurnal variation is not well captured by the model on a few days. Figure 3-2(c) shows the BBOA (biomass burning-like organic aerosol) based on the AMS data and the predicted other primary OC by the UCD/CIT model. The dashed line shows the contributions from predicted open burning and wildfire sources and the solid line shows the contributions from open burning, wildfire and other sources. The predicted biomass burning (open burning and wildfire) alone does not fully explain the BBOA from AMS. Including primary OC from other sources improves the agreement between the observations and predictions but the high concentrations of BBOA on September 2, 3 and 5 are not reproduced. This is likely due to incompleteness in the wildfire emission inventory. Figure 3-2(d) shows the HOA (hydrocarbon-like organic aerosol) from AMS and the predicted primary OC from diesel and gasoline vehicle sources. HOA from AMS data have been considered as mostly due to primary organic aerosols from diesel and gasoline combustions [104] thus allow a direct comparison with the UCD/CIT results. The predicted concentrations of primary OC from diesel and gasoline engines combined are in the range of 0-0.5 μgm^{-3}, which agree well with the AMS measurements. There is no significant episode trend in the observed and predicted concentrations and the diurnal variations are generally well reproduced by the model.

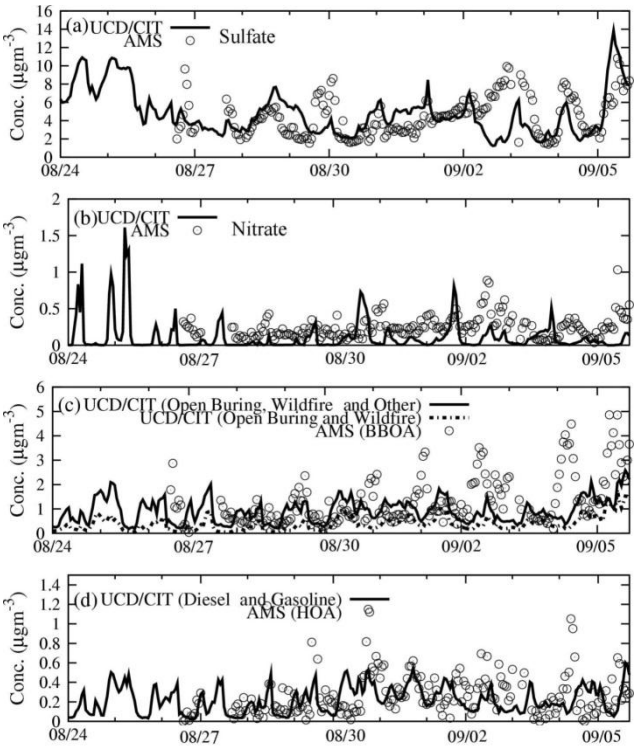

Figure 3-2. Time series of concentrations of $PM_{2.5}$ sulfate (a), nitrate (b), primary organic compounds from biomass burning (c) and diesel and gasoline engines (d) predicted by the UCD/CIT model (lines) and measured by an AMS(open circles).

3.4.2 Comparison with CMB results

The predicted primary PM source apportionment results were compared with the results from an independent CMB source apportionment study that uses organic tracers and 3 inorganic elements to resolve contributions of gasoline vehicles, diesel vehicles, vegetative detritus, meat cooking, wood burning, and road dust to $PM_{2.5}$ OC and mass at three stations (LAPT, HRM3 and HALC). More details about the CMB study can be found in Buzcu et al. [10]. Since the UCD/CIT model does not have explicit vegetation detritus and meat cooking sources, the predicted contributions from these two sources by the CMB model are lumped into the "other" sources in the comparison. The open

burning and wildfire contributions from the UCD/CIT model are combined to compare with the wood burning contributions from CMB. Since open burning contains not only wood combustion but also other types of burnings, this combination may slightly over estimate the actual wood burning contributions.

The CMB analyses were performed for two groups of $PM_{2.5}$ speciation data. One group contains the averaged concentrations for non-smoke days when wildfire influence was small (August 15, 21 and 27, 2000) and other dataset for smoke days (September 2, 14, 20 and 30, 2000). Since the current model episode covers only part of the CMB dataset, averaged results from August 24-27, 2000 were used to compare with the non-smoke day CMB results and results from September 3-5, 2000 were used to compare with the smoke day CMB results. The relative contributions of each source from the CMB analysis are based on the apportioned primary OC and $PM_{2.5}$ mass from each source and the measured $PM_{2.5}$ OC and mass (including secondary PM) reported in Table 2 and Table 3 of Buzcu et al. [10]. The total apportioned percentages shown in Figure 3-3 are the ratio of total primary $PM_{2.5}$ OC and mass to the total measured $PM_{2.5}$ OC and mass. Relative contributions predicted by the UCD/CIT model are based on the predicted primary OC and $PM_{2.5}$ mass and overall $PM_{2.5}$ OC and mass with secondary components.

Figure 3-3(a) and (b) show the comparison of source contributions to primary OC for non-smoke and smoke days, respectively. The UCD/CIT model predicts a much higher primary OC fraction (60-80%) in total OC due to possible under-prediction of secondary organic aerosol [26, 29].On the other hand, the CMB might slightly under-

predict the primary OC from other sources, as some of the CMB reconstructed tracer concentrations are much lower than measurements (see Figure 5 of Buzcu et al., [10]). Both models show obvious diesel and gasoline engines contributions but the UCD/CIT model predicts higher contributions from wood smoke. The UCD/CIT model also predicts larger contributions from the "other" sources. Both models show a slight decrease in primary OC fraction and an increase of OC from wildfire that rivals the contributions from diesel and gasoline engines on smoke days. The predicted contributions from gasoline, diesel and wildfire contributions by the two models agree much better on the smoke days. Figure 3-3 (c) and (d) show the relative contributions to total primary $PM_{2.5}$ on non-smoke and smoke days, respectively. The models agree well that approximately 50% of $PM_{2.5}$ was primary on non-smoke days and 30-40% on smoke days. Both models predict higher contributions from diesel engines to the total $PM_{2.5}$ than gasoline engines. However, the UCD/CIT model again predicts higher contributions from the "other" sources" and wood smoke sources and lower contributions from diesel and gasoline engines.

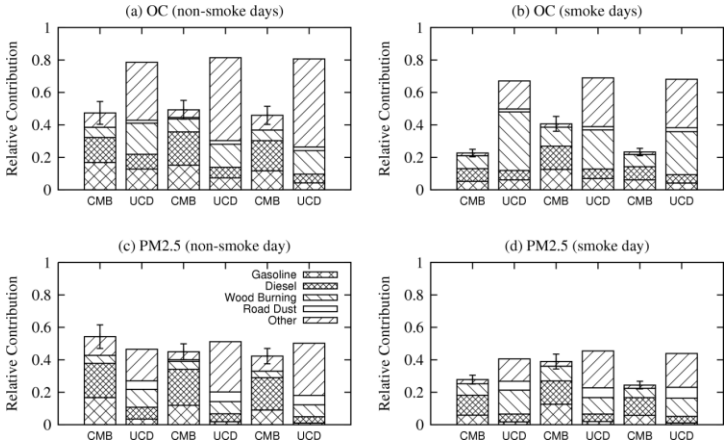

Figure 3-3. Relative source contributions to primary $PM_{2.5}$ OC and mass concentrations by a CMB model and UCD/CIT model at three sites.

The emissions data in Table 3-2 suggests that approximately 40% of primary $PM_{2.5}$ (excluding wildfire) in the 4 km model domain is from the "other" sources. Analysis of the emission inventory shows that approximately 60%of the primary $PM_{2.5}$ in the "other" source category is from industrial point sources (mainly catalyst cracking, process heaters and furnace electrode manufacture) and 40% is from area sources (mainly road construction and commercial charbroiling). Thus, the UCD/CIT model results of significant contributions from the "other" sources are consistent with emission inventory data. The UCD/CIT model predicted OC from diesel and gasoline engines seems agree well with the AMS data, suggesting that the PM emissions from these two sources are generally well represented in the emission inventory. Previous studies showed significant contributions to VOCs in the HGB area from industrial sources [105, 106], so it is expected that they should also contribute to the observed PM concentrations. However, few other independent studies of PM exist so additional analysis is necessary

to validate the PM emission inventory regarding emissions from other sources, especially from industrial sources.

Table 3-2. Daily emission rates of sulfate, nitrate, EC, OC, other components and $PM_{2.5}$ mass for each source on August 31, 2000 in the 4 km model domain. (Units: kg day^{-1}).

Source Types	Sulfate	Nitrate	EC	OC	Other	$PM_{2.5}$
Diesel	260.5	21.2	9650.4	2944.5	99.0	12975.6
Gasoline	105.9	17.7	742.9	3391.9	842.6	5100.9
High Sulfur Fuel	1343.5	28.4	123.8	3008.1	1333.1	5836.9
Open Burning	649.6	60.7	2096.8	6884.8	13064.0	22755.9
Road Dust	50.0	43.1	196.1	2662.0	39826.0	42777.1
Agriculture Dust	3.1	8.7	29.6	435.6	7514.7	7991.7
Other	8238.6	186.2	2246.6	18694.9	35293.2	64659.6
Wildfire	1545.2	153.7	12360.9	59490.0	3708.5	77258.4
Sea Salt	30.6	14.5	0.0	0.0	0.0	384.7
Total	12227.0	534.2	27447.2	97511.7	101681.0	239740.8

3.4.3 Source apportionment of primary particulate matter

Figure 3-4 shows the predicted hourly-averaged relative source contributions to $PM_{2.5}$ EC, OC and primary $PM_{2.5}$ mass at DRPK from sources within the 4 km domain during the study period. The DRPK site is located east of the Houston urban center and is close to the Houston Ship Channel. Contributions to EC at DRPK are mainly from diesel engines (approximately 70%) and open burning (approximately 20%).Contribution from wild fire increases on September 4-5, 2000, with a maximum contribution of approximately 50%. The contributions of gasoline engines and road dust to EC concentrations are small.

Figure 3-4 (b) shows that diesel and gasoline engines combined contribute to approximately 20% of the primary OC, with approximately equal contribution from each source. The diurnal variation in the gasoline contributions is more significant than that of diesel engines. Approximately 20-30% of the OC originate from open burning and 5-10%

from high sulfur fuel. Contributions from road dust to primary OC are small. Other OC sources account for about 40-55%. A further check of the emission data shows that approximately 70% of the OC in the “other” source category are from industrial sources. The contribution from wild fire increases from almost zero to about 80% in September 4-5, 2000.

Figure 3-4 (c) shows the relative contributions to primary $PM_{2.5}$mass. The contributions due to upwind sources are not included so that the sum of the relative contributions is slightly less than 100%on some of the days. Open burning accounts for approximately 20% of the primary $PM_{2.5}$. Contributions from diesel engines are about 15-20%. Road dust is another important source of primary $PM_{2.5}$with relative contributions of 10-20%. Contributions from gasoline engines and high sulfur fuel to primary $PM_{2.5}$vary between 5-10%.Wildfire contributions peak at approximately 30% in the last a few days of the study episode. Large contributions from other sources are likely due to industrial sources, based on an analysis of the emission inventory.

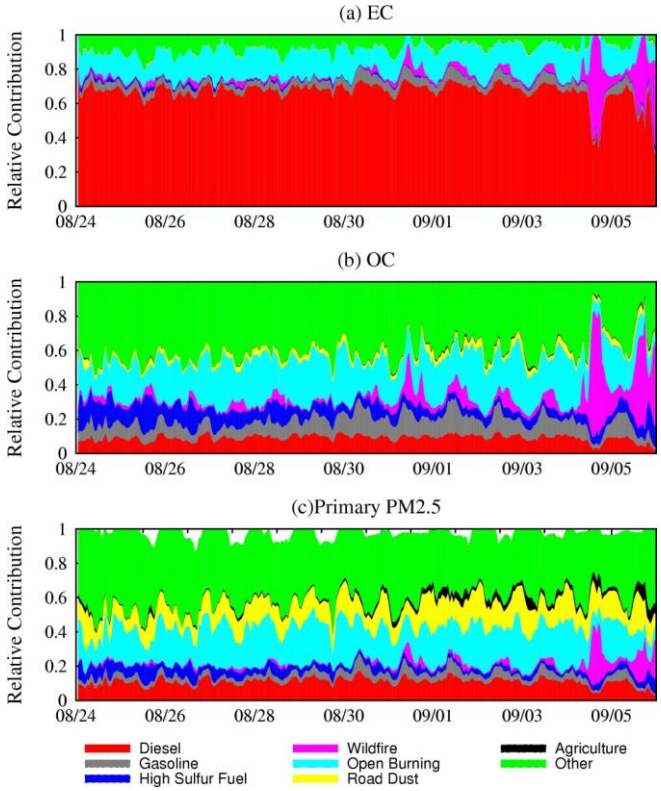

Figure 3-4. Relative source contributions to $PM_{2.5}$ EC (a), primary OC (b), and mass (c) at Deer Park (DRPK).

Figure 3-5 shows the source contributions to $PM_{2.5}$ EC, OC and mass concentrations at CONR. The CONR site is situated in an urban commercial area approximately 40 miles north of Houston, away from major industrial emissions. Figure 3-5(a) shows that 50%-60% EC is from diesel engines. Open burning is the second largest source with relative contributions of approximately 30%. Wildfire contributes to about 50% in the last few days. The combined contributions of road dust, gasoline engines and high sulfur fuel to EC are less than 10%.

Figure 3-5 (b) shows that diesel and gasoline engines account for less than 20% of OC at CONR. The relative contribution from road dust is approximately 5%. Contribution from open burning accounts for about 40% of the total OC. OC from

wildfire dominates the last few days with relative contributions as high as 100% on some hours. Contributions of other sources are approximately 10-20% throughout the episode.

Figure 3-5(c) describes the relative source contributions to primary $PM_{2.5}$ mass at CONR. Open burning and road dust are two main sources and account for approximately 60% of the predicted $PM_{2.5}$ mass concentrations during the entire episode. $PM_{2.5}$ from diesel vehicles is less than 10%. The contribution from wildfire to primary $PM_{2.5}$ mass increases to approximately 25% on September 2, 2000 and even reached approximately 50% on September 4, 2000. Contributions of gasoline vehicles and high sulfur fuel sources are negligible and contributions from other sources are about 20%.

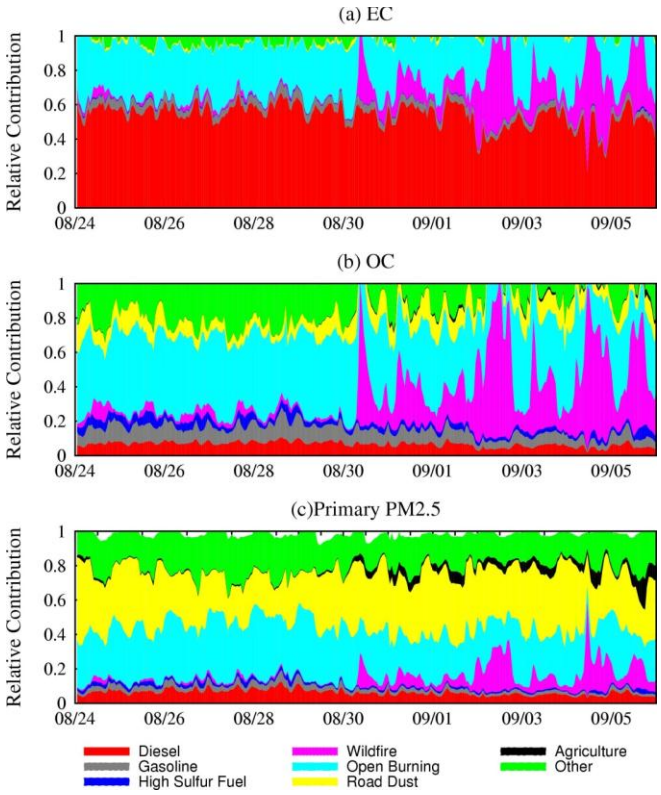

Figure 3-5. Relative source contributions to $PM_{2.5}$ EC (a), primary OC (b), and mass (c) at Conroe (CONR).

Figure 3-6 shows the regional source contributions to episode average $PM_{2.5}$ EC concentrations. The minimum to maximum value scale is used for all the regional figures in this section. To better show the spatial distribution, the maximum values of the scale of some figures are adjusted with the maximum values attached with titles. Figure 3-6(a) shows that high EC concentrations occur in the Houston urban areas with a maximum concentration of 1.93μgm^{-3}.As shown in Figure 3-6(b), the dominant source of EC in the urban area is diesel engines which account for approximately60% of total EC. In addition to diesel vehicles, diesel-powered construction equipment is an important source of diesel emissions. This explains the wider spatial distribution of diesel engine contributions than gasoline engine contributions. Contribution from gasoline engines is also highest in the urban area with a maximum contribution of 0.12μgm^{-3} as shown in Figure 3-6(c). Wildfire dominates local EC concentration with a highest contribution of 1.73μgm^{-3}.Open burning also has wide spatial distribution around the Houston area. All other anthropogenic sources combined contribute to approximately 0.20 μgm^{-3}near the Houston Ship Channel and approximately 0.15μgm^{-3} in the BPA area.

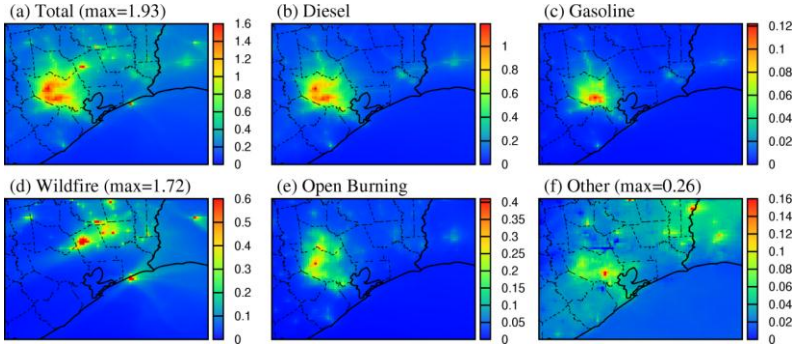

Figure 3-6. Episode-averaged source contributions to $PM_{2.5}$ EC concentrations. Units are μgm^{-3}.

Figure 3-7 shows the predicted source contributions of episode average primary OC from August 24, 2000 to September, 5, 2000. The spatial distribution of OC is similar to that of EC. High OC concentrations occur in the urban areas with maximum concentrations of approximately 3-4 μgm^{-3}. In areas affected by wildfire, the maximum concentration is approximately 9 μgm^{-3} as shown in Figure 3-7(a). As shown in Figure 3-7(b) and (c), maximum contributions from diesel and gasoline engines are approximately 0.36 and 0.55μgm^{-3}, respectively. Wildfires generate a large amount of OC. The highest concentration of OC due to wildfire is approximately 8.32 μgm^{-3} as shown in Figure 3-7(d). Figure 3-7(e) shows that open burning is an important source of OC with a highest average contribution of 1.25 μgm^{-3}.All other sources combined contribute to as high as 2.20 $\mu gm^{-3}$of OC. The highest concentration occurs in industrial areas, further confirming that industrial sources account for majority of the emissions from the "other" source category.

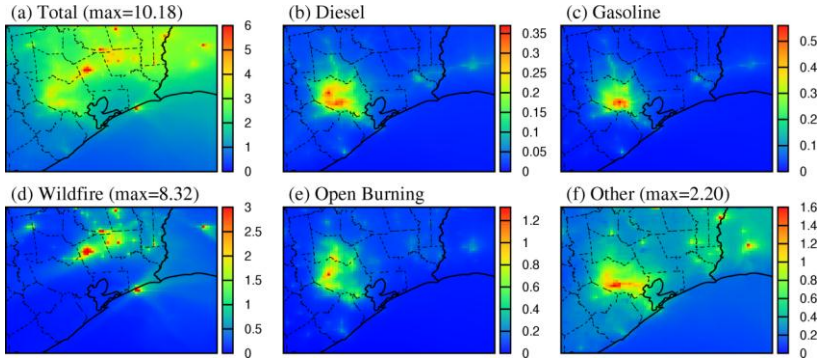

Figure 3-7. Episode averaged source contributions to OC concentrations. Units are μgm^{-3}.

Figure 3-8 shows the predicted episode averaged source contribution to24-hour average primary $PM_{2.5}$ mass concentrations. Figure 3-8(a) shows that primary $PM_{2.5}$

concentrations in the Houston urban and industrial areas are approximately 8-10 μgm^{-3}. The contribution due to upwind sources to primary $PM_{2.5}$ in the 4 km domain is approximately 1%. Highest contribution from diesel engines is approximately 1.6 μgm^{-3}. Contributions from diesel engines are higher than contributions from gasoline engines by approximately a factor of 2. High sulfur fuel contributes less than 0.8 μgm^{-3} in both HGB and BPA areas. Contributions from wood smoke can be as high as 10 μgm^{-3}. Figure 3-8(g) shows that open burning contributes to approximately 25% of the primary $PM_{2.5}$ in urban areas. Figure 3-8(h) illustrates that road dust contributes significantly to primary $PM_{2.5}$ especially in some rural areas north of Houston. The concentration can be as high as 2.52 μgm^{-3}. Analysis of the emissions inventory shows that unpaved road dust emissions account for over 95% of the road dust emissions. Other sources, mostly industrial sources, can contribute to approximately 4-6 $\mu gm^{-3}$of primary $PM_{2.5}$. The contribution from sea salt is confined to the coastal areas and is small compared to other sources.

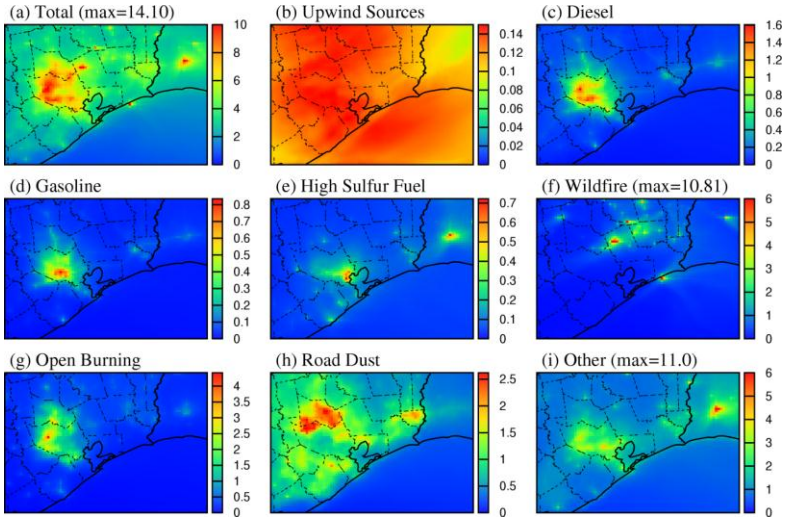

Figure 3-8. Episode averaged source contributions to primary $PM_{2.5}$. Units are μgm^{-3}.

3.4.4 Source apportionment of secondary inorganic components

In previous receptor-oriented source apportionment studies, source contributions to sulfate were not determined because most of the sulfate is secondary. Buzcu et al. [10] suggested that heterogeneous reactions of SO_2on the surface of wood smoke particles could lead to increased sulfate concentrations in areas downwind of wildfires. In this study, we focus on understanding the sources secondary sulfate from major SO_2 sources and the relative contributions from local (sources in the HGB and BPA areas) vs. upwind sources (sources located outside the 4 km domain) without considering the potential heterogeneous pathways.

Figure 3-9 shows the time series of predicted and observed 24-hour averaged $PM_{2.5}$ sulfate concentrations at 7 observation sites. The predicted sulfate concentrations are broken down to show contributions from local sources and upwind sources. In the first two days, most of the sulfate in the domain is due to initial conditions and the

contribution from upwind sources is small. In the rest of the days, predicted concentrations generally agree well with observations at all the sites and upwind sources dominate the sulfate concentration with relative contributions of more than 80% at most stations. Sulfate concentrations are under-predicted on September 1-2, 2000 at most stations in the HGB area, suggesting that a regional sulfate event was not captured by the model.

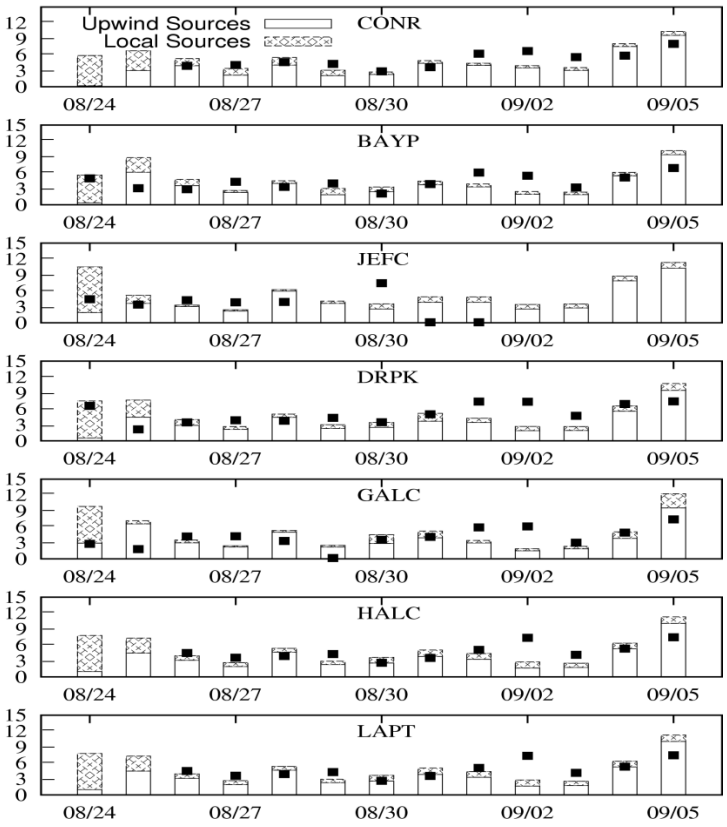

Figure 3-9. Time series of 24-hour averaged observed (closed rectangle) and predicted (stacked bars) $PM_{2.5}$ sulfate concentrations from sources within the 4 km domain (Local Sources) and upwind sources (Upwind Sources). Units are μgm^{-3}.

Figure 3-10 shows the predicted regional contributions to 24-hour averaged secondary $PM_{2.5}$ sulfate concentrations from different SO_2 sources on September 5, 2009, when the concentrations at all observation sites are highest throughout the simulated

episode. The source contributions to $PM_{2.5}$ sulfate (Figure 3-10 (a)) from primary emissions, upwind secondary sources and local sources of high sulfur fuel, coal combustion and other sources are shown on Figure 3-10(b)-(f), respectively. The overall sulfate concentration in HGB area is approximately 8-10 μgm^{-3}. Primary emissions can contribute to as high as 2.2 μgm^{-3} but the contributions from primary emissions to sulfate in HGB and BPA areas are less than 1 μgm^{-3}. Figure 3-10(c) shows that secondary sulfate from upwind sources accounts for almost all regional sulfate in the HGB and BPA areas. Local sources of SO_2 are not major sources of sulfate. SO_2 emitted from local sources of coal combustion contributes to a maximum of 1.8 μgm^{-3} on that day but most of the contributions are seen off the coast due to significant regional transport. Figure 3-10(g)-(i) illustrate the sources that contribute to the upwind secondary sulfate as shown in Figure 3-10(c). Coal combustion is the largest source with contributions of 5-7 μgm^{-3} and high sulfur fuel (mostly natural gas burning) is the second largest source with contributions of 3-4 μgm^{-3}in the HGB and BPA areas. All other sources combined only contribute to less than 1μgm^{-3} in most part of the domain.

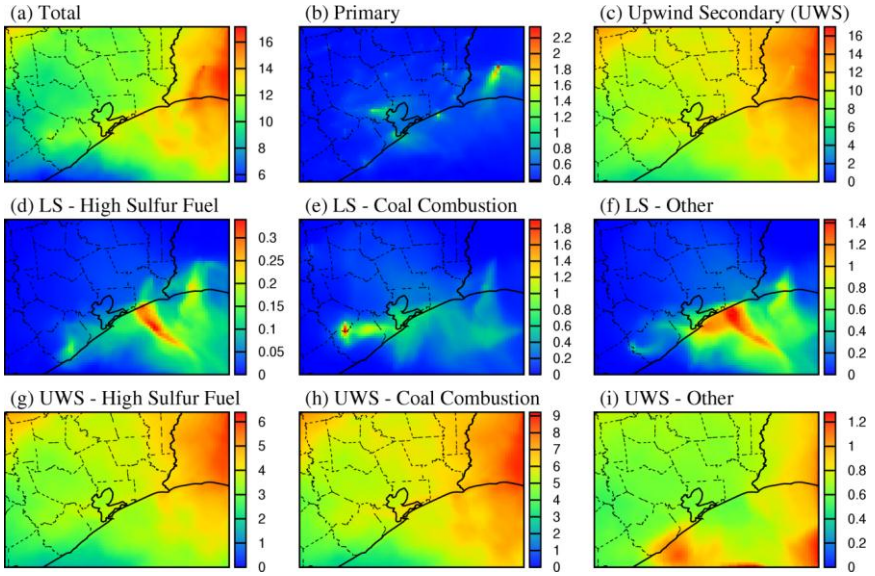

Figure 3-10. Source apportionment of $PM_{2.5}$ sulfate concentrations on September 5, 2000. Units are μgm^{-3}.

The low contributions from local SO_2 sources are expected since the reaction rate of SO_2 with hydroxyl radical (OH) is relatively slow as discussed in Buzcu et al. [10]. The half life of SO_2 assuming a day time average OH concentration of 6 ×106 molecules cm-3 is on the order of 50 hours at room temperature. Using a typical SO_2 concentration of 5 ppb and a reaction time of 10 hours, it can be shown that only 1.5 μgm^{-3} sulfate can be formed. Thus, most of the sulfate observed in the HGB area should be from non-local sources. This analysis agrees with the more detailed model calculations shown in Figure 3-10. It should be noted that the model calculation in this paper does not consider the potential heterogeneous pathways, which may lead to higher local source contributions. However, regional emissions control is necessary to significantly reduce the sulfate contributions in HGB and BPA areas.

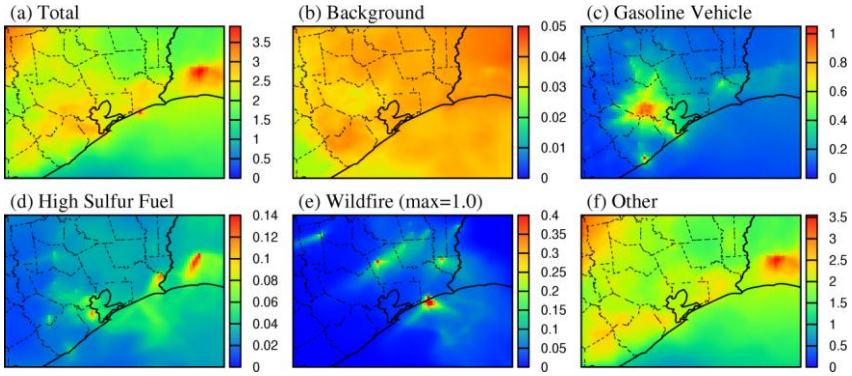

Figure 3-11. Source apportionment of $PM_{2.5}$ ammonium ion concentrations on September 5, 2000. The scale on each panel is different. Units are µg m^{-3}.

Figure 3-11 shows the regional distribution of 24-hour averaged $PM_{2.5}$ ammonium ion concentrations and the major contributing sources on September 5, 2000. Since the PM emission profiles used in the emission processing do not include ammonium ion, the ammonium ion shown in Figure 3-11 is entirely secondary. The maximum 24-hour average $PM_{2.5}$ ammonium ion concentration is approximately 4 µgm^{-3}. Figure 3-11(b) shows an almost uniform regional background ammonium ion concentration of 0.05 µgm^{-3}.This regional background is due to the condensation of ammonia that enters the model simulation through the boundary condition specified for the 36 km parent domain. Figure 3-11(c) shows that the contribution of gasoline engines to ammonium ion is mostly located in urban areas with a maximum value of 1.1µgm^{-3}. Most of the ammonia emissions are from catalyst-equipped light-duty gasoline vehicles [107]. Contributions to ammonium ion due to diesel engines are small and not shown here. Contributions from oil/gas production and high sulfur fuel are generally small. The combined contributions from the two sources are approximately 0.14 µgm^{-3} as shown in Figure 3-11(d).Contribution from wildfires could reach a maximum value of

approximately 1 μgm^{-3} in the vicinity of the fire. Majority of the ammonium ion is from "other" sources category and is mainly due to gas-to-particle partitioning of ammonia emitted from agriculture sources, such as dairy operations and fertilizer applications.

3.5 Conclusions

The nested version of the source-oriented UCD/CIT model was used to simulate the source contributions to primary and secondary inorganic PM during the TexAQS 2000 in the HGB and BPA areas. The predicted concentrations of EC, OC, sulfate, ammonium ion and primary $PM_{2.5}$ mass generally agree with the filter-based observations as well as AMS analysis. Predicted source contributions to primary OC and $PM_{2.5}$ mass are also compared with a CMB model calculation. The UCD/CIT model, based on current emission inventory, shows PM emissions from sources other than diesel/gasoline vehicles and wood burning account for a significant fraction of primary OC and $PM_{2.5}$. Significant emissions of OC and $PM_{2.5}$ are from industrial sources and road construction based on the emission inventory data. This is not in agreement with the CMB results and implies that further investigations on the industrial and other PM emissions are necessary.

The UCD/CIT model predicts that EC was mainly from diesel engines. Majority of the primary OC was from internal combustion engines (diesel and gasoline engines) and industrial sources. Open burning was found to contribute large fractions of EC, OC and primary $PM_{2.5}$ mass in the HGB and BPA areas. Road dust, internal combustion engine sand industrial sources were the major sources of primary $PM_{2.5}$. Wildfire dominated the contributions to all primary PM components and mass in areas near the

fires. Secondary ammonium sulfate accounted for majority of the secondary inorganic PM. Over 80% of the secondary sulfate in the 4 km domain was produced in upwind areas. Coal combustion is largest source of sulfate. Ammonium ion was mainly agriculture sources and contributions from gasoline vehicles are predicted to be significant in urban areas.

4. SECONDARY ORGANIC AEROSOL FORMATION AND SOURCE APPORTIONMENT*

The latest version of US EPA's Community Multi-scale Air Quality (CMAQ v4.7) model with the most recent update on secondary organic aerosol (SOA) formation pathways was adapted into a source-oriented modeling framework to determine the contributions of different emission sources to SOA concentrations from a carbon source perspective in Southeast Texas during the 2000 Texas Air Quality Study (TexAQS 2000) from August 25 to September 5, 2000.A comparison of the VOC and SOA predictions with observations shows that anthropogenic emissions of long chain alkanes and aromatics are likely underestimated in the EPA's Clean Air Interstate Rule (CAIR) inventory and the current SOA mechanism in CMAQ still under-predicts SOA. The SOA peak values can be better predicted when the emissions are adjusted by a factor of 2 based on the observation to prediction ratios of SOA precursors. A linear correlation between SOA and odd oxygen ($\Delta SOA/\Delta O_x$=23.0 μgm^{-3}/ppm O_x, r^2=0.674) can be found when they are formed simultaneously in the air masses passing the urban Houston on high SOA days. As a sensitivity run, the overall SOA can be more accurately predicted by increasing the emissions of the anthropogenic SOA precursors by a factor of 5.

Based on the adjusted emissions, approximately 20% of the total SOA in the Houston-Galveston Bay area is due to anthropogenic sources. Solvent utilization and

---

* Reproduced with permission from Zhang, H.; Ying, Q., Secondary Organic Aerosol Formation and Source Apportionment in Southeast Texas. *Atmospheric Environment* **2011,** *45*(19), 3217-3227. Copyright 2011 Elsevier Ltd.

gasoline engines are the main anthropogenic sources. SOA from alkanes and aromatics accounts for approximately 23-4% and 5-9% of total SOA, respectively. The predicted overall anthropogenic SOA concentrations are not sensitive to the half-life time used to calculate the conversion rate of semi-volatile organic compounds to non-volatile oligomers in the particle phase. The main precursors of biogenic SOA are sesquiterpenes, which contribute to approximately 12-35% of total SOA. Monoterpenes contribute to 3-14% and isoprene accounts for approximately 6-9% of the total SOA. Oligomers from biogenic SOA account for approximately 30-58% of the total SOA, indicating that long range transport is an important source of SOA in this region.

4.1 Introduction

Secondary Organic Aerosol (SOA) is an important group of chemical components of the airborne particulate matter (PM) in the atmosphere that significantly affects regional air quality, global climate and human health [4-6]. SOA can be formed from both anthropogenic and biogenic precursor volatile organic compounds (VOCs). On global and continental scales, biogenic emissions are estimated to contribute much more significantly than anthropogenic sources to the overall SOA [20, 21]. Most of the SOA formed from biogenic sources are believed due to isoprene [22, 23] and monoterpenes emissions [24, 25] because of their high emission rates from various vegetated surfaces. More recent studies also indicate that sesquiterpenes, whose emission rate is only 10-20% of that of monoterpenes, could also be significant contributors to the SOA budget in the atmosphere due to their high aerosol formation potentials [108-110]. On regional and urban scales, however, anthropogenic sources are

believed to account for a significant fraction of the SOA [29, 111]. Most of the anthropogenic SOA is formed from the oxidation of higher alkanes and aromatic compounds [28-30, 111].

The Southeast Texas area in the United States is a place where both biogenic and anthropogenic VOC emissions are significant and thus a unique place to study SOA formation. A large amount of petroleum related industrial facilities around the Houston-Galveston-Brazoria (HGB) and Beaumont-Port-Arthur (BPA) areas emit significant amounts of highly reactive VOCs [112]. These industrial plumes often mix with the emissions from internal combustion engines using fossil fuel in urban areas. The urban and industrial areas are surrounded in three directions by large amounts of vegetation covered rural areas where biogenic emissions become the dominant source of VOCs [113]. This mixture of industrial and urban anthropogenic emissions and rural biogenic emissions provides a unique precursor pool for SOA formation.

Several studies have been conducted to characterize the SOA concentrations and formation pathways in Southeast Texas. Vizuete et al. [114] calculated the emission rates of isoprene, monoterpenes and sesquiterpenes in the HGB area and estimated that the formation flux of biogenic SOA in the central Houston area is in the range of 0.46-4.5 kgC km^{-2} day^{-1} . Dechapanya et al. [18] studied the SOA formation due to precursor emissions from anthropogenic sources in the HGB area using the estimated emission rates of 100 explicit potential SOA precursors in the HGB area and their corresponding aerosol yields based on chamber experiments. It was estimated that although industrial sources account for only 16% of the total VOCs emitted from anthropogenic sources,

they contribute to approximately 53% of the projected anthropogenic SOA in this region. However, neither study performed detailed chemical transport modeling to estimate the actual concentrations of SOA in the atmosphere. Russell and Allen [115] developed a modified SAPRC99 photochemical mechanism to treat the SOA formation from several monoterpene species and three lumped aromatic groups in a regional air quality model and determined that monoterpenes and aromatics are responsible in rural and industrial/urban areas, respectively. Primary organic aerosol concentrations in the domain were not predicted but estimated by spatially interpolating the measured concentrations and no other SOA formation pathways were included. In a more recent study, Bahreini et al. [116] measured the organic aerosol concentrations downwind of the urban and industrial areas in Houston in summer 2006. Their box model simulation results of the SOA formation processes suggest that there is no significant biogenic SOA in the Houston area. However, simple box model simulations may not be able to realistically account for the SOA or precursors transported into the area and thus lead to potential biases. Although these studies improved the understanding of SOA formation, detailed 3D simulations of SOA concentrations are necessary to better quantify the regional distributions of SOA and the contributions of different anthropogenic and biogenic emission sources in this area.

This study reports detailed SOA predictions in Southeast Texas using a revised Community Multi-scale Air Quality (CMAQ) model with the most recent updates on SOA formation pathways. Sensitivities of SOA predictions to some parameters in several new SOA pathways are studied. The timescale of SOA formation in this area

under different meteorology conditions are evaluated through the correlation between SOA and O_x ($=O_3+NO_2$). The CMAQ model was modified in this study to include a source-oriented framework of SAPRC99 photochemical mechanism and a source-oriented SOA module to directly track the regional formation of SOA from different sources. The term "source-oriented" means the capability to resolve the contributions of different sources directly in 3D chemical transport models [82]. It is used to contrast with the receptor-oriented models, which are also used for source apportionment purposes based on solving the algebra equations that relate the ambient measurements, source profiles and source contributions [37]. Contributions from seven sources: biogenic, diesel engines, highway gasoline vehicles, off-highway gasoline engines, solvent utilization, industries and wildfire to SOA in Southeast Texas are quantified in this study.

4.2 Methodology

4.2.1 SOA formation in CMAQ v4.7

The EPA's CMAQ model version 4.7 (CMAQ v4.7) was used as a base model for SOA predictions. This most recent update of the CMAQ model includes the fifth generation aerosol module (AERO5) with more SOA formation pathways and updated thermal dynamic parameters based on recent experimental studies. A detailed description of the CMAQ v4.7 secondary organic aerosol mechanism can be found in Carlton et al. [57] and the references therein so only a brief summary is provided below. A complete list of the SAPRC99 species can be found in Carter [75].

In AERO5, SOA can be formed from seven precursor VOCs species: long chain alkanes (ALK5), high yield aromatics (ARO1), low yield aromatics (ARO2), benzene (BENZ), isoprene (ISOP), monoterpenes (TRP1) and sesquiterpenes (SESQ). The semi-volatile organic compounds (SVOCs) produced from the oxidation of these precursor species are represented by the semi-empirical two-product model proposed by Odum et al. [49]. SOA formation from olefins is not included in current version of the CMAQ model mainly because the SOA yields for olefins are small at all possible ranges of the primary organic aerosol concentrations based on the data used in Strader et al. [117] (Prakash Bhave, personal communication, 2010). Gas/particle distribution of the semi-volatile products is simulated using the equilibrium absorption partition theory of Pankow et al. [118].

The sesquiterpenes pathway is a new addition to the CMAQ model. The emission rate of sesquiterpenes is highly temperature dependent and generally increases exponentially as temperature increases [108, 119]. To calculate sesquiterpenes emissions under a given ambient temperature, a scaling factor is used to adjust the emission rate from a reference temperature to the ambient temperature, as shown in Equation (E4-1):

$$\frac{E_T}{E_{Ts}} = \exp\left[\beta_{SQT}(T - T_s)\right] \quad \text{(E4-1)}$$

where ETs is the emission rate at the reference temperature Ts and ET is the emission rate at ambient temperature T, and β_{SQT} is the temperature dependence parameter. In this study, the sensitivity of the predicted SOA from sesquiterpenes to the temperature dependence parameter is investigated and reported in Section 4.5.

The absorption/partitioning SOA formation pathway is also enhanced by a simplified representation of oligomerization of the condensed particle phase SVOCs, following the treatment of Sakulyanontvittaya et al. [110], which specifies a uniform half-life of 20 hours for all condensed SVOCs. The sensitivity of the model predictions of total SOA and source contributions to the oligomerization time scale is investigated in Section 4.4.5. In addition to oligomerization, non-volatile products from aromatic peroxy radicals with HO_2 under low NO_x conditions [30] and isoprene oxidation products on acidic particles [120] are also simulated. These non-volatile products are assumed not to further react to form oligomers. CMAQ uses a modal representation of particle size distributions and SOA is assumed to form in significant quantities in the fine particle mode only.

4.2.2 Source apportionment of SOA

The gas phase SAPRC99 photochemical mechanism and the SOA module were modified to include a source-oriented treatment of the SOA formation processes. Source-oriented modeling framework has been previously applied in several versions of the UCD/CIT model for the source apportionment of secondary inorganic aerosol (based on a revised SAPRC90 gas phase photochemical mechanism) [45, 121] and secondary organic aerosol (based on the CACM mechanism) [29, 111] as well as primary PM [84]. In a recent study, the source oriented approach is extended to determine the source contributions of VOCs to ozone formation in Southeast Texas [36]. The source-oriented technique introduces additional chemical species to represent the contributions from different sources. A brief explanation of this method is included in the following.

Emissions from different sources are tracked independently through a model simulation of transport, emission, gas phase chemistry, gas/particle partitioning and dry/wet deposition processes. For example, if the superscript X represents VOC emissions from an explicit source X (for example, gasoline engines) and the superscript O represents emissions from all other sources, then the gas phase reaction of ALK5 with OH in the original SAPRC99 mechanism can be expanded into two reactions:

$$\begin{aligned} ALK5^{X} + HO &\rightarrow 0.653RO2\_R + ... + ALK5RXN^{X} \\ ALK5^{O} + HO &\rightarrow 0.653RO2\_R + ... + ALK5RXN^{O} \end{aligned} \quad \text{(R4-1)}$$

where RO2_R is a peroxy radical operator representing NO consumption with organic nitrate formation and ALK5RXN is a counter species to keep track of how much ALK5 is reacted during a model time step. To simplify the text, most of the other products of the actual reaction are not shown. By tracking the ALK5 and ALK5RXN from different sources separately, the amount of SVOCs produced by ALK5 from sources X and O can be determined explicitly:

$$\begin{aligned} \Delta SV\_ALK^{X} &= \alpha_{ALK5} ALK5RXN^{X} \\ \Delta SV\_ALK^{O} &= \alpha_{ALK5} ALK5RXN^{O} \end{aligned} \quad \text{(R4-2)}$$

where ΔSV_ALK is the increase of SVOCs produced from the oxidation of ALK5 at the current time step and αALK5 is the mass based SVOCs yield for ALK5. Subsequently, the amount of aerosol products from each source is determined by the absorption partitioning theory.

The above discussion illustrates a method to track the SVOCs and SOA from an explicit source (X) with emissions from other sources lumped into a single “other” group

(O). Theoretically, it is possible to expand the reactions so that emissions from more than one explicit source can be directly tracked in a single model simulation. The current study chooses to resolve one explicit source at a time. A more detailed discussion of the source apportionment method can be found in Ying and Krishnan [36].

This source apportionment technique is only based on tracking the carbon sources of the precursor VOCs that form SOA. It does not account for the indirect contributions to SOA formation from co-emitted pollutants such as NO_x and primary organic aerosol (POA). For example, in rural areas where biogenic SOA formation is limited by NOx, predicted SOA concentrations are enhanced by increased level of anthropogenic NOx emissions [122]. However, this indirect contribution of anthropogenic emissions to SOA is not included in the current estimation of the anthropogenic source contributions based on the origin of the carbon atoms, leading to an underestimation the overall contribution of anthropogenic sources. Future source apportionment technique should be developed to account for these indirect effects.

4.3 Model application

The CMAQ model with the source-oriented SAPRC99/AERO5 extension is applied to study SOA formation during the 2000 Texas Air Quality Study (TexAQS 2000) episode, from August 25 to September 5, 2000 using a three-level nested domain. Detailed model setup and preparation of emission and meteorology inputs are described in Ying and Krishnan [36] and are briefly summarized below. The coarse domain is for the eastern United States with 36-km horizontal resolution. The 12-km and 4-km resolution nested domains cover the east part of Texas and its surrounding states, and the

HGB and BPA areas in Southeast Texas, respectively. Figure 4-1 shows the Southeast Texas model domain and the location of the seven monitoring stations with 24-hour average organic aerosol concentration measurements during the TexAQS 2000 episode. ▲, ■ and ● symbols represent suburban, urban and industrial sites. La Porte (LAPT) is the site with AMS measurements. Stations with daily VOC measurements are C35C and LAPT. Stations with daily VOC measurements include HALC, CNVW, BAYP, DRPK, GALC and other stations shown in * symbols without labels. In all the three domains, the vertical extent of the model is divided into 14 layers, reaching 21000 m above the surface. The first layer thickness is 42 m. Meteorology inputs needed to drive the CMAQ model are generated by the Meteorology-Chemistry Interface Processor (MCIP) using the output from an MM5 mesoscale meteorology simulation provided by the Texas Commission of Environmental Quality (TCEQ).

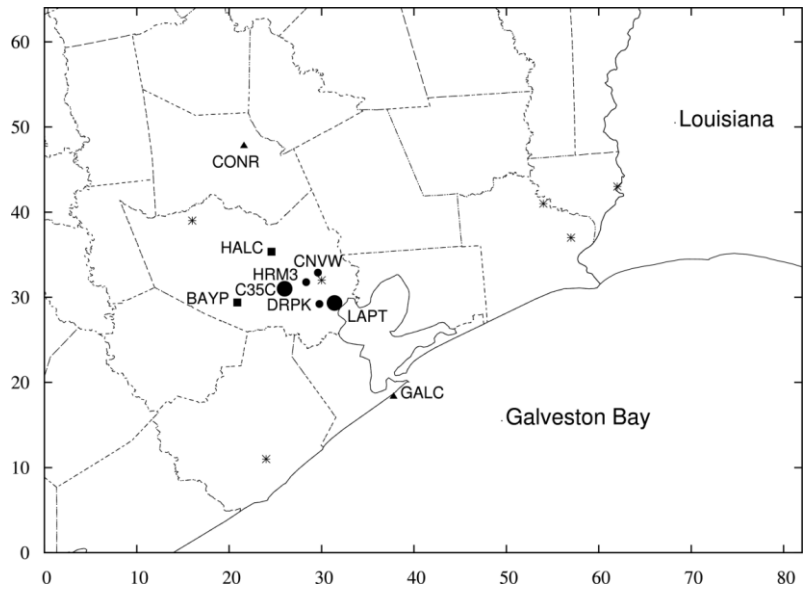

Figure 4-1. The Southeast Texas model domain and the location of stations with 24-hour average organic aerosol measurements during TexAQS 2000.

EPA's 2001 Clean Air Interstate Rule (CAIR) emission inventory is used to generate emission inputs for the TexAQS 2000 episode. Alkenes emissions from industrial sources are increased by a factor of 5 to account for the potential missing high reactive VOCs from these sources [36]. A revised Sparse Matrix Operator Kernel Emissions (SMOKE) emission processing model (version 2.5) from US EPA is used to process the raw emission inventory to generate emissions of gases and PM for each source category. Biogenic emissions are generated using the Biogenic Emissions Inventory System, Version 3 (BEIS3), which includes a 1-km resolution land cover database with 230 different cover types [91]. Most of the emissions are grouped into seven major explicit source categories and the remaining VOC sources are lumped into the "other" source category. VOC speciation profiles used to split total VOC emissions into SAPRC99 model species are based on the SPECIATE 3.2 database (http://www.epa.gov/ttnchie1/software/speciate/speciate32.html) and processed using the emission preprocessor program provided by Dr. William P.L. Carter [123] for application in the SMOKE model. The SCC code to speciation profile mapping is based on the reference file provided by the EPA's 2001 modeling platform (available at ftp://ftp.epa.gov/EmisInventory/2001nmp/). Table 4-1 summarizes the daily emission rates of the SAPRC99 SOA precursor species in the 4-km domain for August 31, 2000.

Table 4-1. Emission rates of gas phase SOA precursor species from each source on August 31, 2000 in the 4-km Southeast Texas model domain. (Units: kmol day^{-1})

Source Types	Gas Phase Precursor Species*							
	ALK5	**ARO1**	**ARO2**	**BENZ**	**ISOP**	**TRP1**	**SESQ**	**Total**
Diesel	40.49	0.00	0.00	0.00	0.00	0.00	0.00	40.49
Highway gasoline	129.20	265.62	199.93	102.57	3.59	0.21	0.00	701.11
Off-highway gasoline	180.64	115.74	187.93	27.46	1.60	3.62	0.00	516.98
Solvent utilization	802.68	211.77	66.50	10.39	0.81	0.05	0.00	1092.21
Industries	336.36	103.03	110.02	107.5	0.31	59.46	0.00	716.67
Other anthropogenic	212.76	71.31	56.62	54.91	5.73	7.49	0.00	408.82
Biogenic	0.00	0.00	0.00	0.00	29943.86	5029.57	807.19	35780.61
Wildfire	199.26	28.85	32.73	0.00	0.00	17.32	0.00	278.16
Total	1702.14	767.47	621.00	302.82	29955.89	5100.40	807.19	39256.90

*See Section 4.2.1 for the detailed description of the precursor species.

4.4 Results and discussion

Evaluation of the predicted gas phase pollutant concentrations against observations is described in greater detail in Ying and Krishnan [36]. In summary, the predicted daily maximum 8-hour ozone concentrations at all surface stations within the 4-km domain are generally within ±20% of the observed concentrations. Concentrations of other gaseous pollutants are also in good agreement with observations but alkanes and aromatics concentrations are under-predicted.

4.4.1 Adjustment of VOC emissions

An Aerodyne Aerosol Mass Spectrometer (AMS) was deployed at La Porte (LAPT, as shown in Figure 4-1) during TexAQS 2000 [103]. The reported 1-hour average OOA (oxygenated organic aerosol) concentrations based on PMF analysis of the aerosol mass spectra, are compared with model predicted 1-hour average SOA concentrations as shown in Figure 4-2. Although the OOA is not equivalent to SOA, it is

generally interpreted as a surrogate for SOA [104]. The base case SOA generally captures the long term variation of the OOA concentrations but fails to predict the daily peak OOA concentrations. Over-prediction of SOA mostly occurs on several nighttime hours with significant regional transport (e.g. August 31 and September 4). A comparison of the predicted and observed wind speed and direction at LAPT shows that the observed wind is usually from the west. The predicted wind directions agree well with the observations but the predicted wind speed is significantly lower. Thus, the over-prediction in the SOA could be caused by slower wind speed that is not fast enough to bring in the low SOA air from the west boundary. The mean fractional error ($mfe = \frac{2}{N}\sum_{i=1}^{N}\left|P_i - O_i\right| / \left(P_i + O_i\right)$, where Pi and Oi denote the ith prediction and observation, respectively, and N is the number of data points) of hourly SOA at LAPT is 0.60.

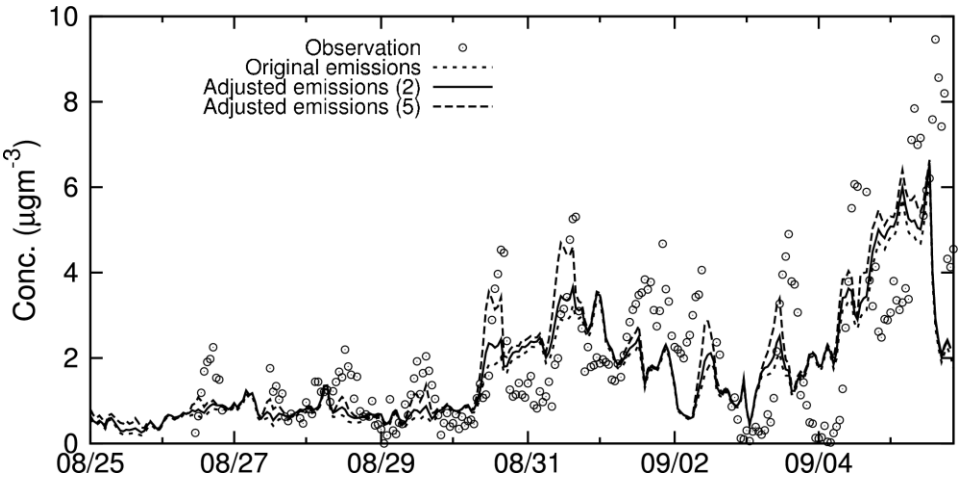

Figure 4-2. Predicted SOA concentrations at La Porte (LAPT) using the original and adjusted emissions and the observed OOA concentrations from AMS.

Underestimation of modeled SOA was reported in many previous studies. Volkamer et al. [124] compared zero-dimensional model predictions of SOA with OOA concentrations in Mexico City and found that the predicted SOA concentrations were a factor of 4-8 lower than the observations. Chen et al. [125] reported that overall organic aerosol from an SOA module coupled with the CACM mechanism was under-predicted by a factor of 2-8 in the east US. Matsui et al. [58] showed that the predicted SOA concentrations in the metropolitan areas of Tokyo were a factor of 5 lower than the observed OOA concentrations and the differences could be reduced if emissions from anthropogenic emissions were increased.

Several possible factors can contribute to the underestimation of SOA concentrations. Firstly, not all possible SOA formation pathways are included in the current AERO5 aerosol module, such as SOA from the oxidation of alkenes and polycyclic aromatic hydrocarbons (PAHs). The importance of these pathways to ambient SOA formation is still under investigation. Matsui et al. [58] showed that SOA from alkenes and PAHs only accounted for a very small fraction of the overall SOA in the metropolitan areas of Tokyo. However, Chan et al. [47] found that the SOA yield of PAHs may be higher than previously estimated and could potentially be a significant contributor to atmospheric SOA. In this study, a separate sensitivity run was conducted by implementing the olefin SOA formation mechanism from a previous version of CMAQ (v4.6) [126]. The maximum of the 1-hour average SOA from this pathway is approximately 0.003 μg m-3 and thus it is not included in this study. The importance of

the PAH pathway is not evaluated in this study due to lack of proper emission data for PAHs.

Secondly, the mechanisms of additional SOA formation in the aerosol-phase [52-54] and aqueous-phase [55, 56] are not well understood and could be another source of under-prediction. In the current study, SOA production within the aqueous phase is not considered although CMAQ v4.7 does include an updated treatment of aqueous SOA production from glyoxal and methylglyoxal. A sensitivity simulation using the non-source-oriented CMAQ v4.7 with aqueous SOA production shows that the maximum increase in the 1-hour average SOA in all model layers during the entire modeling episode is less than 0.01 μgm^{-3}. Thus, the in-cloud SOA production process is omitted from the source-oriented model calculations.

Thirdly, previous studies clearly demonstrated that VOC emissions were under-represented in Southeast Texas. A comparison of the VOCs/NOx ratio data from the emission inventory with the ambient data collected during 2000 and 2001 in Houston area showed that total VOC emissions were underrepresented in the emissions inventory by a factor of 2-10 and aromatics and alkanes were underrepresented by a factor of 2-5 and 3-8 at most of the study sites [127]. Buzcu and Fraser [10]compared the VOC source apportionment results based on PMF analysis and the emission inventory data and found that alkanes emissions were underestimated by a factor of 2-3 from industrial sources.

Simulation results from this study also support the conclusion that VOCs emissions were underestimated. Figure 4-3 shows the ratio of observed and predicted 24-hour average (at 12 stations) and hourly (at LAPT and C35C) concentrations (O/P ratio)

of alkanes and aromatic precursor species for the original emissions (panel a), a factor of 2 increase (panel b) and a factor of 5 increase (panel c) of the precursor emissions. The left and right part of each panel is for 24-hour average data and hourly data, respectively. The box shows the 25^{th} and 75^{th} percentile, the bar in the box shows the median and the whiskers show the minimum and maximum of the data. The dots in the plot show the average O/P ratios where observed concentrations are larger than the median concentration. The upper limit O/P ratios that exceed the scale are shown in the panels. The speciated VOC observation data were from the AIRS database of US EPA and grouped into SAPRC99 model species. The O/P ratios generally range between 1 and 5 with median values around 2 with the original emission rates. For the data points with the observed concentrations higher than the median concentration, the average O/P ratios are higher. Median O/P ratios based on the hourly data at C35C and LAPT are approximately 2 for all the hours and are more close to 5 for the hours when concentrations are higher than the median value.

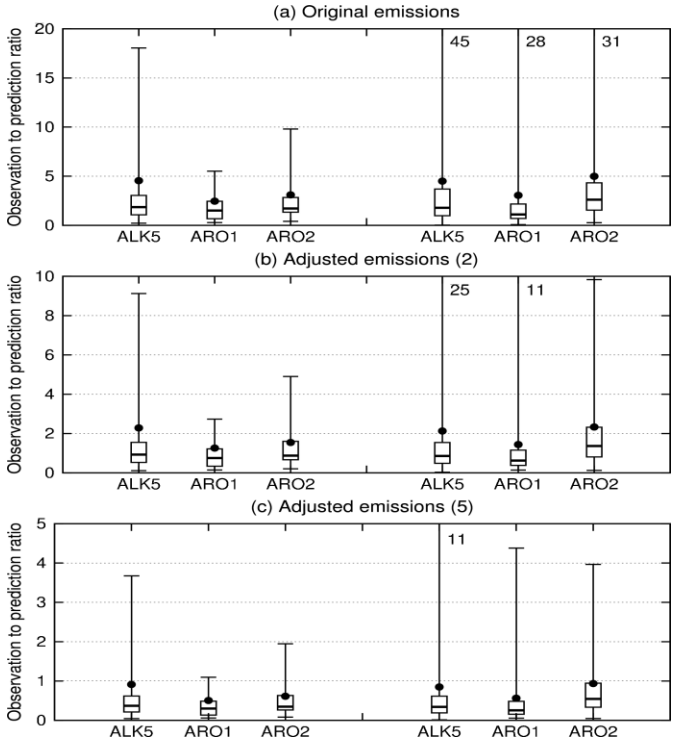

Figure 4-3. Box-whisker plot of O/P ratios for ALK5, ARO1 and ARO2 during the simulation episode for the original and adjusted emissions.

Although the predicted O/P ratios are more close to 1 when the emissions are doubled than when the emissions are increased by a factor of 5, as seen in Figure 4-2, the predicted SOA at LAPT is more close to the observed OOA peaks when the emissions are increased by a factor of 5 on most of the days in August and on September 2-3 (Figure 4-2). The MFE for the two sensitivity simulations are 0.58 and 0.52, respectively. No significant increase of the total SOA is predicted for September 4-5 and the predictions are still significantly lower than the AMS OOA results. Increasing the alkanes and aromatics emissions also generally improves the predicted peak ozone concentrations on high ozone days and does not significantly change the predictions on

most of the remaining days. This result indirectly supports our assessment of the potential VOC underestimation in the emission inventory.

As the O/P ratio data suggests, the actual bias in the emission varies among different species and is also space and time dependent. In the following sections, the results from the simulation with a uniform emission scaling factor of 2 were used to evaluate the regional SOA prediction and assess the relative contributions of anthropogenic and biogenic sources in Southeast Texas. Since the factor of 2 still under-predicts the SOA peak concentrations, a sensitivity case that uses a scaling factor of 5 is also conducted. It does not mean that the emissions are actually uniformly under-represented in the emission inventory by a factor of 5. Instead, this emission adjustment should be considered as an empirical approach to account for the missing SOA precursors and pathways of SOA formation as well as errors in the SOA model parameters in the CMAQ v4.7 code.

4.4.2 Predicted vs. observed organic aerosol (OA)

During the simulated TexAQS 2000 episode, 24-hour average organic carbon (OC) mass concentrations were measured daily at seven monitoring sites (Figure 4-1). The Houston Deer Park (DRPK), Haden Road (HRM3), Channelview (CNVW) and La Porte (LAPT) sites are under significant influence from the industrial emissions in the Houston Ship Channel. The Houston Aldine (HALC) and Bayland Park (BAYP) sites are urban sites within commercial/residential surroundings. The Conroe (CONR) site is a suburban site and the Galveston Airport (GALC) site is also a suburban site on the Gulf Coast.

Figure 4-4 shows the time series of the observed and predicted 24-hour average organic aerosol (OA) mass at the monitoring sites. A factor of 1.4 was used to convert observed OC to OA. The predicted OA mass concentration based on adjusted emissions is split into POA and SOA. The lines on the plot show that OA predictions based on the original emissions are only slightly lower than the predictions based on the adjusted emissions. This is because the adjusted emissions mostly affect SOA concentrations at the peak hours on a few days (for example, see Figure 4-2) and only a fraction of the total OA is SOA. The OA concentrations are generally the lowest in the coastal site (GALC). At the suburban inland site CONR, POA concentrations are lower than the urban/industrial sites but the SOA concentrations are higher. The model successfully reproduced the day-to-day variation of the observed OA concentrations at all stations. In general, OA decreases during August 25-30 and increases significantly on September 3-5. This is mainly due to a substantial increase in the SOA concentrations. Analysis of the wind field shows significant north-to-south transport on September 4-5, when the OA concentrations are highest at all stations. The model under-predicts the concentrations at most stations by 2-4 μgm^{-3}. Since there are no major anthropogenic SOA sources in the near upwind direction and there lacks a strong correlation between SOA and ozone (see Section 4.4.3), the under-prediction is likely caused by the underestimation of aged biogenic SOA from upwind.

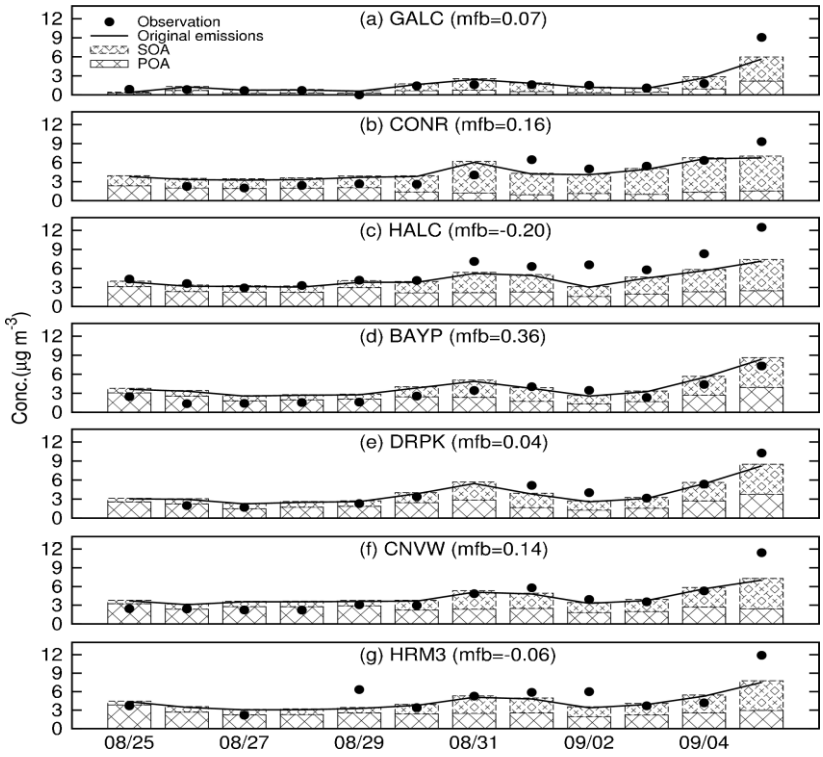

Figure 4-4. Time series of 24-hour average observed $PM_{2.5}$ OA mass (closed dots) and predicted POA and SOA (stacked bar plots) at seven stations. Solid line shows the predicted total OA with the original anthropogenic emissions. Units are μgm^{-3}.

4.4.3 SOA-O_X relationships

Both SOA and O_x are formed as products of VOCs oxidation. It is expected that the SOA and O_x concentrations are correlated if they are formed on similar timescales and at the same location. In fact, a linear correlation between SOA and O_x has been reported previously in both experimental and modeling studies [58, 103, 128]. Since the timescale of O_x is approximately a few hours, a lack of strong correlation between O_x and SOA will usually implies that the timescale of SOA formation is longer and a significant amount of SOA could come from transport over long distances. In addition, since the O_3 formation process is well represented in photochemical models while there

are still significant uncertainties in the SOA predictions, comparing the modeled and observed correlation between SOA and O_x can be a useful method to test whether the SOA mechanism and the inputs to the mechanism capture the overall SOA formation.

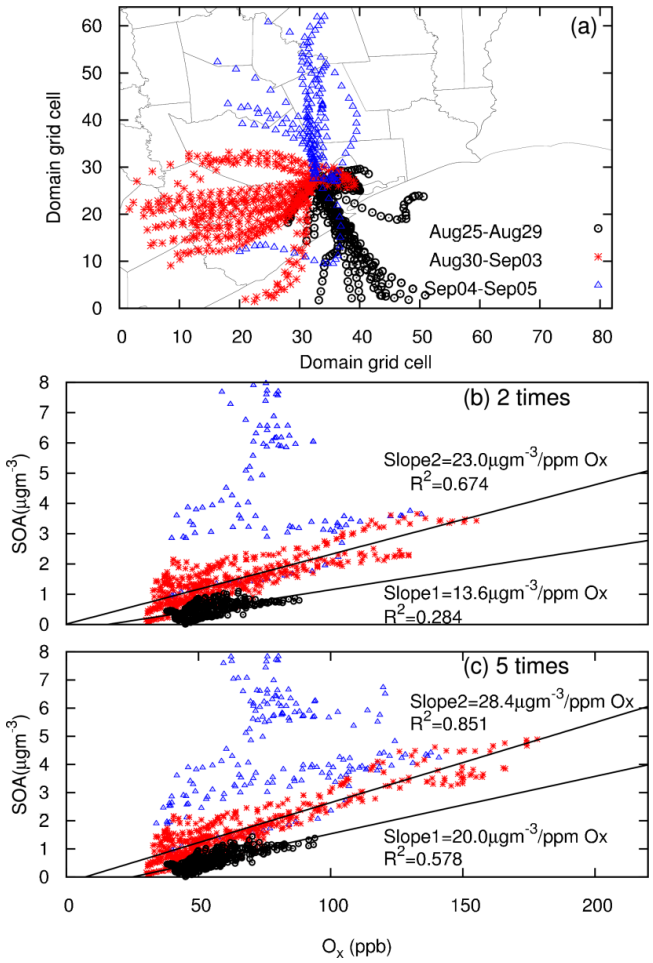

Figure 4-5. Back trajectory analysis of SOA and O_x formation under three meteorology patterns. 8-hour back trajectories on different days (a); Correlations of predicted SOA with Ox along the trajectories when emissions of alkanes and aromatics from anthropogenic sources are increased by a factor of 2 (b) and 5 (c).

In this study, back trajectory analysis is used to examine the histories of the air masses that lead to high SOA concentrations at LAPT. The trajectories are calculated using an in-house back-trajectory program using the MM5 predicted hourly wind fields.

Figure 4-5 shows the positions of the air parcels and the correlations between the SOA and O_x concentrations along the 8-hour back trajectories arriving at LAPT at daily peak SOA hours (1300-1800 CST on August 25-September 3 and 1000-1800 CST on September 4-5).

The areas where the air masses pass through may have important effects on SOA and Ox concentrations. Generally, three trajectory patterns with distinct SOA formation characteristics were found as shown in Figure 4-5(a). From August 25-29, the air masses arriving at LAPT on high SOA hours are from the Gulf of Mexico with low precursor VOCs and NO_x concentrations. SOA and O_x concentrations are generally low but linearly correlated, suggesting that the increases in the SOA and O_x along the trajectories are due to simultaneous local photochemical productions in the air masses. The slope of a linear fit ($\Delta SOA/\Delta O_x$) is 13.6 μgm^{-3} SOA / ppm O_x for adjusted emission case and 20.0 μgm^{-3} SOA / ppm O_x for the sensitivity case.

From August 30 to September 3 (except September 1), the SOA peak concentrations are generally well captured by the model simulation (Figure 4-2). The air masses arriving at LAPT at these hours come from the west, slowly passing through the areas influenced by urban emissions before arriving at LAPT in the afternoon. It indicates that the high SOA concentrations at LAPT are caused by a significant amount of anthropogenic emissions emitted from the upwind Houston urban area. $\Delta SOA/\Delta O_x$ is 28.4 μgm^{-3}/ppm O_x for adjusted emission and 28.4 μgm^{-3}/ppm O_x for the sensitivity case. The sensitivity case is more close to the experimental value of 32 μgm^{-3} OOA/ppm O_x during the same period [103].

On the last two days of the episode (September 4-5), air masses arrive at the Houston area from the northeast, bringing secondary PM pollutants with high concentrations via the north boundary conditions [76]. Predicted SOA concentrations along the trajectories reach approximately 10 μg m-3 but there is no clear linear correlation between SOA and O_x. The SOA is mostly biogenic in nature and is composed of mostly aged SOA products such as non-volatile products and oligomers instead of semi-volatile components.

4.4.4 Source contributions to SOA

Figure 4-6 shows the time series of SOA source apportionment results based on adjusted emissions at LAPT from August 25, to September 5, 2000. SOA produced from anthropogenic sources contributes to 5-20% of total SOA on average. The contributions of anthropogenic SOA are highest during August 30 to September 3, when the westerly wind brings precursors from urban areas. At the peak hours, solvent utilization and industries account for 15% and 5% of total SOA, respectively. Highway gasoline vehicles account for approximately 5-10% and off highway gasoline engines account for approximately 5% of total SOA. Diesel vehicles, wildfire and other sources have minor contributions to SOA. For the sensitivity case, wildfire has approximately 5% contributions on September 4 when wind blows from the wood smoke areas.

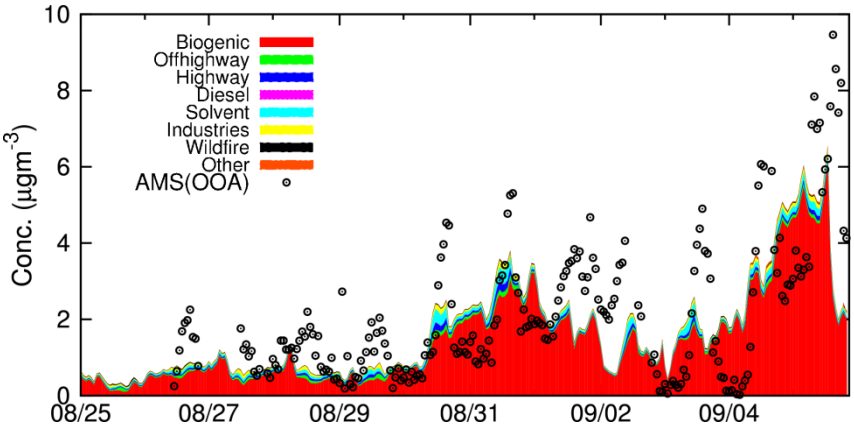

Figure 4-6. Hourly predicted SOA and AMS OOA concentrations at LAPT.

Table 4-2 shows the episode average fractional contributions of different SOA precursors to the predicted SOA concentrations at the four monitoring stations of the adjusted emission case and the sensitivity case. The predicted SOA concentrations are in the range of 1.0-2.7 μgm^{-3}, with the highest concentration at CONR and the lowest at GALC. SOA from sesquiterpenes (ASQTJ) accounts for approximately 12-35% of the total SOA in urban and industrial areas. Monoterpenes (ATRPJ) contribute to 3-14% and isoprene (AISOPJ) contributes to 6-9%. AOLGBJ, non-volatile OA due to oligomerization of biogenic SOA in the condensed phase, contributes to approximately 30-58% of the overall SOA. The contribution of AOLGBJ is higher at GALC where local SOA production is the least significant due to the lack of local precursor sources. SOA from long chain alkanes (AALKJ), low yield aromatics (AXYLJ) and high yield aromatics (ATOLJ) are approximately 2-6% individually while benzene contributes to less than 1% of the total SOA. Non-volatile anthropogenic OA from oligomerization reactions (AOLGAJ) accounts for another 3-8% of total SOA. Overall, SOA from all biogenic sources (BSOA) accounts for more than 80% of total SOA at all sites while

SOA from all anthropogenic sources (ASOA) contributes to approximately 10-20%. The sensitivity case gives higher contributions from anthropogenic sources and lower contributions from biogenic sources.

Table 4-2. SOA concentrations averaged from August 25, 2000 to September 5, 2000 and fractional contributions from different SOA formation pathways to the average SOA concentrations for the adjusted emissions (left of the slash) and the sensitivity case (right of the slash).

	GALC	CONR	BAYP	LAPT
SOA(μg m^{-3})*	**1.15/1.25**	**3.08/3.31**	**1.77/1.95**	**1.69/1.89**
AALKJ	2.1/4.3%	1.7/3.4%	3.4/6.6%	3.1/6.5%
ABNZJ	0.8/0.8%	0.3/0.3%	0.6/0.5%	0.6/0.5%
AXYLJ	3.9/6.0%	2.2/3.7%	3.7/6.4%	3.4/5.6%
ATOLJ	5.5/6.5%	2.6/3.8%	4.3/5.7%	4.3/5.7%
AOLGAJ	7.9/8.1%	3.4/3.7%	5.3/5.3%	5.6/5.8%
ASOA	**20.2/25.7%**	**10.2/14.9%**	**17.3/24.5%**	**17.0/24.1%**
ATRPJ	3.1/3.1%	14.5/14.0%	5.5/5.1%	5.5/5.2%
AISOPJ	6.4/6.0%	9.5/8.9%	7.8/7.2%	7.2/6.6%
ASQTJ	12.3/11.8%	35.5/33.8%	27.6/25.5%	26.0/22.2%
AOLGBJ^	57.9/53.4%	30.328.3%	41.8/37.7%	44.3/39.9%
BSOA	**79.8/74.3%**	**89.8/85.1%**	**82.7/75.5%**	**83.0/75.9%**

* Based on adjusted VOCs emissions

^ The relative contributions of isoprene, monoterpenes and sesquiterpenes to the predicted AOLGBJ in the 4-km domain are approximately 24%, 20% and 55%, based on the average concentrations of AISOPJ, ATRPJ and ASQTJ concentrations in the 12-km domain.

Figure 4-7 shows the regional source contributions to the episode average SOA in the 4-km domain. High SOA concentrations of approximately 3-4 μgm^{-3} occur at the northeast boundary. Concentrations at urban Houston are approximately 1-2 μgm^{-3}. Highway gasoline vehicles and off-highway gasoline engines combined account for a majority of the anthropogenic SOA in the Houston area. SOA from solvent utilization has a highest concentration of 0.12 μgm^{-3} in the Houston downtown area. Industrial sources contribute to approximately 0.1 μgm^{-3} of SOA in the Houston Ship Channel area

and other industrial regions in the domain. Diesel vehicles have only slight contributions to the total SOA due to low emission rates of precursor VOCs. Contributions from other anthropogenic VOC sources can be as high as 0.08 μgm^{-3} near offshore drilling areas. Contributions from wildfires are small and are included in the "other" source category. On average, contributions from anthropogenic VOC emissions to SOA can be as high as 20-24% in the urban and industrial areas, as illustrated in Figure 4-7(i). For the sensitivity case, the contributions from anthropogenic sources are 50%-100% higher than the adjusted emissions case.

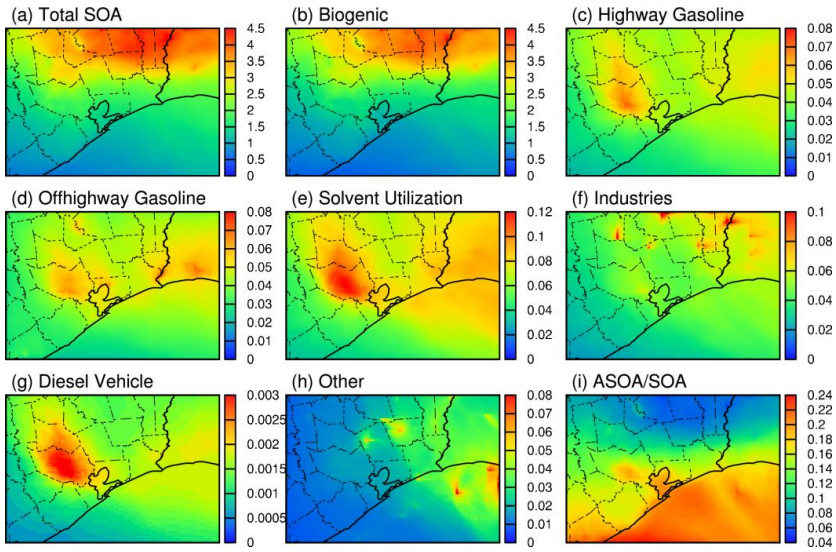

Figure 4-7. Source contributions to 24-hour average SOA during the entire model episode (a-h) and the ratio of ASOA to total SOA (i). Units are μgm^{-3} for (a)-(h).

4.4.5 Sensitivity analysis

In AERO5, oligomerization reactions and oxidation of sesquiterpenes are two new pathways of SOA formation. Table 4-2 shows that products from oligomerization reactions of the semi-volatile components account for a significant fraction of the predicted SOA concentrations. However, modeling the complex oligomerization

processes as a first order reaction is an extremely simplified approach. The sensitivity of the model predictions of oligomers to the choice of the half-life time needs to be studied. In addition, a significant amount of SOA in Southeast Texas is produced from sesquiterpenes (Table 4-2), especially under northerly wind conditions (Figure 4-5). The sensitivity of the predicted sesquiterpene SOA due to uncertainty in the sesquiterpene emission rates also needs to be evaluated.

The default half-life time adopted in the CMAQ model and used in the simulation described in the previous sections is 20 hours. Figure 4-8 shows the change in the predicted concentrations of episode-average AOLGAJ and AOLGBJ as a function of the half-life time at 5 different sites. Figure 4-8(a) shows that the AOLGAJ concentrations throughout the region are not particularly sensitive to the half-life time. Decreasing the half-life time to 5 hours and 1 hour only increases the AOLGAJ concentrations by approximately 0.04 and 0.08 μgm^{-3}, respectively. This is because most of the semi-volatile SOA products from anthropogenic sources are produced within the HGB area and the amount of time they continue to stay in the model domain is small, not allowing much of the anthropogenic SOA to be converted to non-volatile oligomers before being removed through deposition processes or transported to other regions. The AOLGBJ concentrations in the HGB area are more sensitive to the half-life time because a large amount of the biogenic SOA is produced in the upwind areas, especially during the days when north-to-south transport is significant. A shorter half-life will allow more semi-volatile biogenic SOA to be converted into AOLGBJ before reaching the HGB area.

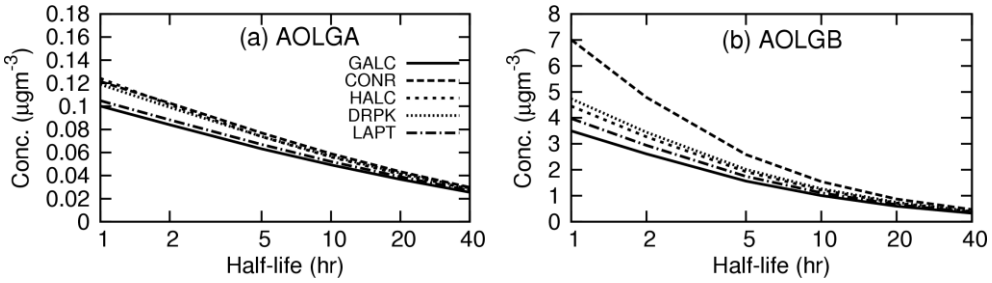

Figure 4-8. Episode average concentrations of oligomers from (a) anthropogenic sources (ALOGAJ) and (b) biogenic sources (ALOGBJ) as a function of the half-life time.

To conclude, the amount of SOA produced through the oligomerization process can vary significantly, based on the half-life time chosen. The half-life time could greatly affect the prediction of the amount of oligomerized biogenic SOA in Southeast Texas. However, oligomerized anthropogenic SOA are not expected to contribute much to the overall SOA under reasonable choices of the half-life time in this area.

Two sources of uncertainty in the sesquiterpenes emission calculation is the base emission rate at the reference temperature E0 and the temperature dependence parameter β_{SQT}. Base on Helmig et al. [119], E_0 varies significantly while β_{SQT} is more consistent among different pine species tested. The current β_{SQT} value for sesquiterpenes used in AERO5 of CMAQ v4.7 is 0.170 $℃^{-1}$ at a reference temperature of 30 ℃. The emission rates of sesquiterpenes almost doubles while the emission rates of monoterpenes only increased by approximately 10-15%.

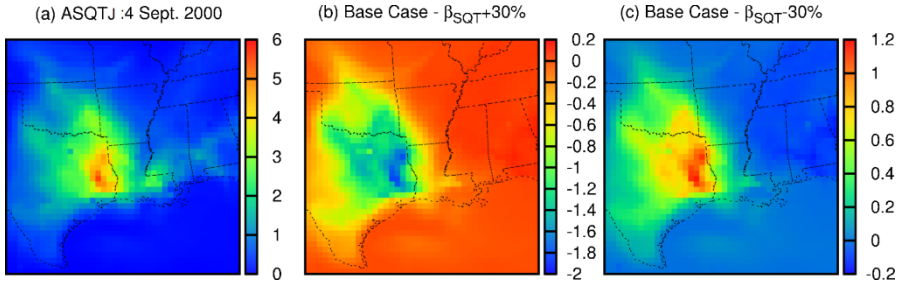

Figure 4-9. Base case (a) and changes ((b) and (c), base case minus sensitivity cases) in the predicted SOA from sesquiterpene oxidation products (ASQTJ) due to ±30% change in the sesquiterpene emission temperature dependence parameter β_{SQT}. Units are µgm^{-3}.

Two simulations were performed to study the sensitivity of the predicted sesquiterpenes emissions and the resultant SOA concentrations to the variations in β_{SQT}. The emission rates of sesquiterpenes in the entire eastern United States due to ±30% change of β_{SQT} from the default value on September 4, 2000, a high SOA day with significant emissions of sesquiterpenes. The ±30% range is based on the reported uncertainty (0.170±0.05) in Helmig et al. [119]. Figure 4-9 shows the difference in the predicted 24-hour average SOA concentrations from sesquiterpenes. Results from the 36-km domain simulation are used to better illustrate the spatial distribution of SOA in the eastern United States. The maximum base case concentration of SOA from sesquiterpenes is approximately 6 µgm^{-3} on September 4, 2000 and is located just to the north of the Houston area. Decreasing β_{SQT} by 30% decreases the maximum concentration by 1.2 µgm^{-3} (20%), while increasing β_{SQT} by 30% significantly increases the sesquiterpenes SOA by 2 µg m^{-3} (33%). Overall, ±30% changes in β_{SQT} lead to 10-15% decrease or 15-25% increase of total SOA. These results suggest that the temperature

dependence parameter could be a significant source of uncertainty in sesquiterpenes SOA predictions.

4.5 Conclusions

Evidence from SOA measurements at LAPT and VOCs measurements at various sites in the HGB area suggests that alkanes and aromatics emissions from anthropogenic sources are underestimated in the current inventory. The predictions for long chain alkanes (ALK5) and aromatics (ARO1 and ARO2) agree better with observations when their emissions are increased by a factor of 2 from all anthropogenic sources. However, the agreement between the observed OOA and the predicted SOA concentrations is improved by increasing the emissions of anthropogenic alkanes and aromatics by a factor of 5, suggesting that the current SOA mechanism in CMAQ still under-predicts SOA concentrations.

Both biogenic and anthropogenic sources are important contributors to the overall SOA concentrations in Southeast Texas. The relative importance of the two source categories depends on the dominant wind directions. Models that do not consider the long range transport of SOA from biogenic sources realistically are likely going to underestimate the contributions from biogenic sources, especially under northerly wind conditions. The newly added formation pathways of SOA from sesquiterpenes and oligomerization are important, and are predicted to account for 12-35% and 34-64% of the total SOA concentrations in Southeast Texas, respectively. When the air masses pass though the urban Houston areas, a strong linear correlation between SOA and O_x

formation is predicted ($\Delta SOA/\Delta O_x$=23.0 μgm^{-3}/ppm O_x; r^2=0.674). Major sources of anthropogenic SOA are solvent utilization and gasoline engines.

5. SECONDARY ORGANIC AEROSOL FROM POLYCYCLIC AROMATIC HYDROCARBONS[*]

Recent chamber studies show that low-volatility gas phase precursors such as polycyclic aromatic hydrocarbons (PAHs) can be a significant source of secondary organic aerosol (SOA). In this work, formation of SOA from the photo-oxidation products of PAHs is added to the SOA modeling framework of the Community Multiscale Air Quality (CMAQ) model to determine the regional distribution of SOA products from PAHs (PAH-SOA) and the contributions from sources in southeast Texas during the Texas Air Quality Study 2006 (TexAQS 2006). Results show that PAHs released from anthropogenic sources can produce SOA mass as much as 10% of that from the traditional light aromatics or approximately 4% of total anthropogenic SOA. In areas under the influence of wild fire emissions, the amount of PAH-SOA can be as much as 50% of the SOA from light aromatics. A source-oriented modeling framework is adopted to determine the major sources of PAH-SOA by tracking the emitted PAHs and their oxidation products in the gas and aerosol phases from different sources separately. Among the eight sources (vehicles, solvent utilization, residential wood, industries, natural gas combustion, coal combustion, wild fire and other sources) that are tracked in the model, wild fire, vehicles, solvent and industries are the major sources of

---

[*] Reproduced with permission from Zhang, H.; Ying, Q., Secondary Organic Aerosol from Polycyclic Aromatic Hydrocarbons in Southeast Texas. *Atmospheric Environment* **2012,** Accepted for publication. Copyright 2012 Elsevier Ltd.

PAH-SOA. Coal and natural gas combustion appear to be less important in terms of their contributions to PAH-SOA.

5.1 Introduction

Organic Aerosol (OA) is an important constituent of atmospheric airborne particulate matter (PM) [129] that contributes to degradation of visibility, negatively affects human health, and influences climate directly by absorbing and reflecting solar radiation and indirectly by affecting cloud formation [4-6]. OA consists of primary organic aerosol (POA), which is directly emitted as PM and secondary organic aerosol (SOA), which is formed from oxidation products of volatile organic compounds (VOCs). Traditional aerosol models generally under-predict SOA due to missing SOA precursors, incomplete SOA formation pathways as well as underestimation of VOC emissions [58, 124, 125, 130, 131].

Polycyclic aromatic hydrocarbon (PAH) species, which are mostly formed from incomplete fuel combustion associated with both anthropogenic and biogenic processes [132, 133], are on the candidate list of missing SOA precursors. Potential large contributions to SOA from PAHs (referred to as PAH-SOA here after) have been proposed based on recent chamber studies [47, 48]. Chan et al. [47] estimate that PAHs can yield 3-5 times more SOA than light aromatic compounds and can account for up to 54% of the total SOA from diesel emissions. In a separate chamber study, Shakya and Griffin [48] report similar SOA yields and estimate that SOA production from oxidation of PAHs emitted from mobile sources in Houston could account for more than 10% of the SOA formed from mobile sources. However, the environmental conditions in

chamber studies are usually different from ambient conditions where multiple precursors and oxidants coexist and usually in much lower concentrations.

Few regional PAH-SOA modeling studies have been reported in the literature. A regional SOA simulation using the Caltech Atmospheric Chemical Mechanism (CACM) [134] in conjunction with an equilibrium partitioning model [135] shows that PAH-SOA can contribute to approximately 4% of total SOA in the South Coast Air Basin in California [29]. The CACM model predicts the semi-volatile products from PAHs using a single lumped PAH species, whose reaction is represented by 1,2-dimethylnaphthalene [134]. The semi-volatile products from the PAH+OH reaction are partitioned into the organic phase based on their estimated saturation vapor pressure. Although it is a more mechanistic treatment of the PAH-SOA formation processes, it has not been strictly evaluated against chamber data. In addition, using 1,2-dimethylnaphthalene to represent the lumped PAH group might not be appropriate in many cases because naphthalene is usually the most abundant gas phase PAH emitted [136-138], which has different SOA yield and OH reaction rate constant than 1,2-dimethylnaphthalene [47]. Regional simulations of PAH-SOA that incorporate data derived from recent chamber experiments have not been performed. No regional PAH-SOA studies have been reported for the Houston-Galveston Bay (HGB) area, which is unique due to its large industrial emissions [139] and strong interactions of biogenic emissions with anthropogenic emissions [36, 131] .

Sources of PAH species are generally well understood. Important sources of PAHs include vehicles, waste incineration, coal combustion, wild fire, and commercial

products usage [140]. This conclusion has been supported by various receptor oriented source apportionment techniques using data collected in various urban areas including the United States [141], the United Kingdom [142] and China [143]. However, contributions of different PAH sources to SOA formation is less well understood. Depending on the saturation vapor pressure, some PAH species reside predominantly in the gas phase (mostly two or three-ring PAHs) while most of the other PAHs are more preferentially partitioned into the aerosol phase. For the PAH species that are emitted as gas phase species, reactivity and SOA yield can be significantly different. Thus, more work is needed to better quantify the potential of PAHs in producing SOA under ambient conditions and to understand the contributions of different PAH sources to SOA formation.

In this study, SOA formation pathways from the photo-oxidation products of PAHs are added to the SOA modeling framework of the Community Multiscale Air Quality (CMAQ) model version 4.7 (CMAQ 4.7) from the United States Environmental Protection Agency (U.S. EPA) to determine the regional distribution of PAH-SOA and their responsible sources in Southeast Texas during the Texas Air Quality Study 2006 (TexAQS 2006).

5.2 Methodology

The condensed gas phase SAPRC07 photochemical mechanism [144] and AERO5 aerosol module of CMAQ 4.7 are modified to include reactions of PAH species with OH and allow their photochemical products to form SOA. A source-oriented version of the mechanism is also developed to determine the contributions to PAH-SOA

from major emission sources of PAHs. Implementation of the SAPRC07 mechanism in the CMAQ model has been described in detailed in a separate manuscript [145]. The implementation of the PAH-SOA formation pathways and the source apportionment technique in the CMAQ model are discussed in detail in the following sections.

5.2.1 Formation pathways of PAH-SOA

Three PAHs (naphthalene, methylnaphthalene, and dimethylnaphthalene) are treated as explicit model species and their gas phase reactions with OH are extracted directly from the detailed explicit SAPRC07 mechanism [146]. In addition, six other 2 and 3-ring PAHs are also treated as explicit species and their gas phase reactions are based on these three explicit species [146]. Emissions of all other gas phase PAHs are lumped into a single model species called PAH2. The reaction rate constant of PAH2 with OH and its gas phase oxidation products follow those of fluorene + OH reaction. Table 5-1 lists the species added to the gas phase reactions and their OH reaction rate constants [147-149].

The standard absorption partitioning theory [118] and the two-product method [49] are used to model SOA from PAH-OH reactions. Figure 5-1 shows the model representation of different pathways of SOA formation from PAH species. For PAH1 group, these species are treated as explicit model species and thus the reaction rate of the species with OH radical is different for each species. However, the semi-volatile products from these species are identical in the current model, as experimental data for species other than naphthalene are limited. As illustrated in Figure 5-1, the semi-volatile organic compounds (SVOCs) from the explicit species are lumped into one set of species

(SV_PAH1_1 and SV_PAH1_2), while the SVOCs from the lumped PAH2 species are represented by a second set of species (SV_PAH2_1 and SV_PAH2_2). The products from explicit PAH species (termed PAH1 species hereafter) are lumped because experimental data on SOA formation from PAH species are very limited. The lumped SVOCs are then partitioned into the organic phase of the fine particle mode to form SOA. It is assumed that, similar to aromatic compounds, non-volatile SOA products (mostly peroxides) form under low NO_x conditions. The NO_x dependence of the SOA products is modeled based on the approach described in Carlton et al. [57].

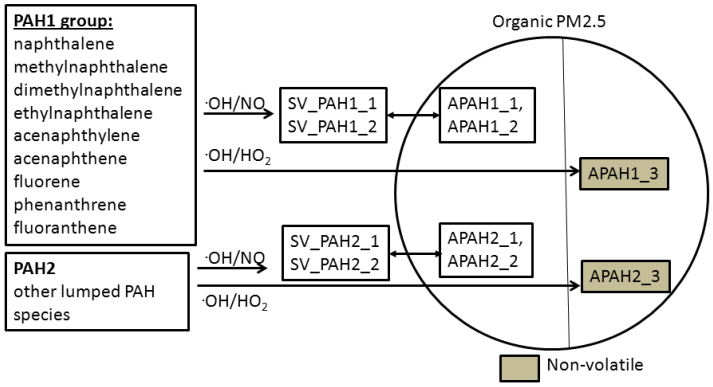

Figure 5-1. Model representation of different pathways of SOA formation from PAH species.

The following reactions illustrate how SOA formation from naphthalene is represented in the model. Reactions (R5-1)-(R5-3) are gas phase reactions and PAH1RO2 is a reaction counter that records how many molecules are reacted with OH to form peroxy radicals in one time step. Reactions (R5-2) and (R5-3) introduce a competition for the peroxy radicals among NO and HO_2. Under high NOx conditions, reaction (R5-2) will be more significant and thus produce more counter species (PAH1NRXN) for semi-volatile products. Under high HO_2 conditions, reaction (R5-3)

will dominate and more non-volatile SOA counter species (PAH1HRXN) will be generated:

$$NAPH + OH \rightarrow ... + PAH1RO2 \quad \text{(R5-1)}$$

$$PAH1RO2 + NO \rightarrow NO + PAH1NRXN,\ k=2.7\times10^{-12}\exp(360/T) \quad \text{(R5-2)}$$

$$PAH1RO2 + HO2 \rightarrow HO2 + PAH1HRXN,\ k=1.9\times10^{-13}\exp(1300/T) \quad \text{(R5-3)}$$

Oxidation products in reaction (R5-1) are not shown. A complete version of reaction (R5-1) can be found in Table 5-1. The reaction rate constants (k) are in units of $cm^3 molecules^{-1}$. The expressions for the rate constants are identical to those used for aromatics species [57]. Temperature (T) is in units of Kelvin. For each explicit PAH species, a gas phase reaction similar to reaction (R5-1) is included in the modified mechanism (See Table 5-1). Three additional reactions are used to represent PAH2 species.

The concentrations of the counter species are passed into the modified aerosol module to calculate the formation of PAH-SOA. Reactions (R5-4.1), (R5-4.2) and (R5-5) show the formation of semi-volatile and non-volatile PAH-SOA based on the counter species:

$$\Delta SV\_PAH1\_1 = \alpha_1 \cdot PAH1NRXN,\ \Delta SV\_PAH1\_2 = \alpha_2 \cdot PAH1NRXN \quad \text{(R5-4.1)}$$

$$SV\_PAH1\_1 \leftrightarrow APAH1\_1,\ SV\_PAH1\_2 \leftrightarrow APAH1\_2 \quad \text{(R5-4.2)}$$

$$\Delta APAH1\_3 = \alpha_3 \cdot PAH1HRXN \quad \text{(R5-5)}$$

As illustrated in reaction (R5-4.1), by multiplying the counter species PAH1NRXN with yield parameters α_1 and α_2 the amount of high and low semi-volatile organic compounds

(SVOCs) generated in a chemistry time step (ΔSV_PAH1_1 and ΔSV_PAH1_2) can be calculated. Subsequently the total concentrations of the SVOCs (SV_PAH1_1 and SV_PAH1_2) are updated. The SVOCs go through equilibrium partitioning process and form high and low volatility SOA products (APAH1_1 and APAH1_2). Reaction (R5-5) shows the formation of non-volatile SOA products directly from counter species PAH1HRXN and the yield parameter α_3. All the counter species are reset to zero after each time step.

Table 5-1. Species added to the gas phase mechanism.

Species	**k_{OH}^ ($\times 10^{-11}$)**	**Reaction**
Naphthalene	2.30	NAPH + OH = 0.236HO2 + 0.15xHO2 + 0.102OH + 0.479RCO3 + 0.15RO2C + 0.033RO2XC + 0.033zRNO3 + 0.15xGLY + 0.236CRES + 0.06xAFG1 + 0.09xAFG2 + 0.102AFG3 + 0.183yRAOOH + 1.0PAH1RO2
Methyl naphthalene	1.59	MENAPH + OH = 0.236HO2 + 0.225xHO2 +0.075OH + 0.414RCO3 + 0.225RO2C + 0.005RO2XC + 0.005zRNO3 + 0.125xGLY +0.1xMGLY + 0.236*CRES + 0.09xAFG1 + 0.135xAFG2 +0.075AFG3 +0.275yRAOOH + 1.0PAH1RO2
Dimethyl naphthalene	7.68	DMNAPH + OH = 0.236HO2 + 0.3xHO2 +0.048OH + 0.35RCO3 + 0.3RO2C + 0.066RO2XC + 0.066zRNO3 + 0.1xGLY +0.2xMGLY + 0.236CRES + 0.12xAFG1 + 0.18xAFG2 +0.048AFG3 +0.366yRAOOH + 1.0PAH1RO2;
Ethylnaphthalene	3.83	1.0 MNAPH
Acenaphthylene	11.0	0.5 NAPH + 0.5 MNAPH
Acenaphthene	10.0	0.5 NAPH + 0.5 MNAPH
Fluorene	1.30	0.5 MNAPH + 0.5DMNAPH
Phenanthrene	3.10	0.5 MNAPH + 0.5DMNAPH
Fluoranthene	13.0	0.5 MNAPH + 0.5DMNAPH
All other PAHs	13.0	PAH2 + OH = 0.236HO2 + 0.263xHO2 +0.062OH + 0.382RCO3 + 0.263RO2C + 0.035RO2XC + 0.035zRNO3 + 0.113xGLY +0.15xMGLY + 0.236CRES + 0.105xAFG1 + 0.153xAFG2 + 0.062AFG3 +0.32yRAOOH + 1.0PAH2RO2

The mass-based stoichiometric SOA yields (α) and effective saturation concentrations (K_p) for PAH1 species are derived from the chamber study of Chan et al.

[47] by averaging the reported α and K_p values for naphthalene, methylnaphthalene and dimethylnaphthalene based on their overall emissions rate in southeast Texas. Shakya and Griffin [48] tested some different species under high NOx conditions and their results of yields are within the range of those of Chan et al. [47]. The final data used in the model are summarized in Table 5-2 (base case rows). The α and K_p values for PAH2 products are assumed to be the same as those for PAH1 products, lacking of experimental data. To calculate the mass concentrations of PAH-SOA from mole concentrations, the molecular weights of SVOCs from PAH1 and PAH2 species are estimated to be 264 and 360 $gmol^{-1}$, respectively. They are obtained by assuming that each SVOC molecule from PAH1 and PAH2 species on average contains 11 and 15 carbon atoms, respectively, and both have an SOA/SOC ratio of 2. The SOA/SOC ratio is also used to estimate the molecular weight of SVOCs from aromatic compounds in the AERO5 of the original CMAQ model. Enthalpies of vaporization of SVOCs are taken from Allen [150].

Table 5-2. SOA yields from semi-volatile products of oxidation of PAHs and their effective saturation concentrations for base case and sensitivity case.

		α_1 μg/μg	$1/K_{p1}$ μg m^{-3}	α_2 μg/μg	$1/K_{p2}$ μg m^{-3}	α_3 μg/μg
High-NOx	Base case	0.32	2.34	1.07	270.27	-
	Sens. case	0.55	1.69	1.07	270.27	-
Low-NOx	Base case	-	-	-	-	0.64
	Sens. case	-	-	-	-	0.73

5.2.2 Source apportionment technique

Contributions to PAH-SOA due to different PAH sources are determined based on a source-oriented reactive tracer method [45, 85, 121] which has recently been applied in the CMAQ model to study source contributions to SOA due to alkanes,

aromatics, isoprene, monoterpenes and sesquiterpenes in Southeast Texas [131]. The source-oriented extension of the CMAQ model to track SOA from PAHs is briefly described below.

Additional species are introduced to track source-origin of PAH species, their reaction counters and semi-volatile/non-volatile products in the gas phase photochemical mechanism and the aerosol module. Using naphthalene (NAPH) as an example, reaction (R1) is expanded into n reactions (n is the number of sources the model can track simultaneously in one simulation). As illustrated in reaction set (R5-1'), a total number of n reactions with tagged NAPH and PAH1RO2 species are introduced into the mechanism to represent NAPH and the peroxy radical products from n number of sources.

$$NAPH^{i} + OH \rightarrow ... + PAH1RO2^{i} \quad ,i=1,2,...n \qquad \text{(R5-1')}$$

Similarly, reactions (R5-2)-(R5-5) described in the previous section are also expanded to include additional tagged species to track the sources of PAHs and their products. With this source-oriented approach, the source contributions of PAH-SOA from each source type can be directly determined.

This source apportionment technique only tracks the direct contributions of each source to SOA based on partitioning of semi-volatile or non-volatile products emitted from the source. The indirect contributions of each source to PAH-SOA due to emissions of other reactive gas species that affect the production rate of condensable VOC species or POA that affects gas-particle absorption partitioning are not quantified.

This non-linearity of the source contributions due to indirect effects should be explored in future studies.

5.3 Model application

CMAQ 4.7 with the source-oriented SAPRC07/AERO5 extension is applied to study SOA formation from PAHs during TexAQS 2006, from August 28 to September 12, 2006. August 28 is used as a spin-up day and results from that day are not used in the data analysis. Three nested domains are used in the simulation. The horizontal grid resolutions are 36 km, 12 km and 4 km, respectively. The 36-km horizontal resolution parent domain covers the eastern United States, the 12km domain covers the east part of Texas and neighbor states and the 4-km domain covers Southeast Texas. The map of the 4-km domain together with the locations of the observation sites used to validate the model performance can be found in previous sections. The model covers a vertical extend of approximately 21000 m above surface using 14 vertical layers with increasing thickness from the ground level. The first model layer has a thickness of 42 m.

The MM5 meteorology simulation results provided by Texas Commission on Environmental Quality (TCEQ) are processed using the Meteorology-Chemistry Interface Processor (MCIP) to generate inputs for the CMAQ model. The MM5 results are used in TCEQ's State Implementation Plan (SIP) development and have been evaluated against observations extensively. The initial conditions (ICs) for all the domains and boundary conditions (BCs) for the 36-km parent domain are generated based on the default CMAQ profiles.

Emissions of CO, NO_x, SO_2, VOCs, NH_3 and primary PM from anthropogenic sources are based on the 2005 National Emission Inventory (NEI) (2005-Based Modeling Platform, version 4, downloaded from ftp://ftp.epa.gov/EmisInventory/2005v4/) and processed using a modified Sparse Matrix Operator Kernel Emission (SMOKE) model (version 2.5) to generate CMAQ model ready emissions. Emissions from port activities in the 2005 NEI v4 are actually 2002 emissions based on a top-down estimation method and this method is thought to overestimate emissions from diesel fuel commercial marine vessel (CMV) (SCC codes 2280002x00) (Rich Mason, personal communication, May 12, 2011). Reported NO_x emission from the diesel CMV in the Port of Houston in the 2005 NEI v4 is approximately 82500 ton $year^{-1}$(tpy). However, based on a documentation from TCEQ, CMV NO_x emission in the HGB area in 2007 is approximately 5091 tpy [151]. Thus the actual NO_x and VOC emissions from the diesel CMV in the 2005 NEI v4 are reduced by a factor 16 to match the TCEQ emission estimates. VOC and NO_x emissions from industrial point sources in the HGB and Beaumont Port Arthur (BPA) areas are generated from the TCEQ's hourly special inventory (version 9) (from ftp.tceq.state.tx.us/pub/OEPAA/TAD/Modeling/HGB8H2/ei/point/2006/special_inventory on January 15, 2011, but currently unavailable as the time of the writing) using an in-house program. The sources included in the special inventory are removed from the 2005 NEI to avoid double counting of the emissions.

Total VOC emissions are speciated into explicit and lumped model VOCs using the speciation profiles extracted from the SPECIATE 4.2 database from U.S. EPA

(downloaded from http://www.epa.gov/ttn/chief/software/speciate/index.html). The original SPECIATE 4.2 profiles are in the form of mass split factors of individual VOC species or compound groups. These profiles are processed using the emission preprocessor program provided by Dr. William P.L. Carter [123] to generate profiles that match the modified SAPRC07 model with explicit and lumped PAH species. Speciation profiles to process the TCEQ special VOC emission inventory are taken from the data files included in Dr. Carter's preprocessor program. Biogenic emissions (excluding wild fire) are generated using the Biogenic Emission Inventory System Version 3 (BEIS3) imbedded in the SMOKE model.

Table 5-3. Daily emission rates of PAH species in the 4-km domain for different emission sources on August 31, 2006. Units are kmol day^{-1}.

	Vehicles	Solvent	Industries	Natural gas	Coal	Wild fire	Other
NAPH	1.4552	1.5008	2.6689	0.0319	0.0011	11.0796	0.6119
MENAPH	0.5928	0.6121	0.5103	0.0004	0.0000	11.0870	0.1508
DMNAPH	0.2311	0.1769	0.6346	0.0000	0.0000	10.6376	0.1533
ETNAPH	0.1803	0.0851	0.3173	0.0000	0.0000	0.0000	0.0733
ACNAPHY	0.0344	0.0000	0.0266	0.0000	0.0000	1.6414	0.0060
ACNAPHT	0.0093	0.0000	0.0002	0.0000	0.0000	0.5522	0.0000
FLUORENE	0.0155	0.0000	0.0124	0.0000	0.0001	1.6718	0.0027
PHENAPH	0.0390	0.0000	0.0687	0.0001	0.0002	2.4957	0.0157
FLUORAPH	0.0196	0.0000	0.0102	0.0000	0.0000	0.0719	0.0024
PAH2	0.1717	0.1131	0.0000	0.0000	0.0000	3.0023	0.0007
Total	2.7489	2.4879	4.2492	0.0325	0.0014	42.2395	1.0168

The fire emissions are based on Fire Inventory from NCAR (FINN) version 1.0 [152]. The emissions of PAHs from fires are estimated based on the wood burning speciation profiles by Hays et al. [153]. Almost none of the SPECIATE 4.2 speciation profiles for coal and natural gas combustions contain PAH species. These profiles are

modified to include naphthalene and some other PAH species based on emission factors recommended in the AP-42, Compilation of Air Pollutant Emission Factors [154].

The original SMOKE model is modified to generate emissions for specific emission source categories by using a Source Classification Code (SCC) filter [36]. In this study, total emissions of PAH species are grouped into eight sources: vehicles, solvent utilization, residential wood, industries, natural gas combustion, coal combustion, wild fire and other sources. Table 5-3 shows the total emission rates of PAH species for these source categories within the 4-km Southeast Texas domain on August 31, 2006. As discussed in the previous paragraph, PAH emissions from coal combustion and natural gas combustion sources are not well represented in the original SPECIATE profiles. Although corrections were made to include naphthalene and some other PAH species emissions, the emissions rates of other PAH species from these two sources are likely under-estimated.

5.4 Results

5.4.1 Model evaluation

In previous experimental and modeling studies, it has been demonstrated that SOA concentrations in this area can be strongly correlated with O_x (O_3 + NO_2) concentrations because both are generated during oxidation processes of the VOCs [58, 128, 131, 155]. Thus, correctly predicting O_3 and NO_2 is a necessary condition to ensure reasonable SOA predictions.

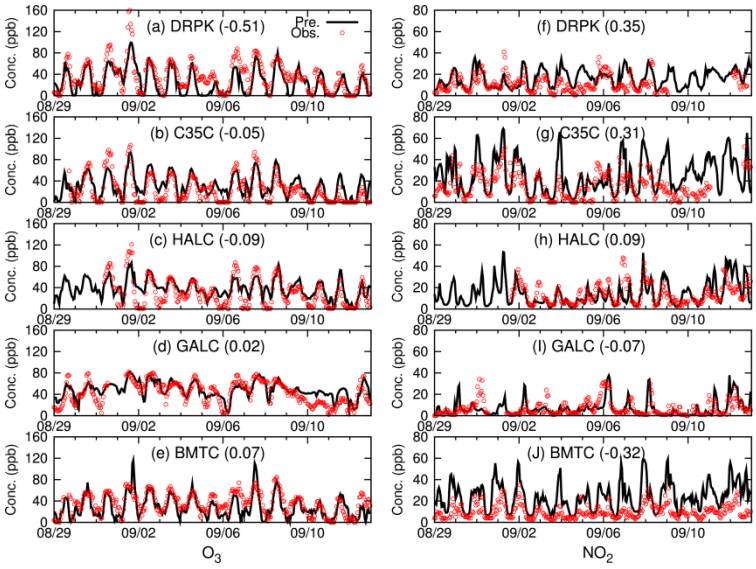

Figure 5-2. Comparison of predicted and observed hourly O_3 and NO_2.

Figure 5-2 shows the comparison of predicted and observed hourly O_3 and NO_2 concentrations together with the mean fractional bias

($MFB = \frac{2}{N}\sum_{i=1}^{N}(P_i - O_i)/(P_i + O_i)$, where P_i and O_i denote the i^{th} prediction and observation, respectively, and N is the number of data points) at 5 stations. Deer Park (DRPK) is an urban site to south of the Houston Ship Channel. Clinton Driver (C35C) is an urban site in Houston under the influence of industrial emissions. Aldine (HALC) is a suburban site to the north of Houston. Galveston (GALC) is located on the Galveston Island, and can be seen as a coastal site. Beaumont (BMTC) is an industrial site in Jefferson County, Texas. The model well captures the O_3 trend in all the stations. O_3 peaks in days such as from August 29 to September 1 and from September 6 to September 7 and DRPK, C35C, and HALC are under-predicted. The under-prediction of peak hour O_3 concentrations in this area has bas been studied extensively and has been

attributed to potential underestimation of VOCs from industrial sources [36]. The model also overestimates nighttime O_3 concentrations at HALC and GALC. This overestimation of O_3 is likely due to overestimations of vertical turbulent diffusion coefficient near the surface, which brings too much O_3 from upper air into the surface layer. At BMTC, which is very close to several of the wild fire events during the modeling episode, peak O_3 concentrations are over-predicted on two days, which could be caused by an overestimation of the wild fire emissions. Uncertainties in the vertical distributions or diurnal variations of wild fire emissions can also be contributed to the O_3 overestimation. MFB values for O_3 performance at DRPK, C35C and HALC are -0.51, -0.05, -0.09, respectively. Over-predictions of NO_2 happen at DRPK and C35C (MFB values are 0.35 and 0.31, respectively) while under-prediction happens at BMTC (MFB value is -0.32). Despite the discrepancies, the general agreement between O_3 and NO_2 shows that the model reasonably simulates the emissions and reactions of VOCs and NOx that lead to O_3 formation.

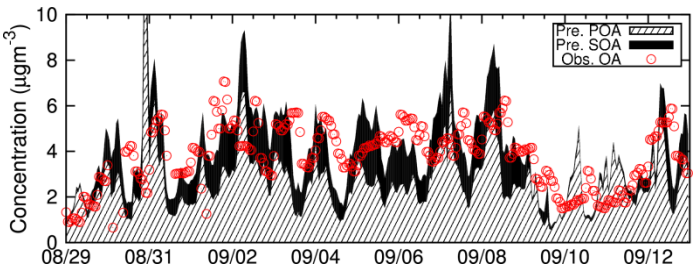

Figure 5-3. Observed OA and predicted POA and SOA at DRPK.

Hourly organic carbon (OC) observation at DRPK is acquired from TCEQ. A scaling factor of 1.4 is used to convert OC concentrations to organic aerosol (OA) concentrations [156 and the references therein]. Figure 5-3 shows the predicted POA and

SOA, and observed OA at DRPK from August 29 to September 12. Elevated OA concentrations of more than 3 μg m^{-3} are observed from August 31 to September 8. The modeled SOA concentrations are also high during these days and contributions of SOA to total OA are significant. Overall the model over estimate OA with an MFB value of 0.58, although this is well within the model performance criteria suggested by Boylan and Russell [102]. A detailed examination of the regional OA distributions shows that the emissions from wild fire near the border of Texas and Louisiana reach urban Houston on some of the high SOA days, likely contributing to the predicted SOA at DRPK. Sometimes the timing of the peaks is slightly off and the magnitude of the peaks is slightly higher than observations. Since the wildfire emissions are provided in daily resolution without vertical injection information, uncertainties in the assignment of diurnal variation and vertical distribution of the emissions might be responsible. It is also possible that the OA/OC ratio might be too small as there are evidences that this ratio could be higher than 1.4 [156-158]. If a higher ratio, such as 1.6, was used, the prediction would agree better with the observed OA. Overall, the model appears to reproduce O_3, NO_2, and OA at locations where observations are available.

Although direct measurements of SOA or PAH species are not available during this episode, TCEQ has auto Gas Chromatograph (GC) measurements for selected PAH species at DPRK in Houston since 2007. Daily concentrations of naphthalene, acenaphthene, acenaphthylene, fluorene, and phenanthrene are available every 6 days. Though these data cannot be directly used to validate the model performance on PAHs species, it gives some qualitative measure on how well the PAH species are predicted.

Predicted 24-hour average concentrations in 2006 and observed concentrations of these species from 2007 to 2010 are shown in Figure 5-4.Figure 5-4 (a) shows that model predicted naphthalene concentrations in 2006 are close to observations in 2007 and slightly higher than observations in other three years. Based on the observed concentrations in these four years, it is expected that actual concentrations in 2006 are likely similar in magnitude and the model is capable of reproducing the observed naphthalene concentrations. For all other PAH species, the model predicted concentrations are all significantly lower than observations. Acenaphthene, acenaphthylene, fluorene, and phenanthrene are under-predicted by a factor of 2-7, 5-10, 3-5, and 2-4, respectively (Figure 5-4 (b)-(e)). Based on these results, the emissions of naphthalene are reasonably represented by the model but emissions of other PAH species are underestimated. Although the absolute concentrations of these PAH species are significantly lower than those of naphthalene, the OH reaction rate constants of acenaphthene, acenaphthylene and fluorene are approximately a factor of 5-10 faster. Thus, it is expected that the overall PAH-SOA concentrations, as reported in the following sections, are under-predicted.

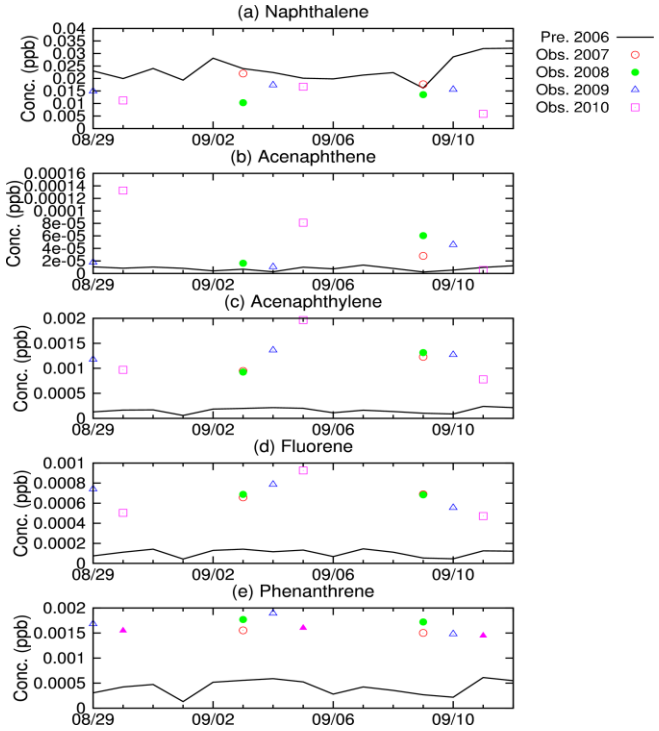

Figure 5-4. Comparison of predicted 24-hour averaged naphthalene (a), acenaphthene (b), acenaphthylene (c), fluorene (d), and phenanthrene (e) and relevant observation from 2007 to 2010 at DRPK.

5.4.2 PAH-SOA formation

Figure 5-5 shows the SOA formed from explicit PAH species (APAH1, which equals the sum of APAH1_1, APAH1_2 and APAH1_3) and lumped PAH species (APAH2, which equals the sum of APAH2_1, APAH2_2 and APAH2_3) and the ratio of total PAH-SOA (APAHT=APAH1+APAH2) to SOA formed from aromatics (AROT) at four stations. Conroe (CONR) is a rural site approximately 40 miles north of Houston. APAH1 is approximately 0.005 to 0.02 μgm^{-3} at CONR and APAH2 is very small. A concentration peak of more than 0.04μgm^{-3} due to wild fire occurs on September 5. The APAHT/AROT ratio is within a range of 5-10% and is generally correlated with APAHT concentration. As shown in Figure 5-5(b) and (c), in the urban areas, the

APAH1 concentration is around 0.01 μgm^{-3} while APAH2 is up to 0.005 μgm^{-3} at peaks time and remains small on other times. The APAHT/AROT ratio correlates with APAHT when it is high but remains 5-10% when APAHT is lower than 0.005 μg m^{-3} such as the first day and the last few days of the episode. At BMTC, the station closer to frequent wild fire activities, APAHT concentration is generally around 0.01 to 0.02 μg m^{-3} with peaks higher than 0.1 μg m^{-3} when wildfire influence is significant. The APAHT/AROT can be as high as about 50% on these high wildfire days.

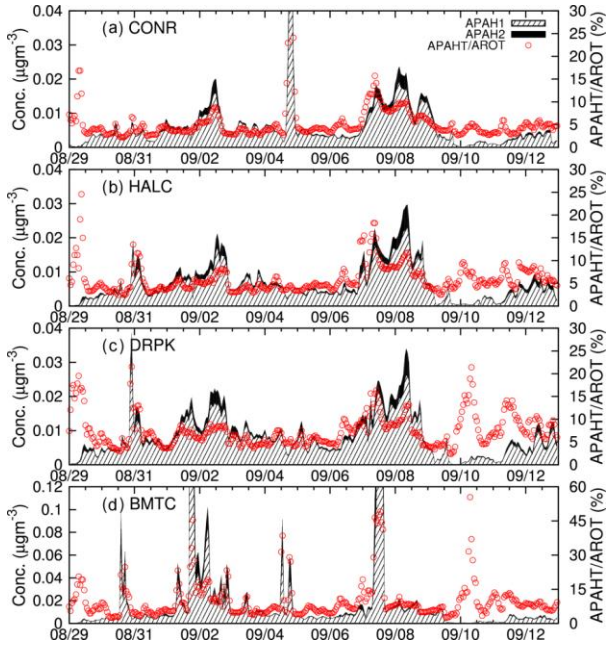

Figure 5-5. Model predicted APAH1 and APAH2 concentrations as well as the APAHT/AROT ratio at four stations.

Figure 5-6 shows the episode averaged regional distribution of APAH1 and APAH2 in the 4-km domain as well as APAHT/AROT and the ratio of APHAT to total anthropogenic SOA (ASOA). The highest APAH1 and APAH2 concentrations are at the Northeast of the domain where wildfires are reported during the episode (see Figure 5-6 (a) and (b)). The maximum values for APAH1 and APAH2 are 0.02 and 0.005 μgm^{-3},

respectively. At urban area, APAH1 is about 0.01μgm^{-3} while APAH2 is about 0.002 μgm^{-3}. APAHT/AROT is approximately 6% throughout the domain except in the urban and wildfire areas. It is 8-10% in urban Houston and higher than 10% in areas affected by wild fire emissions. APAHT/ASOA has similar regional distribution but with lower values. In urban areas the ratio is approximately 4-5% in general while up to 6% near wild fire regions, as shown in Figure 5-6(d).

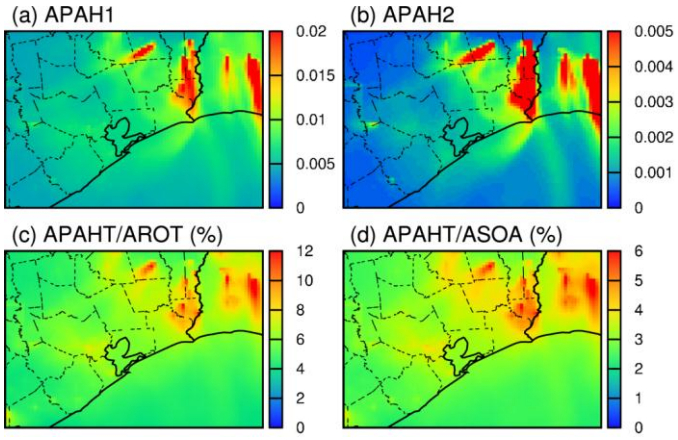

Figure 5-6. Regional distribution of episode averaged APAH1 and APAH2 concentrations (a, b) and APAHT/AROT and APAHT/ASOA ratios (c, d). Units are μgm^{-3} for (a) and (b) and % for (c) and (d).

5.4.3 Source contributions to PAH-SOA

Figure 5-7 shows the contribution of PAHs from each source type to SOA in the entire 36km domain over the Eastern US. Figure 5-7 (a) shows that the maximum amount of SOA from PAHs emitted from vehicles (including gasoline and diesel engines) is approximately 0.002 μgm^{-3} averaged over the entire episode. High concentrations occur at large cities such as Houston, Dallas, and Atlanta. In most rural and suburban areas, the concentrations are about 0.0005-0.0015 μgm^{-3}. Highest PAH-SOA concentrations due to solvent utilization sources happen in Illinois and Indiana with a

maximum concentration of 0.01μgm^{-3} as shown in Figure 5-7 (b). Residential wood burning contributions are in Northern areas such as Missouri, North Georgia, South Carolina, North Carolina, Virginia as well as New York City area. The highest concentrations are about 0.002μgm^{-3}. As shown in Figure 5-7(d), PAHs from industries are important sources to SOA at Central Texas and Alabama. Although clear spatial distributions of SOA concentrations can be seen in Figure 5-7(e) and 8(f), PAHs from natural gas and coal combustion sources are much lower and have a negligible contribution to overall PAH-SOA. Wild fire is the most important source of PAH-SOA. During the simulation episode, there are significant wildfire activities near the bordering area of Texas and Louisiana. The SOA formed are transported to surrounding areas such as Houston. The concentrations of PAH-SOA near the fire locations are higher than 0.01 μgm^{-3} and have about 0.002-0.004 μgm^{-3} effects to Houston (see Figure 5-7(g)). PAHs from other sources contribute less than 0.001μgm^{-3} to episode averaged SOA. Figure 5-7(i) shows the total SOA formed from all PAHs sources is approximately 0.01-0.02μgm^{-3}. Texas, Louisiana, Alabama, and Indiana are the states with higher PAH-SOA concentrations.

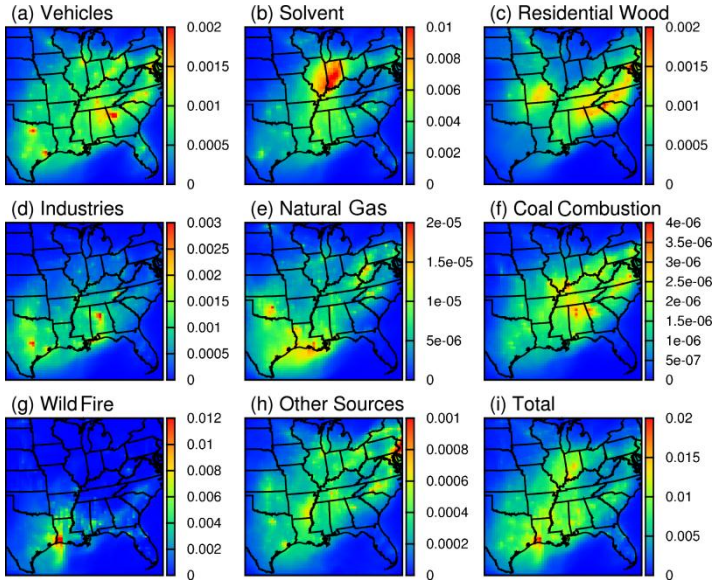

Figure 5-7. Source contributions to 24-hour average SOA from PAHs (a-h) and total SOA from PAHs (i) during the episode in 36km domain. Units are μgm^{-3}.

The regional distribution of SOA from each PAHs source in southeast Texas is shown in Figure 5-8. SOA formed by PAHs from vehicles is about 0.0014 μgm^{-3} in urban Houston as shown in Figure 5-8(a). Solvent utilization contributes about 0.0015 μgm^{-3} in urban Houston while about 0.002 μgm^{-3} in Lake Charles, Louisiana. Contributions of PAHs from residential wood to SOA are negligible in the domain (direct emissions of PAHs from residential wood is zero). A small background concentration is due to upwind sources (see Figure 5-8(c)). In Houston Ship Channel and Texas City areas, SOA concentrations are highest and with maximum of 0.0016 μgm^{-3}. PAH emissions from natural gas and coal combustions give very low concentrations of SOA as shown in Figure 5-8(e) and 8(f). Figure 5-8(g) shows that PAH-SOA produced from wild fire activities can be as high as 0.02 μgm^{-3} but it contributes to SOA in the urban Houston area is only 0.002 μgm^{-3}. PAHs from other sources generate less than

0.001 μgm^{-3} of SOA in the domain with higher concentrations confined in urban and industrial areas. Overall, PAH-SOA accounts for approximately 0.01 μgm^{-3} of total SOA in southeast Texas during this summer episode.

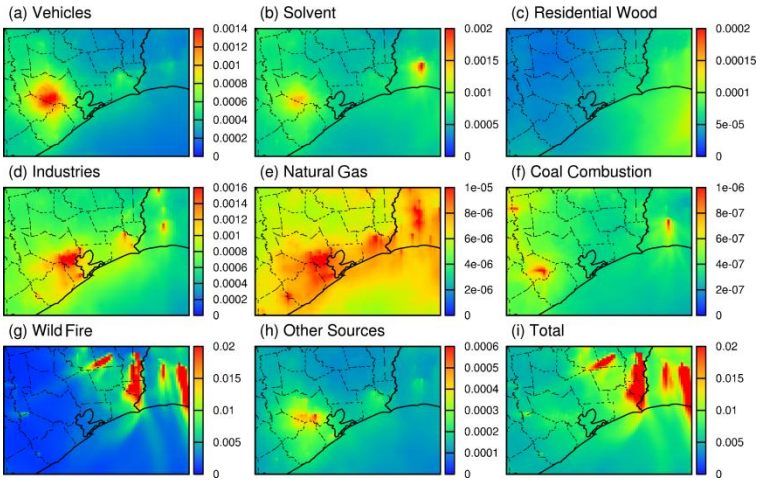

Figure 5-8. Source contributions to 24-hour average SOA from PAHs (a-h) and total SOA from PAHs (i) during the episode in 4km domain. Units are μgm^{-3}.

The contributions of coal and natural gas combustion to the overall PAH-SOA are low based on this study. As noted in Section 5.5.3, part of this might due to lack of proper VOC speciation profiles of PAHs in the existing SPECIATE 4.2 for these two source types. Although emission factors for naphthalene are appended to the relevant profiles, other PAH species are not included. This may lead to under-estimation of their contributions to the overall PAH-SOA.

5.4.4 Uncertainties analysis

Factors that may affect the formation of SOA from PAHs include the accuracy of the emissions of gas phases PAHs, the biases on meteorological predictions, and the parameters used in the current model scheme. In the previous section, possible under-

prediction due to under-prediction of non-naphthalene PAH species has been discussed. In this section, the effects of SOA yield and temperature on predicted SOA concentrations are further studied.

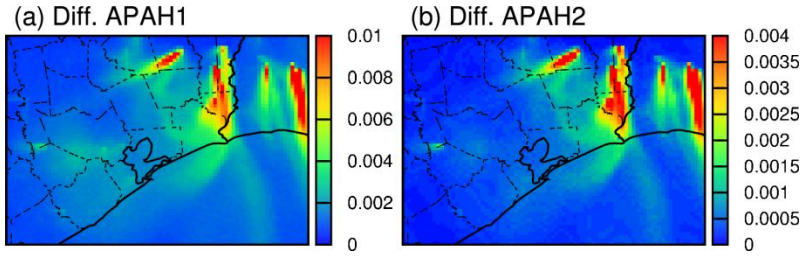

Figure 5-9. Regional distribution of episode averaged difference between sensitivity case and base case (sensitivity case – base case) for APAH1 (a) and APAH2 (b). Units are μgm^{-3}.

SOA yields and effective saturation concentrations for semi-volatile products of PAHs are important to predict PAH-SOA concentrations. However, only a few PAHs species have been studied in chamber and can be used to derive parameters for model simulation. For base case simulations reported in the previous sections, the emission-averaged parameters are used. A sensitivity case is run with SOA yields set to the upper-range and effective saturation concentrations to the lower-range of the experimental data of Chan et al. [47]. Table 5-2 lists the parameters for sensitivity run. This simulation represents an upper limit estimation of the PAH-SOA based on current chamber data and emission inventory.

Figure 5-9 shows the regional difference of predicted APAH1 and APAH2 between the sensitivity case and base case. The sensitivity case can produce 0.01 μgm^{-3} more APAH1 near wild fire locations and 0.004 μgm^{-3} more in urban Houston compared to base case. Similarly, sensitivity case can produces 0.005 μgm^{-3} more APAH2 near

wild fire while about 0.001 μgm^{-3} in urban Houston. Since the base case concentrations of APAH1 are slight higher than 0.01 μg m^{-3} in urban Houston, the change in the predicted concentrations is approximately 40%, which is quite significant.

Temperature affects SOA formation by altering the saturation vapor pressures of semi-volatile SOA species. Bias on meteorological predictions will lead to uncertainties of SOA formed from PAHs through gas-particle partitioning processes. To test effect of temperature, sensitivity runs are conducted by increasing or decreasing the temperature domain-wide evenly by 5 ℃. Due to the large enthalpies of vaporization of PAHs species, predicted PAH-SOA concentrations are not sensitive to the variation of temperature.

5.5 Discussions

The overall amount of PAH-SOA reported in this study is likely underestimated. It does not consider gas-particle partitioning of PAH species as well as heterogeneous or aerosol phase PAH oxidation reactions that would lead to the formation of additional SOA products [159-161]. Reactions of gas phase PAH species with other potential oxidants such as O_3 and NO_3 are also neglected. Zhou and Wenger [162] determined that the lifetimes of acenaphthene and acenaphthylene are shorter under typical NO_3 and O_3 concentrations than under typical OH concentrations. Although no SOA yield is determined in that study, less volatile products are identified in the particle phase. Follow up studies are necessary to include these processes to better estimate the contribution of PAHs to OA loading in the atmosphere and to estimate their climate and health impacts.

6. MODELING OF AGE DISTRIBUTON OF ELEMENTAL CARBON

Experimental studies show distinguished differences in the optical and hygroscopic properties between fresh and aged soot particles, which have significant implications in estimating the effect of atmospheric particles on air quality, weather and climate. In this study, the source-oriented UCD/CIT model described in Section 3 is expanded to track the regional age distribution of elemental carbon (EC) and organic carbon (OC) in Southeast Texas.

The model correctly predicts the overall concentrations of EC and OC when compared to a base case simulation without age-resolved particle representation. EC and OC emitted within 0-3 hours contribute approximately 70-90% in urban Houston and about 20-40% in rural areas. Significant diurnal variations in the relative contributions to EC are predicted by the model. Highest contributions of fresh particles occur at morning and early evening traffic hours due to increased emission and lower mixing. The closer to the emission sources, the fresher the EC and OC would be. The concentrations of EC and OC that spend more than 9 hours in the air are low over land but almost accounts for 100% of the total EC and OC over the ocean. The high level of fresh EC in the Southeast Texas area means that they could have a strong regional impact on aerosol optical and hygroscopic properties, and thus affect cloud formation and radiation balance.

6.1 Introduction

Elemental carbon (EC, often used interchangeably as black carbon (BC)) emitted from fossil-fuel combustion, vehicles, aircrafts, and biomass burning, is an important

components of tropospheric particulate matter (PM) [163-165]. EC has adverse effects on visibility, human health, atmospheric radiation as well as climate change [165-169]. Once emitted into the atmosphere, EC will go through aging processes such as absorption or condensation of gaseous species, coagulation with other preexisting aerosols, homogeneous and heterogeneous reactions [60, 61]. The variability in morphology, hygroscopicity, and optical properties of EC aerosols due to atmospheric aging has been observed by laboratory experiments and ambient measurements [59, 60, 166, 170]. The changes of properties of EC enhance its abilities on solar radiation absorption and it can act as cloud condensation nuclei (CCN) which impact cloud formation and the lifetime and albedo of clouds after being converted to hydrophilic by deposition of water and other chemical species [165, 171].

Aging of EC and its impact on air quality, weather and climate have been extensively investigated through modeling and experiments. Parameterized aging rates were commonly in the last decade in climate models due to computational limitations and the results are very sensitive to the chosen rates [172-174]. Riemer et al. [62, 63] conducted models that explicitly treat aging process and found that the aging time scales significantly change when the dominating aging processes switch. During the day, the absorption and condensation of secondary pollutants are the most important processes and the time scales are from a few minutes to less than 10 hours. At night, coagulation dominates the aging process due to decreasing of secondary pollutants formation and the time scales are about 10-50 hours. More recently, by incorporating the gradual aging process of EC into AURAMS (A Unified Regional Air-quality Modeling System), Park

et al. [175] found that model performance on EC concentration predictions was improved and wet deposition of EC was enhanced.

Moffet and Prather [176] show that in the Mexico city, fresh soot particles account for the majority of the absorption coefficient in the early morning and at night because of the absence of photochemistry, while aged soot particles are responsible for the majority of the midday absorption when the solar irradiance is the highest, which promotes the formation of secondary semi-volatile vapors that can condense onto existing particles. Correct spatial and temporal distributions of the particle and their aging status are needed to evaluate the impact of air quality on climate or regional or global scale. This information might be available in the future directly with satellite-based retrieval methods but such remote sensing techniques have not been reported so far. Although chemical transport model can provide regional distributions of EC no modeling studies have been reported that determine the distribution of particle aging statues in regional/global scales.

Similar to EC, primary emitted organic carbon (OC) also goes through atmospheric transformations through heterogamous reactions, gas-to-particle partitioning and reactions in the particle phase. These processes also change the physical and chemical properties of aerosols, which in turn affects the formation of secondary organic aerosol (SOA), air quality, and climate. In this section, the source-resolved air quality UCD/CIT model is enhanced with an age-resolved particle representation so that it is not only possible to determine the temporal and spatial variations of the particles and their source-origins but also their “aging” status (chemical compositions, optical properties) in

regional scales. This model development will improve the understanding of aging distribution of primary EC and OC and will eventually lead to an increase in the ability of air quality and climate models to better predict the feedback of particles on weather and climate.

6.2 Methodology

Most existing air quality models do not keep track of the source or age information of the particulate matter in the simulation. Typically, emissions from different sources at a given time are mixed with preexisting particles, which are represented as an internal mixture of different chemical components. The physical and chemical properties of the particles, which are needed for gas-to-particle partitioning and cloud chemistry, are based on the internally mixed particles, assuming that particles of the same size have identical chemical compositions. In coupled air quality-meteorology models, the PM optical properties that link the air quality and meteorology models are also based on the internally mixed aerosol assumptions.

The externally-mixed particle representation as implemented by Kleeman and coworkers [27, 45, 177] is capable of resolving particles from multiple sources independently. Their treatment, however, does not account for the fact that the chemical, physical and optical properties of particles of different ages are different. In the age-resolved air quality model proposed in this study, particles emitted at different times will be explicitly represented in the model and their evolution in the atmosphere will be tracked separately. This provides a more realistic representation of the mixing state of the particles in the atmosphere.

As shown in Figure 6-1, the aerosol module in the externally-mixed host model will be expanded to include n time bins. Different time bins will be used to represent particles of different age groups. The emissions of the current model time-step will always go to the fresh aerosol bin. At the end of each hour, the particles in the i^{th} age group will be moved to the $(i+1)^{th}$ age group. The last age group will be used to account for aerosols in the air that are emitted earlier than particles in previous time bins. The total number of the time bins can be selected so that the last time bin does not account for a significant amount of particle mass during all the hours of the simulation. The time bin advance process can be written mathematically in eq. (E5-1),

$$C^{i+1}=C^{i},\ i=N_b-2,\ N_b-3,\ldots,1 \qquad \text{(E5-1)}$$

$$C^{N_b}=C^{N_b}+C^{N_b-1}$$

where C represents aerosol concentration, i is the time bin index and N_b is the total number of time bins.

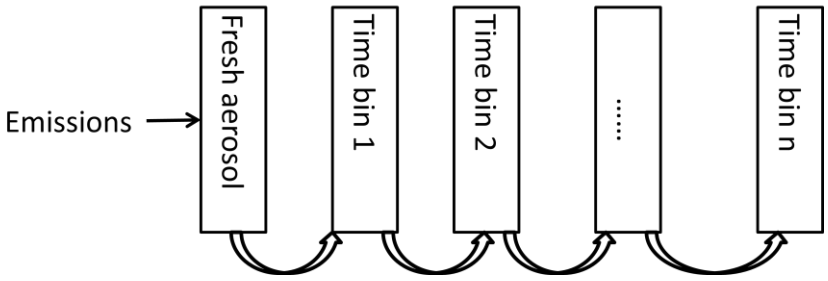

Figure 6-1. Schematic diagram of aerosol aging process (n is the total number of time bins).

As a demonstration of the ability of the time-resolved regional modeling, this technique is applied to primary PM species and emissions from different emission

sources are lumped in the model simulation (i.e., it does not keep track of the source information of the particles) in the current study. In follow up studies, the gas-to-particle partitioning processes that form secondary inorganic and organic components as well as in-particle processes such as aqueous chemistry and SOA oligomerization will be simulated for all particles. In addition, particle cores emitted from different source will be tracked separately in as a full external-mixture. Since the freshly emitted particles and particles of different ages will have different morphology and chemical composition (for example, freshly emitted particles from combustion sources are likely to be more hygrophobic than aged particles), the amount of semi-volatile gases condenses onto particles of different ages and sources will be different even for the same particle size. This difference is likely going to affect the further chemical/physical evolution of the particles. Figure 6-2 illustrates this source and age resolved external mixture concept using two particle sources (wildfire and sea salt) and three time bins. Note that Figure 6-2 does not illustrate the time evolution of the particles but shows a snapshot of the aerosol population at a given time.

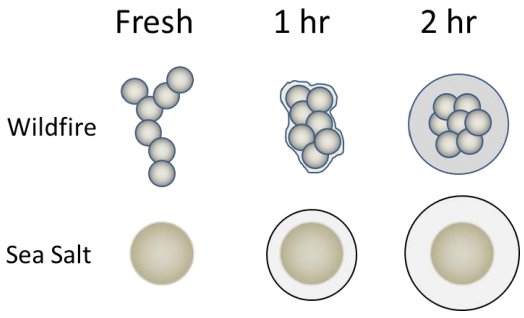

Figure 6-2. Source and age resolved representation of aerosols from wildfire and sea salt sources. The change of the morphology of particles emitted from wildfire and difference in the amount of secondary components among particles of different ages and types are illustrated.

6.3 Model application

In this study, the nested version of the UCD/CIT model coupled with age-resolved feature is applied to simulate the age distribution of EC and primary OC in Southeast Texas during a 6-day (August 24, 2000 to August 29, 2000) air quality episode in the TexAQS 2000 study. The first day is used as spin-up and not used for analysis. The domain settings and model inputs are same as study in Section 3, so here only a summary is shown.

The horizontal grid size for the three nested domains are 36km (62×67), 12km (89×89) and 4km (83×65), respectively. All domains use same 14 vertical layers that reach approximately 15km above surface are used. The meteorology fields were generated using the PSU/NCR mesoscale model (MM5) by the Texas Commission of Environmental Quality (TCEQ) and were converted into the data format required by the UCD/CIT model using a preprocessing program. Emissions of EC, primary OC and other PM components were based on the 2001 Clean Air Interstate Rule (CAIR) emission inventory. Emissions of wildfire during the modeling episode were based on the data provided from the Center for Energy and Environmental Resources at the University of Texas at Austin.

In this study, the model tracks age information of primary species (EC and OC) in the 4-km domain using 10 time bins. The first nine time bins have a resolution of 1 hour, i.e., the particles in the i^{th} time bin are particles that released between i-1 and i hours before the current model time. Since the particles in the 36-km and 12-km simulations are not age-resolved, the particles that enter the 4-km domain as boundary

conditions are put into the last time bin, assuming these are relatively aged particles. Gas phase reactions and gas-to-particle conversion of inorganic and organic materials are not simulated.

6.4 Results

The EC and OC predicted by the age-resolved simulation has to be compared with a base case simulation that does not treat particles are age-resolved mixtures to ensure that the time advancing scheme is programmed correctly. Figure 6-3 shows the comparison of the predicted total EC and OC concentrations by the age-resolved model with the base case model results. 24-hour averaged concentrations at 6 stations, whose locations can be found in Figure 4-1, are extracted for the comparison. The age-resolved model predicts similar but slightly lower EC and OC concentrations compared to base case results. This is likely caused by the numerical error accumulated in the finite-element based advection solver used in the simulation. The base case simulation includes coagulation while the time-resolved simulation does not. This leads to differences in the particle number concentrations and diameters. The difference in the model configuration may also lead to difference in the predictions. A new simulation using the same model configurations will be needed to further evaluate the correctness of the model.

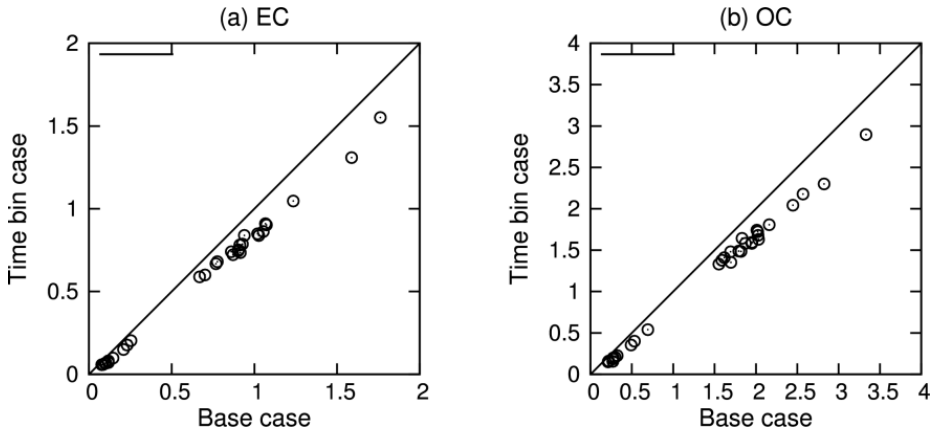

Figure 6-3. Comparison of 24-hour averaged EC and OC predicted by base case and this time bin case, units are μgm^{-3}.

Figure 6-4 shows the time evolution of the age distribution of EC and OC at Deer Park (DRPK, an industrial station near the Ship Channel), Conroe (CONR, a suburban site to the north of Houston), and Huntsville (HSVL, a rural town to the north of Houston) from August 25 to 29, 2000. The concentrations are grouped to 4 age ranges: 0-3 hours, 3-6 hours, 6-9 hours, and more than 9 hours old. EC concentrations are about 1.5 μg m^{-3} at morning and afternoon peaks at DRPK. Majority of them are fresh EC less than 3 hours old. EC 3-6 hours old can be as high as 0.5 μg m^{-3} for morning peaks like August 26 and 27 but remains negligible in other times. At DRPK, EC emitted more than 6 hours ago accounts for a very small faction of the total EC. In contrast, at CONR the amount of 6-9 hours old EC is higher and can be as much as 0.5 μg m^{-3} as shown in Figure 6-4 (b). In HSVL, EC concentrations are lower than at other sites. Although EC 0-3 hours old still dominates the overall EC concentrations, older EC becomes more significant, especially EC older than 9 hours. OC aging distributions are shown in Figure 6-4 (d), (e), and (f). Mostly the age distributions are similar to EC at each station.

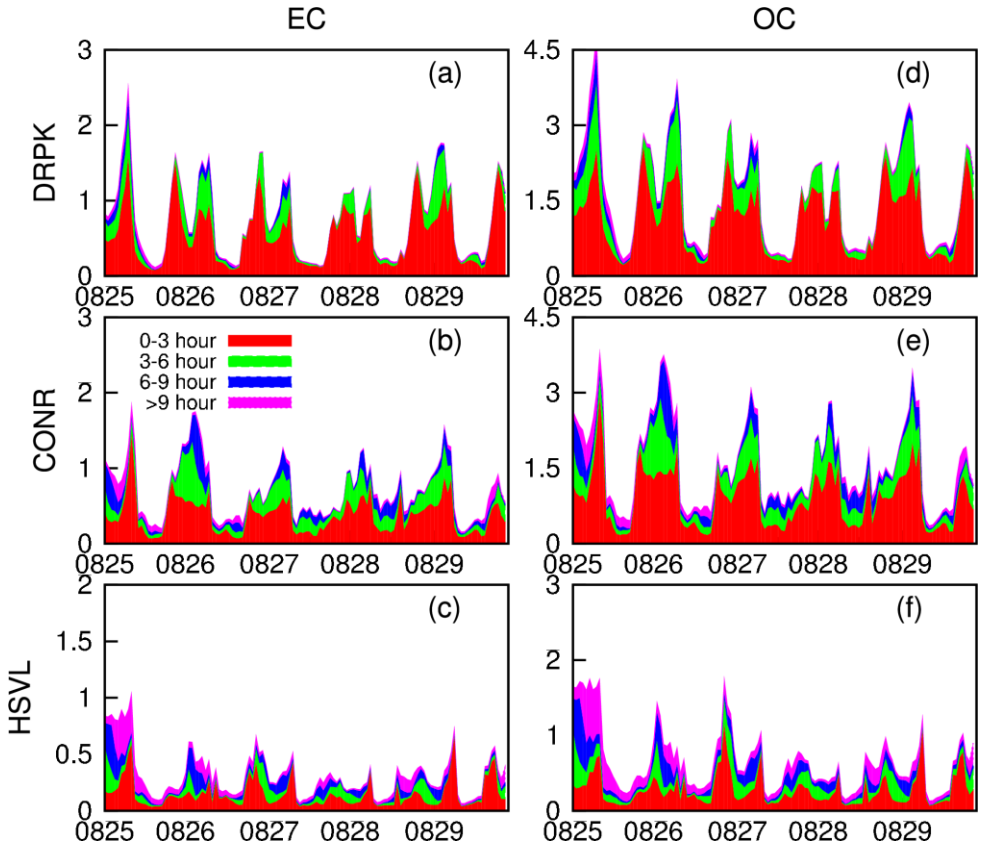

Figure 6-4. Time series of aging distribution for EC and OC concentrations at three stations, units are μgm^{-3}.

To better illustrate the relative importance of EC and OC of difference ages to the overall concentrations, episode averaged diurnal variation of the fractional contributions of different age groups to overall EC and OC at DRPK, CONR, and HSVL are shown in Figure 6-5. At DRPK, EC and OC have same pattern through 24 hours. The contributions from the freshest particles (0-3 hours old) contribute to more than 60% from midnight to early evenings. The fraction of fresh particles starts to increase at1600 local time and reaches 90% at 2000 hours. This increase is likely due to vehicle emissions from traffic hours. Particles 3-6 hours old contribute to approximately 15% of

total EC and OC except early evening hours. Contributions from particles 7-9 hours old increase gradually from midnight and are approximately 10% from early morning to noon. The oldest particles (> 9 hours old) are low in the morning but can contribute up to 15% of EC and OC in the afternoon. Contribution of each age group to total EC and OC in suburban site CONR is shown in the second row of Figure 6-5. Contributions of particles 0-3 hours old decrease to 40-60% and other three age groups increase. In addition to the early evening traffic peak that leads to fresh particles as high as 80%, there is another peak of fresh particles appears at 0800 hours with a highest contribution of approximately 70%. This peak is likely due to increased vehicle emissions during morning commute. At HSVL, the rural site, contributions from 0-3 hours old particles are low at approximately 30% from late night to early morning. During the morning traffic peak hours, contributions from 0-3 hours old particles can still reach 70%. Highest contributions from 4-6 hour range are synchronous with the lowest contributions from b1-3 hour range and as high as 40%. Contributions from 7-9 hour range peak at early morning. The >10 hour rage contributes to about 40% at whole daytime. The results suggest that freshly emitted particles dominate the particle population not only in large urban areas with a lot of emissions but also in suburban and rural areas in the morning and evening traffic hours. The closer a place to the emission source, the fresher the pollutants will be. From urban area to rural area, the contributions of the 0-3 hours old particles decrease from more than 60% to 30-40% at non-traffic-peak hours while the contributions of the more than 9 hours old particles increase from 10% to 40%.

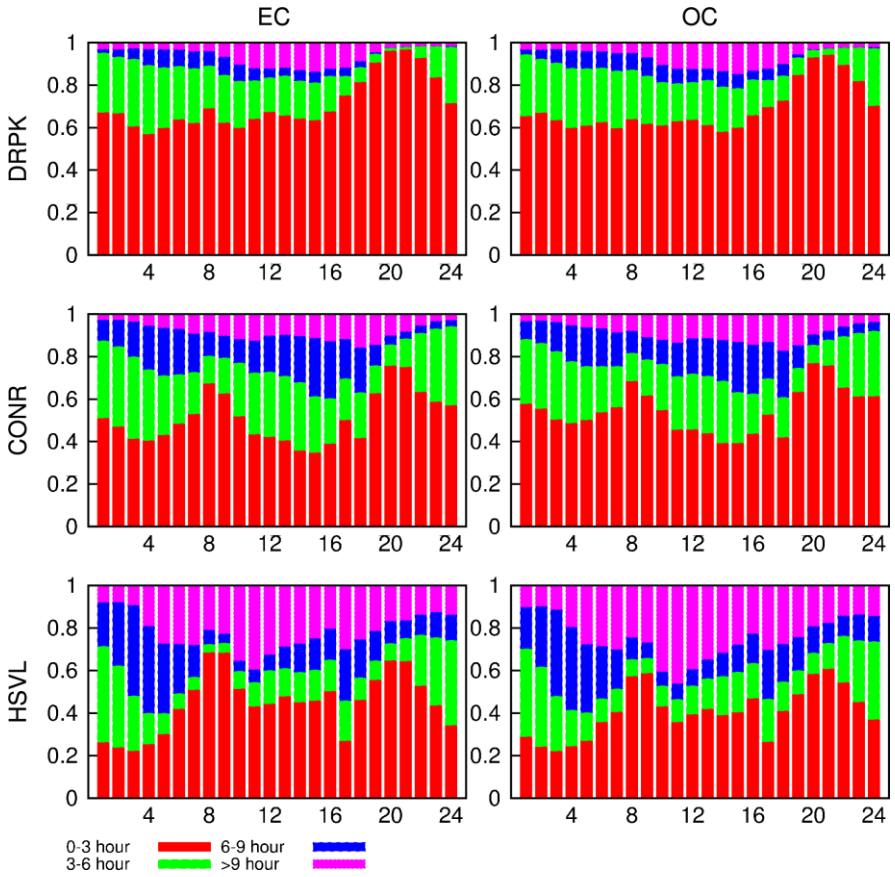

Figure 6-5. Episode averaged diurnal variation of the contributions of aging particles to EC and OC concentration at three stations.

Figure 6-6 shows the regional distribution of EC concentrations for different age groups. From Figure 6-6(a) to (c), the transport of EC from its major emission area in urban Houston area and the decrease of concentrations as they are transported downwind can be easily observed. After every 3 hours, the peak concentrations decrease to approximately 30% of the peak concentrations of the previous 3-hour age group. This also gives a rough estimation of the half life time of 2 hours for EC. Figure 6-6(d) shows the EC concentrations in the particles after they are emitted into the atmosphere for more than 9 hours are approximately 5% of the first age group, indicating that the number of time bins used in this study is sufficient to resolve the age distribution of EC in the

Houston area. The spatial distribution for different age groups of OC are similar to that of EC and are not presented.

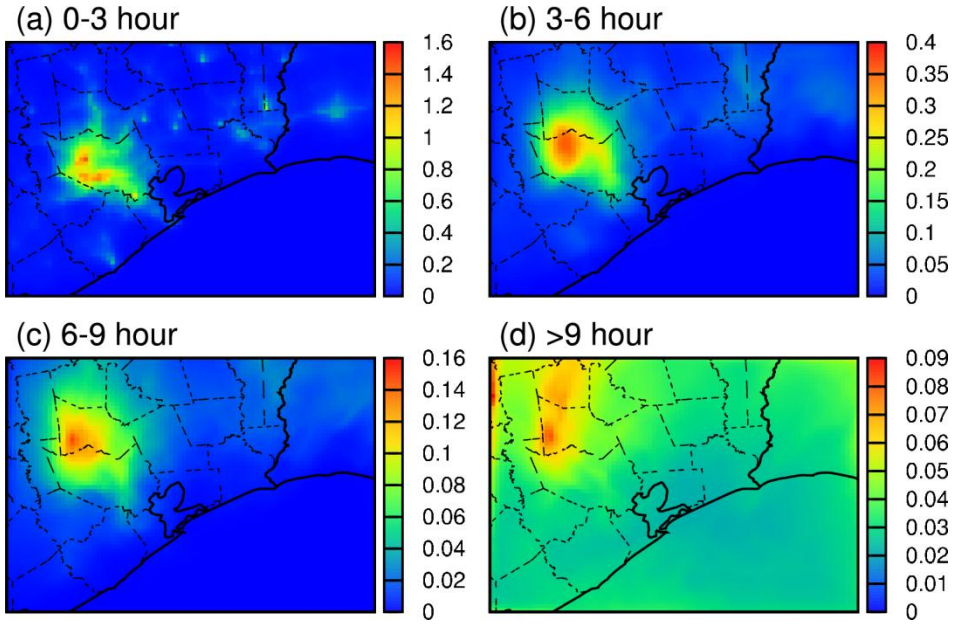

Figure 6-6. Regional distribution of episode average EC concentrations in Southeast Texas for different age groups. Units are μgm^{-3}.

Figure 6-7 shows the episode average factional contribution of each age group to the overall EC loading in southeast Texas. Figure 6-7(a) illustrates that the fraction of fresh EC can reach 70-90% in urban areas and 40-50% in areas long major freeways. In addition, wild fires can also contribute to as much as 80-90% of fresh EC in some isolated locations. Even in rural areas over land, its contributions are generally more than 20%. The high level of fresh EC means that they could have a regional impact on aerosol optical and hygroscopic properties, and thus affect cloud formation and radiation balance. Figure 6-7(b) shows that EC 3-6 hours old accounts for majority of the EC loading near the emission sources with a maximum contribution of 45%. In most areas on land in the southeast Texas, the contributions of these particles to the overall EC loading are on the

order of 20-30%. Figure 6-7(c) shows that further away from the urban emissions the contributions of EC 6-9 hours old dominate with a highest contribution of approximately 40% in the northwest corner of the domain. Figure 6-7(d) shows that aged EC particles more than 9 hours old have lowest contributions near the emission sources. Their factional contribution over land is approximately 20-40%. Near the Gulf coast and over the ocean, all most 100% percent of the EC are more than 9 hours old. The influence of fresh emissions in southeast Texas to the EC concentrations over the ocean is small, and a sharp gradient of EC age exists along the coastal line. The regional distributions for OC is similar to those of EC shown in Figure 6-7 and thus are not shown.

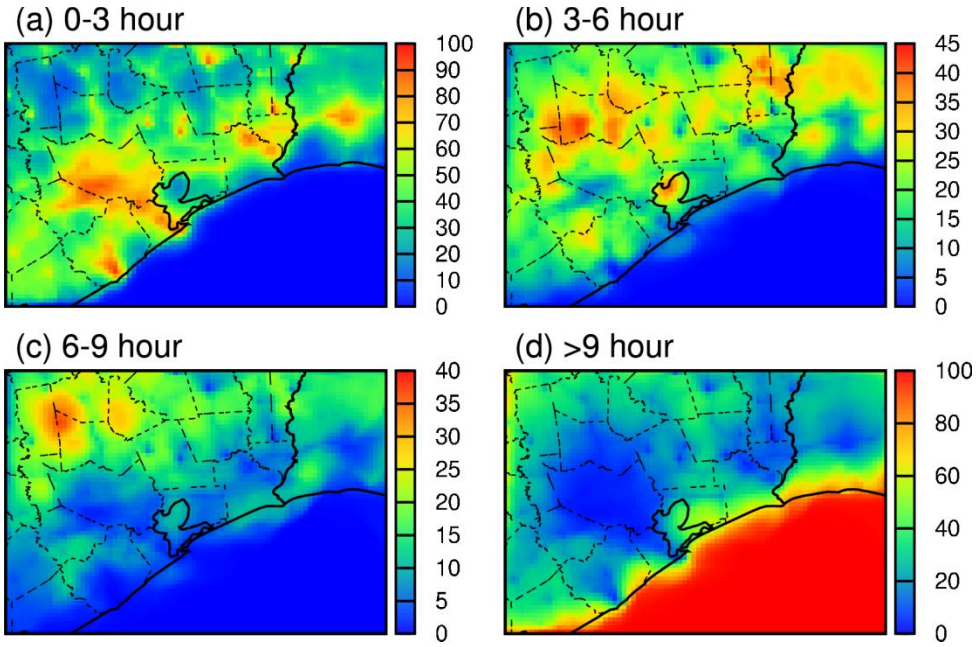

Figure 6-7. Regional distribution of episode average fractional EC concentrations to overall EC loading in Southeast Texas for different age groups. Units are %.

6.5 Conclusions

In this study, the source-oriented UCD/CIT model is expanded with multiple time bins to track the contribution of particles emitted at different times to elemental

carbon (EC) and organic carbon (OC) concentrations in Southeast Texas. The model correctly predicts the overall concentrations of EC and OC when compared to a base case simulation without age-resolved particle representation. EC and OC emitted within 0-3 hours contribute approximately 70-90% in urban Houston and about 20-40% in rural areas. Significant diurnal variations in the relative contributions to EC are predicted by the model. Highest contributions of fresh particles occur at morning and early evening traffic hours due to increased emission and lower mixing. The closer to the emission sources, the fresher the EC and OC would be. The concentrations of EC and OC that spend more than 9 hours in the air are low over land but almost accounts for 100% of the total EC and OC over the ocean. The high level of fresh EC in the Southeast Texas area means that they could have a strong regional impact on aerosol optical and hygroscopic properties, and thus affect cloud formation and radiation balance.

7. CONCLUSION

7.1 Summary

The overall object of this study is to develop source and age resolved 3D air quality models and apply them in Southeast Texas. From Section 2 to Section 6, the development and application of these models to O_3, primary PM, secondary inorganic aerosol, SOA, and EC/OC age distribution are presented.

In Section 2, the CMAQ model with a modified SAPRC-99 photochemical mechanism was used to investigate the contributions of local and upwind NO_x sources to O_3 concentrations in Southeast Texas during TexAQS 2000 from August 25 to September 5, 2000. Contributions from eight different local NO_x source types and eight different source regions to the 8-hour average daytime O_3 concentrations from 1100 to 1800 CST (referred to as AD O_3 hereafter) are determined. Both diesel engines and highway gasoline vehicles account for 25 ppb of AD O_3 in the urban Houston area. NO_x from natural gas combustion produces 35 ppb of AD O_3 in the industrial area of Houston. Contributions from industrial sources and coal combustion to AD O_3 have comparatively less broad spatial distribution with maximum values of 14 ppb and 20 ppb, respectively. Although the local sources are the most important sources, upwind sources have non-negligible influences (20-50%) on AD O_3 in the entire domain, with a maximum of 50 ppb in rural and coastal areas and 20 ppb in urban and industrial areas. To probe the origins of upwind sources contributions, NO_x emissions in the entire eastern United States are divided into eight different regions and their contributions to O_3

concentrations in the Houston-Galveston-Brazoria (HGB) and Beaumont-Port Arthur (BPA) areas are determined. Among the various NO_x source regions resolved in this study, other Texas counties near the HGB and BPA areas and southeastern states are the most important non-local sources of O_3. Under favorable transport conditions, emissions from neighbor states and northeastern states could also contribute to non-negligible O_3 concentrations (7-15%) in the HGB and BPA areas. This indicates that in addition to reduce local emissions, regional NO_x emission controls, especially from the neighbor counties and states, are also necessary to improve O_3 air quality in Southeast Texas.

In Section 3, a nested version of the source-oriented externally mixed UCD/CIT model was developed to study the source contributions to PM during a two-week long episode during TexAQS 2000. Contributions to primary PM and secondary ammonium sulfate were determined within the 4 km resolution domain that covers HGB and BPA areas. The predicted 24-hour EC, OC, sulfate, ammonium ion and primary $PM_{2.5}$ mass are in good agreement with filter-based observations. Predicted hourly sulfate, ammonium ion, and primary OC from diesel and gasoline engines at the La Porte agree well with measurements from an AMS. The predicted contributions to biomass burning OC is also in general agreement with BBOA resolved by the AMS. The comparison between predicted source contributions to primary OC and $PM_{2.5}$ and a CMB model suggests that, based on current emission inventory, PM emissions from industrial sources account for a significant fraction of primary OC and $PM_{2.5}$. This implies that further investigations on the industrial PM emissions are necessary. EC is mainly from diesel engines and majority of the primary OC is from internal combustion engines and

industrial sources. Open burning contributes large fractions of EC, OC and primary $PM_{2.5}$ mass. Road dust, internal combustion engines and industrial sources are the major sources of primary $PM_{2.5}$. Wildfire dominates the contributions to all primary PM components in areas near the fires. Secondary ammonium sulfate accounts for majority of the secondary inorganic PM. Over 80% of the secondary sulfate in the 4 km domain is produced in upwind areas. Coal combustion is the largest source of sulfate. Ammonium ion is mainly from agriculture sources and contributions from gasoline vehicles are significant in urban areas.

In Section 4, CMAQ v4.7 model with the most recent update on SOA formation pathways was adapted into a source-oriented modeling framework to determine the contributions of different emission sources to SOA concentrations from a carbon source perspective in Southeast Texas during TexAQS 2000. A comparison of the VOC and SOA predictions with observations shows that anthropogenic emissions of long chain alkanes and aromatics are likely underestimated in the EPA's CAIR inventory and the current SOA mechanism in CMAQ still under-predicts SOA. The SOA peak values can be better predicted when the emissions are adjusted by a factor of 2 based on the observation to prediction ratios of SOA precursors. A linear correlation between SOA and odd oxygen ($\Delta SOA/\Delta O_x$=23.0 μgm^{-3}/ppm O_x, r^2=0.674) can be found when they are formed simultaneously in the air masses passing the urban Houston on high SOA days. As a sensitivity run, the overall SOA can be more accurately predicted by increasing the emissions of the anthropogenic SOA precursors by a factor of 5. Based on the adjusted emissions, approximately 20% of the total SOA in the Houston-Galveston Bay area is

due to anthropogenic sources. Solvent utilization and gasoline engines are the main anthropogenic sources. SOA from alkanes and aromatics accounts for approximately 23-4% and 5-9% of total SOA, respectively. The predicted overall anthropogenic SOA concentrations are not sensitive to the half-life time used to calculate the conversion rate of semi-volatile organic compounds to non-volatile oligomers in the particle phase. The main precursors of biogenic SOA are sesquiterpenes, which contribute to approximately 12-35% of total SOA. Monoterpenes contribute to 3-14% and isoprene accounts for approximately 6-9% of the total SOA. Oligomers from biogenic SOA account for approximately 30-58% of the total SOA, indicating that long range transport is an important source of SOA in this region.

In Section 5, formation of SOA from the photooxidation products of PAHs is added to the SOA modeling framework of CMAQ model to determine the regional distribution of SOA products from PAHs (PAH-SOA) and the contributions from sources in southeast Texas during TexAQS 2006. Results show that PAHs released from anthropogenic sources can produce approximately 10% of the SOA mass as those from the traditional light aromatics or approximately 4% of total anthropogenic SOA. In areas under the influence of wild fire emissions, the amount of PAH-SOA can be as much as 50% of the SOA from light aromatics. A source-oriented modeling framework is adopted to determine the major sources of PAH-SOA by tracking the emitted PAHs and their oxidation products in the gas and aerosol phases from different sources separately. Among the eight sources (vehicles, solvent utilization, residential wood, industries, natural gas combustion, coal combustion, wild fire and other sources) that are tracked in

the model, wild fire, vehicles, solvent and industries are the major sources of PAH-SOA. Coal and natural gas combustion appear to be less important in terms of their contributions to PAH-SOA.

In Section 6, the source-oriented UCD/CIT model is expanded to track the contribution of particles emitted at different times. It is applied to study the age distribution of EC and OC in Southeast Texas. The model correctly predicts the overall concentrations of EC and OC when compared to a base case simulation without age-resolved particle representation. EC and OC emitted within 0-3 hours contribute approximately 70-90% in urban Houston and about 20-40% in rural areas. Significant diurnal variations in the relative contributions to EC are predicted by the model. Highest contributions of fresh particles occur at morning and early evening traffic hours due to increased emission and lower mixing. The closer to the emission sources, the fresher the EC and OC would be. The concentrations of EC and OC that spend more than 9 hours in the air are low over land but almost accounts for 100% of the total EC and OC over the ocean. The high level of fresh EC in the Southeast Texas area means that they could have a strong regional impact on aerosol optical and hygroscopic properties, and thus affect cloud formation and radiation balance.

7.2 Recommendations for future research

This dissertation provides information on source contributions to O_3 and PM in Southeast Texas, improving model prediction of SOA, and gives distribution of BC during aging time in the atmospheric.

In section 2, source apportionment of O_3 due to NO_x emissions are determined. However, VOCs also plays crucial role in ground O_3 formation. Since the nonlinearity of reactions that forms O_3, O_3 concentrations may not be reduced to designed values according to NO_x emissions control only. Ying and Krishnan [36] used same technique and gave the contributions of each VOCs source to net O_3 formation rate. But the contributions of different VOCs sources to absolute O_3 concentrations for Southeast Texas are not clear to policy makers. Furthermore, NO_x and VOCs are emitted concurrently from most sources, so it is most likely that both of them will be reduced if measures are taken to a certain source type. Therefore, combined source apportionment results of NO_x and VOCs are needed.

In Section 2, 3 and 4, it has been noticed that regional transport is important to secondary pollutants (O_3, sulfate, and SOA) in Southeast Texas. Although the contributions of regional transport are estimated in those sections, uncertainties remain. For instance, excluding the long range transport of SOA from biogenic sources is likely to underestimate the contributions from biogenic sources, especially under northerly wind conditions. Thus, further investigation is recommended.

In Section 4, the under-prediction of SOA by various chemical transport models is discussed. Possible reasons include missing SOA formation pathways are included in the current AERO5 aerosol module, such as SOA from the oxidation of alkenes and polycyclic aromatic hydrocarbons (PAHs), missing mechanisms of additional SOA formation in the aerosol-phase and aqueous-phase, as well as underestimation of VOC emissions. Results in Section 4 and Section 5 show that increase of VOCs emissions and

including PAHs to SOA precursors increase SOA predictions. However, not all possible reasons are tested.

Source-oriented 3D Eulerian air quality model is able to estimate the contribution to gas and PM pollutants. The accuracy of the model results is essential to policy makers. However, in this dissertation the calculated source contributions to O3 and PM are affected by various uncertainties in model inputs. It is important to quantify the uncertainties due to the emission profiles used for each emission source type, the meteorological fields used, as well as the algorithms. Sensitivity simulations such as perturbing the emission source profiles or using Monte Carlo simulation are useful.

In Section 6, the aging distribution of primary elemental carbon (EC) and organic carbon (OC) is presented. However, due to the computational limitation, the aging distribution of EC and OC from different source types and the formation of secondary pollutants are not simulated. In future, the computational ability should be improved to simulate the whole processes that particles go through in the atmosphere. In addition, criteria should be developed to judge the status of each particle so the model can predict its properties and evaluate the effects to air quality, weather and climate.

REFERENCES

1. Lippmann, M., Health effects of tropospheric ozone. *Environmental Science & Technology* **1991,** *25*, (12), 1954-1962.

2. Chappelka, A. H.; Samuelson, L. J., Ambient ozone effects on forest trees of the eastern United States: a review. *New Phytologist* **1998,** *139*, 91-108.

3. Fuhrer, J., Agroecosystern responses to combinations of elevated CO2, ozone, and global climate change. *Agriculture Ecosystems & Environment* **2003,** *97*, 1-20.

4. Cruz, C. N.; Pandis, S. N., A study of the ability of pure secondary organic aerosol to act as cloud condensation nuclei. *Atmospheric Environment* **1997,** *31*, (15), 2205-2214.

5. Liao, H.; Zhang, Y.; Chen, W. T.; Raes, F.; Seinfeld, J. H., Effect of chemistry-aerosol-climate coupling on predictions of future climate and future levels of tropospheric ozone and aerosols. *Journal of Geophysical Research-Atmospheres* **2009,** *114*.

6. Poschl, U., Atmospheric aerosols: Composition, transformation, climate and health effects. *Angewandte Chemie-International Edition* **2005,** *44*, (46), 7520-7540.

7. Banta, R. M., C. J. Senff, J. Nielsen-Gammon, L. S. Darby, T. B. Ryerson, R. J. Alvarez, S. P. Sandberg, E. J. Williams, and M. Trainer, A bad air day in Houston. *Bull. Am. Meteorol. Soc.* **2005,** *86*, 657-669.

8. Kleinman, L. I.; Daum, P. H.; Imre, D.; Lee, Y.-N.; Nunnermacker, L. J.; Springston, S. R.; Weinstein-Lloyd, J.; Rudolph, J., Ozone production rate and hydrocarbon reactivity in 5 urban areas: A cause of high ozone concentration in Houston. *Geophysical Research Letters* **2002,** *29*, (10), 105.

9. U.S.EPA, Region 6: State Designations for the 1997 8-Hour Ozone Standard (http://www.epa.gov/ozonedesignations/1997standards/regions/region6desig.htm). In 2004.

10. Buzcu, B.; Fraser, M. P., Source identification and apportionment of volatile organic compounds in Houston, TX. *Atmospheric Environment* **2006,** *40*, (13), 2385-2400.

11. Buzcu, B.; Yue, Z. W.; Fraser, M. P.; Nopmongcol, U.; Allen, D. T., Secondary particle formation and evidence of heterogeneous chemistry during a wood smoke episode in Texas. *Journal of Geophysical Research-Atmospheres* **2006,** *111*, (D10).

12. Nopmongcol, U.; Khamwichit, W.; Fraser, M. P.; Allen, D. T., Estimates of heterogeneous formation of secondary organic aerosol during a wood smoke episode in Houston, Texas. *Atmospheric Environment* **2007,** *41*, (14), 3057-3070.

13. Atkinson, R., Atmospheric chemistry of VOCs and NOx. *Atmospheric Environment* **2000,** *34*, (12-14), 2063-2101.

14. Finlayson-Pitts, B. J.; Pitts, J. N., Tropospheric air pollution: Ozone, airborne toxics, polycyclic aromatic hydrocarbons, and particles. *Science* **1997,** *276*, (5315), 1045-1052.

15. Fiore, A. M.; Jacob, D. J.; Logan, J. A.; Yin, J. H., Long-term trends in ground level ozone over the contiguous United States, 1980-1995. *Journal of Geophysical Research-Atmospheres* **1998,** *103*, (D1), 1471-1480.

16. Kanakidou, M.; Seinfeld, J. H.; Pandis, S. N.; Barnes, I.; Dentener, F. J.; Facchini, M. C.; Van Dingenen, R.; Ervens, B.; Nenes, A.; Nielsen, C. J.; Swietlicki, E.; Putaud, J. P.; Balkanski, Y.; Fuzzi, S.; Horth, J.; Moortgat, G. K.; Winterhalter, R.; Myhre, C. E. L.; Tsigaridis, K.; Vignati, E.; Stephanou, E. G.; Wilson, J., Organic aerosol and global climate modelling: a review. *Atmospheric Chemistry and Physics* **2005,** *5*, 1053-1123.

17. Yu, S. C.; Bhave, P. V.; Dennis, R.; Mathur, R., Seasonal and regional variations of primary and secondary organic aerosols over the Continental United States: Semi-empirical estimates and model evaluation. *Environmental Science & Technology* **2007,** *41*, 4690-4697.

18. Dechapanya, W.; Russell, M.; Allen, D. T., Estimates of anthropogenic secondary organic aerosol formation in Houston, Texas. *Aerosol Science and Technology* **2004,** *38*, 156-166.

19. deGouw, J. A.; Middlebrook, A. M.; Warneke, C.; Goldan, P. D.; Pszenny, A. A. P.; Keene, W. C.; Marchewka, M.; Bertman, S. B.; Bates, T. S., Bydget of organic carbon in a polluted atmosphere: Results from the New England Air Quality Study in 2002. *Journal of Geophysical Research-Atmospheres* **2002,** *110*, (D16305).

20. Griffin, R. J.; Cocker, D. R.; Seinfeld, J. H.; Dabdub, D., Estimate of global atmospheric organic aerosol from oxidation of biogenic hydrocarbons. *Geophysical Research Letters* **1999,** *26*, (17), 2721-2724.

21. Liao, H.; Henze, D. K.; Seinfeld, J. H.; Wu, S. L.; Mickley, L. J., Biogenic secondary organic aerosol over the United States: Comparison of climatological simulations with observations. *Journal of Geophysical Research-Atmospheres* **2007,** *112*, (D6).

22. Henze, D. K.; Seinfeld, J. H., Global secondary organic aerosol from isoprene oxidation. *Geophysical Research Letters* **2006,** *33*, (9).

23. Kroll, J. H.; Ng, N. L.; Murphy, S. M.; Flagan, R. C.; Seinfeld, J. H., Secondary organic aerosol formation from isoprene photooxidation. *Environmental Science & Technology* **2006,** *40*, (6), 1869-1877.

24. Hoffmann, T.; Odum, J. R.; Bowman, F.; Collins, D.; Klockow, D.; Flagan, R. C.; Seinfeld, J. H., Formation of organic aerosols from the oxidation of biogenic hydrocarbons. *Journal of Atmospheric Chemistry* **1997,** *26*, (2), 189-222.

25. Yu, J. Z.; Cocker, D. R.; Griffin, R. J.; Flagan, R. C.; Seinfeld, J. H., Gas-phase ozone oxidation of monoterpenes: Gaseous and particulate products. *Journal of Atmospheric Chemistry* **1999,** *34*, (2), 207-258.

26. Chen, J.; Ying, Q.; Kleeman, M. J., Source Apportionment of Wintertime Secondary Organic Aerosol During the California Regional PM10/PM25 Air Quality Study. *Atmospheric Environment* **2009,** *In Press, Accepted Manuscript*.

27. Kleeman, M. J., Cass, G. R., Eldering, A., Modeling the airborne particle complex as a source-oriented external mixture. *Journal of Geophysical Research* **1997,** *102*, 21355-21372.

28. Johnson, D.; Jenkin, M. E.; Wirtz, K.; Martin-Reviejo, M., Simulating the formation of secondary organic aerosol from the photooxidation of aromatic hydrocarbons. *Environmental Chemistry* **2005,** *2*, (1), 35-48.

29. Kleeman, M. J.; Ying, Q.; Lu, J.; Mysliwiec, M. J.; Griffin, R. J.; Chen, J. J.; Clegg, S., Source apportionment of secondary organic aerosol during a severe photochemical smog episode. *Atmospheric Environment* **2007,** *41*, (3), 576-591.

30. Ng, N. L.; Kroll, J. H.; Chan, A. W. H.; Chhabra, P. S.; Flagan, R. C.; Seinfeld, J. H., Secondary organic aerosol formation from m-xylene, toluene, and benzene. *Atmospheric Chemistry and Physics* **2007,** *7*, 3909-3922.

31. Dunker, A. M.; Morris, R. E.; Pollack, A. K.; Schleyer, C. H.; Yarwood, G., Photochemical modeling of the impact of fuels and vehicles on urban ozone using auto oil program data. *Environmental Science & Technology* **1996,** *30*, (3), 787-801.

32. Yang, Y. J.; Wilkinson, J.; Russell, A. G., Fast, direct sensitivity analysis of multidimensional photochemical models. *Environmental Science & Technology* **1997,** *31*, 2859-2868.

33. Hakami, A.; Odman, M. T.; Russell, A. G., High-order, direct sensitivity analysis of multidimensional air quality models. *Environmental Science & Technology* **2003,** *37*, (11), 2442-2452.

34. Cohan, D. S.; Hakami, A.; Hu, Y. T.; Russell, A. G., Nonlinear response of ozone to emissions: Source apportionment and sensitivity analysis. *Environmental Science & Technology* **2005,** *39*, (17), 6739-6748.

35. Dunker, A. M.; Yarwood, G.; Ortmann, J. P.; Wilson, G. M., Comparison of source apportionment and source sensitivity of ozone in a three-dimensional air quality model. *Environmental Science & Technology* **2002,** *36*, (13), 2953-2964.

36. Ying, Q.; Krishnan, A., Source contributions of volatile organic compounds to ozone formation in southeast Texas. *J. Geophys. Res.* **2010,** *115*, (D17), D17306.

37. Watson, J. G.; Zhu, T.; Chow, J. C.; Engelbrecht, J.; Fujita, E. M.; Wilson, W. E., Receptor modeling application framework for particle source apportionment. *Chemosphere* **2002,** *49*, 1093-1136.

38. Bullock, K. R.; Duvall, R. M.; Norris, G. A.; McDow, S. R.; Hays, M. D., Evaluation of the CMB and PMF models using organic molecular markers in fine particulate matter collected during the Pittsburgh Air Quality Study. *Atmospheric Environment* **2008,** *42*, 6897-6904.

39. Lane, T. E.; Pinder, R. W.; Shrivastava, M.; Robinson, A. L.; Pandis, S. N., Source contributions to primary organic aerosol: Comparison of the results of a source-resolved model and the chemical mass balance approach. *Atmospheric Environment* **2007,** *41*, 3758-3776.

40. Robinson, A. L.; Subramanian, R.; Donahue, N. M.; Bernardo-Bricker, A.; Rogge, W. F., Source apportionment of molecular markers and organic aerosols. 3. Food cooking emissions. *Environmental Science and Technology* **2006,** *40*, 7820-7827.

41. Schauer, J. J.; Cass, G. R., Source apportionment of wintertime gas-phase and particle-phase air pollutants using organic compounds as tracers. *Environmental Science and Technology* **2000,** *34*, (1821-1832).

42. Zheng, M.; Cass, G. R.; Schauer, J. J.; Edgerton, E. S., Source apportionment of PM2.5 in the Southeastern United States using solvent-extractable organic compounds as tracers. *Environmental Science and Technology* **2002,** *36*, 2361-2371.

43. Bhave, P. V.; Pouliot, G. A.; Zheng, M., Diagnostic model evaluation for carbonaceous PM2.5 using organic markers measured in the southeastern US. *Environmental Science & Technology* **2007,** *41*, (5), 1577-1583.

44. Wagstrom, K. M.; Pandis, S. N.; Yarwood, G.; Wilson, G. M.; Morris, R. E., Development and application of a computationally efficient particulate matter apportionment algorithm in a three-dimensional chemical transport model. *Atmospheric Environment* **2008,** *42*, (22), 5650-5659.

45. Ying, Q.; Kleeman, M. J., Source contributions to the regional distribution of secondary particulate matter in California. *Atmospheric Environment* **2006,** *40*, (4), 736-752.

46. Jimenez, J. L.; Canagaratna, M. R.; Donahue, N. M.; Prevot, A. S. H.; Zhang, Q.; Kroll, J. H.; DeCarlo, P. F.; Allan, J. D.; Coe, H.; Ng, N. L.; Aiken, A. C.; Docherty, K. S.; Ulbrich, I. M.; Grieshop, A. P.; Robinson, A. L.; Duplissy, J.; Smith, J. D.; Wilson, K. R.; Lanz, V. A.; Hueglin, C.; Sun, Y. L.; Tian, J.; Laaksonen, A.; Raatikainen, T.; Rautiainen, J.; Vaattovaara, P.; Ehn, M.; Kulmala, M.; Tomlinson, J. M.; Collins, D. R.; Cubison, M. J.; Dunlea, E. J.; Huffman, J. A.; Onasch, T. B.; Alfarra, M. R.; Williams, P. I.; Bower, K.; Kondo, Y.; Schneider, J.; Drewnick, F.; Borrmann, S.; Weimer, S.; Demerjian, K.; Salcedo, D.; Cottrell, L.; Griffin, R.; Takami, A.; Miyoshi, T.; Hatakeyama, S.; Shimono, A.; Sun, J. Y.; Zhang, Y. M.; Dzepina, K.; Kimmel, J. R.; Sueper, D.; Jayne, J. T.; Herndon, S. C.; Trimborn, A. M.; Williams, L. R.; Wood, E. C.; Middlebrook, A. M.; Kolb, C. E.; Baltensperger, U.; Worsnop, D. R., Evolution of Organic Aerosols in the Atmosphere. *Science* **2009,** *326*, (5959), 1525-1529.

47. Chan, A. W. H.; Kautzman, K. E.; Chhabra, P. S.; Surratt, J. D.; Chan, M. N.; Crounse, J. D.; Kurten, A.; Wennberg, P. O.; Flagan, R. C.; Seinfeld, J. H., Secondary organic aerosol formation from photooxidation of naphthalene and alkylnaphthalenes: implications for oxidation of intermediate volatility organic compounds (IVOCs). *Atmospheric Chemistry and Physics* **2009,** *9*, (9), 3049-3060.

48. Shakya, K. M.; Griffin, R. J., Secondary organic aerosol from photooxidation of polycyclic aromatic hydrocarbons. *Environmental Science & Technology* **2010,** *44*, 8134-8139.

49. Odum, J. R.; Hoffmann, T.; Bowman, F.; Collins, D.; Flagan, R. C.; Seinfeld, J. H., Gas/Particle Partitioning and Secondary Organic Aerosol Yields. *Environmental Science & Technology* **1996,** *30*, (8), 2580-2585.

50. Griffin, R. J.; Dabdub, D.; Kleeman, M. J.; Fraser, M. P.; Cass, G. R.; Seinfeld, J. H., Secondary organic aerosol 3. Urban/regional scale model of size- and composition-resolved aerosols. *J. Geophys. Res.* **2002,** *107*, (D17), 4334.

51. Johnson, D.; Jenkin, M. E.; Wirtz, K.; Martin-Reviejo, M., Simulating the Formation of Secondary Organic Aerosol from the Photooxidation of Toluene. *Environmental Chemistry* **2004,** *1*, (3), 150-165.

52. Gao, S.; Keywood, M.; Ng, N. L.; Surratt, J.; Varutbangkul, V.; Bahreini, R.; Flagan, R. C.; Seinfeld, J. H., Low-molecular-weight and oligomeric components in secondary organic aerosol from the ozonolysis of cycloalkenes and alpha-pinene. *J Phys Chem A* **2004,** *108*, (46), 10147-10164.

53. Jang, M. S.; Czoschke, N. M.; Lee, S.; Kamens, R. M., Heterogeneous atmospheric aerosol production by acid-catalyzed particle-phase reactions. *Science* **2002,** *298*, (5594), 814-817.

54. Kroll, J. H.; Ng, N. L.; Murphy, S. M.; Flagan, R. C.; Seinfeld, J. H., Secondary organic aerosol formation from isoprene photooxidation under high-NOx conditions. *Geophysical Research Letters* **2005,** *32*, (18).

55. Chen, J.; Griffin, R. J.; Grini, A.; Tulet, P., Modeling secondary organic aerosol formation through cloud processing of organic compounds. *Atmospheric Chemistry and Physics* **2007,** *7*, (20), 5343-5355.

56. Ervens, B.; Carlton, A. G.; Turpin, B. J.; Altieri, K. E.; Kreidenweis, S. M.; Feingold, G., Secondary organic aerosol yields from cloud-processing of isoprene oxidation products. *Geophysical Research Letters* **2008,** *35*, (2).

57. Carlton, A. G.; Bhave, P. V.; Napelenok, S. L.; Edney, E. D.; Sarwar, G.; Pinder, R. W.; Pouliot, G. A.; Houyoux, M., Model representation of secondary organic aerosol in CMAQv4.7. *Environmental Science and Technology* **2010,** *44*, (8553-8560).

58. Matsui, H.; Koike, M.; Takegawa, N.; Kondo, Y.; Griffin, R. J.; Miyazaki, Y.; Yokouchi, Y.; Ohara, T., Secondary organic aerosol formation in urban air: Temporal variations and possible contributions from unidentified hydrocarbons. *Journal of Geophysical Research-Atmospheres* **2009,** *114*.

59. Zhang, R. Y.; Khalizov, A. F.; Pagels, J.; Zhang, D.; Xue, H. X.; McMurry, P. H., Variability in morphology, hygroscopicity, and optical properties of soot aerosols during atmospheric processing. *Proceedings of the National Academy of Sciences of the United States of America* **2008,** *105*, (30), 10291-10296.

60. Moffet, R. C.; Prather, K. A., In-situ measurements of the mixing state and optical properties of soot with implications for radiative forcing estimates. *Proc. Natl. Acad. Sci. U. S. A.* **2009,** *106*, 11872-11877.

61. Zhang, R.; Khalizov, A. F.; Pagels, J.; Zhang, D.; Xue, H.; McMurry, P. H., Variability in morphology, hygroscopicity, and optical properties of soot aerosols during atmospheric processing. *Proc. Natl. Acad. Sci. U. S. A.* **2008,** *105*, 10291-10296.

62. Riemer, N.; Vogel, H.; Vogel, B., Soot aging time scales in polluted regions during day and night. *Atmospheric Chemistry and Physics* **2004,** *4*, 1885-1893.

63. Riemer, N.; West, M.; Zaveri, R.; Easter, R., Estimating black carbon aging time-scales with a particle=resolved aerosol model. *Aerosol Science* **2010,** *41*, 143-158.

64. U.S.EPA, National Ambient Air Quality Standards (NAAQS). In Agency, U. S. E. P., Ed. http://www.epa.gov/air/criteria.html: 2008.

65. U.S.EPA, National Ambient Air Quality Standards for Ozone. *Federal Register* **2010,** *75*, (11), 2938-3049.

66. Darby, L. S., Cluster analysis of surface winds in Houston, Texas, and the impact of wind patterns on ozone. *Journal of Applied Meteorology* **2005,** *44*, 1788-1806.

67. Daum, P. H.; Kleinman, L. I.; Springston, S. R.; Nunnermacker, L. J.; Lee, Y. N.; Weinstein-Lloyd, J.; Zheng, J.; Berkowitz, C. M., Origin and properties of plumes of high ozone observed during the Texas 2000 Air Quality Study (TexAQS 2000). *Journal of Geophysical Research-Atmospheres* **2004,** *109*, (D17), -.

68. Nielsen-Gammon, J.; Tobin, J.; McNeel, A.; Li, G. H. *Conceptual Model for Eight-Hour Exceedences in Houston, Texas Part I: Background Ozone Levels in Eastern Texas, Houston*; Adv. Res. Cent.: Houston, Texas, 2005.

69. Langford, A. O.; Senff, C. J.; Banta, R. M.; Hardesty, R. M.; Alvarez, R. J.; Sandberg, S. P.; Darby, L. S., Regional and local background ozone in Houston during Texas Air Quality Study 2006. *Journal of Geophysical Research-Atmospheres* **2009,** *114*.

70. Pierce, R. B.; Al-Saadi, J.; Kittaka, C.; Schaack, T.; Lenzen, A.; Bowman, K.; Szykman, J.; Soja, A.; Ryerson, T.; Thompson, A. M.; Bhartia, P.; Morris, G. A., Impacts of background ozone production on Houston and Dallas, Texas, air quality during the Second Texas Air Quality Study field mission. *Journal of Geophysical Research-Atmospheres* **2009,** *114*.

71. Xiao, X.; Cohan, D. S.; Byun, D. W.; Ngan, F., Highly nonlinear ozone formation in the Houston region and implications for emission controls. *Journal of Geophysical Research* **2010,** *115*, (D23309, doi:10.1029/2010JD014435).

72. Kim, S.; Byun, D. W.; Cohan, D., Contributions of inter- and intra-state emissions to ozone over Dallas-Fort Worth, Texas. *Civil Engineering and Environmental Systems* **2009,** *26*, (1), 103-115.

73. Yang, Q.; Cunnold, D. M.; Choi, Y. J.; Wang, Y.; Nam, J.; Wang, H.; Froidevaux, L.; Thompson, A. M.; Bhartia, P. K., A study of tropospheric ozone column enhancements over North America using satellite data and a global chemical transport mode;. *Journal of Geophysical Research-Atmospheres* **2010,** *115*, D08302.

74. Zhang, Y.; Vijayaraghavan, K.; Seigneur, C., Evaluation of three probing techniques in a three-dimensional air quality model. *Journal of Geophysical Research* **2005,** *110*, D02305.

75. Carter, W. P. L. *Documentation of the SAPRC-99 Chemical Mechanism for VOC Reactivity Assessment, Report to the California Air Resources Board. Available at http://cert.ucr.edu/~carter/absts.htm#saprc99 and http://www.cert.ucr.edu/~carter/reactdat.htm.;*May 8, 2000.

76. Zhang, H.; Ying, Q., Source apportionment of airborne particulate matter in Southeast Texas using a source-oriented 3D air quality model. *Atmospheric Environment* **2010,** *44*, (29), 3547-3557.

77. Ying, Q.; Fraser, M. P.; Griffin, R. J.; Chen, J. J.; Kleeman, M. J., Verification of a source-oriented externally mixed air quality model during a severe photochemical smog episode. *Atmospheric Environment* **2007,** *41*, (7), 1521-1538.

78. Fraser, M. P.; Yue., Z. W.; Buzcu, B., Source apportionment of fine particulate matter in Houston, TX, using organic molecular markers. *Atmospheric Environment* **2003,** *37*, 2117-2123.

79. Byun, D. W.; Kim, S. T.; Kim, S. B., Evaluation of air quality models for the simulation of a high ozone episode in the Houston metropolitan area. *Atmospheric Environment* **2007,** *41*, (4), 837-853.

80. Nam, J.; Kimura, Y.; Vizuete, W.; Murphy, C.; Allen, D. T., Modeling the impacts of emission events on ozone formation in Houston, Texas. *Atmospheric Environment* **2006,** *40*, (28), 5329-5341.

81. Vizuete, W.; Kim, B. U.; Jeffries, H.; Kimura, Y.; Allen, D. T.; Kioumourtzoglou, M. A.; Biton, L.; Hendersona, B., Modeling ozone formation from industrial emission events in Houston, Texas. *Atmospheric Environment* **2008,** *42*, (33), 7641-7650.

82. Kleeman, M. J.; Cass, G. R., A 3D Eulerian source-oriented model for an externally mixed aerosol. *Environmental Science & Technology* **2001,** *35*, (24), 4834-4848.

83. Ying, Q.; Lu, J.; Kleeman, M. J., Modeling air quality during the California Regional PM10/PM2.5 Air Quality Study (CRPAQS) using the UCD/CIT

sourceoriented air quality model – part III. Regional source apportionment of secondary and total airborne particulate matter. *Atmospheric Environment* **2009,** *43*, 419-430.

84. Ying, Q.; Lu, J.; Allen, P.; Livingstone, P.; Kaduwela, A.; Kleeman, M. J., Modeling air quality during the California Regional PM10/PM2.5 Air Quality Study (CRPAQS) using the UCD/CIT source-oriented air quality model – Part I. Base case model results. *Atmospheric Environment* **2008,** *42*, 8954-8966.

85. Ying, Q.; Lu, J.; Kaduwela, A.; Kleeman, M., Modeling air quality during the California Regional PM10/PM2.5 Air Quality Study (CPRAQS) using the UCD/CIT Source Oriented Air Quality Model - Part II. Regional source apportionment of primary airborne particulate matter. *Atmospheric Environment* **2008,** *42*, (39), 8967-8978.

86. Carter, W. P. L., A detailed mechanism for the gas-phase atmospheric reactions of organic compounds. *Atmospheric Environment. Part A. General Topics* **1990,** *24*, (3), 481-518.

87. Gong, S. L.; Barrie, L. A.; Blanchet, J. P.; von Salzen, K.; Lohmann, U.; Lesins, G.; Spacek, L.; Zhang, L. M.; Girard, E.; Lin, H.; Leaitch, R.; Leighton, H.; Chylek, P.; Huang, P., Ganadian aerosol module: A size-segregated simulation of atmospheric aerosol processes for climate and ari quality models - 1. module development. *Journal of Geophysical Research-Atmospheres* **2003,** *108*, (D1).

88. Zhang, L. M.; Gong, S. L.; Padro, J.; Barrie, L. A., A size-segregated particle dry depostion scheme for an atmospheric aerosol module. *Atmospheric Environment* **2001,** *35*, (3), 549-560.

89. Byun, D.; Schere, K. L., Review of the Governing Equations, Computational Algorithms, and Other Components of the Models-3 Community Multiscale Air Quality (CMAQ) Modeling System. *Applied Mechanics Reviews* **2006,** *59*, (2), 51-77.

90. Byun, D.; Ching, J., Science Algorithms of the EPA Models-3 Community Mutiscale Air Quality Modeling System EPA/600/R-99/030, US Environmental Protection Agency, Office of Research and Development. In Washington, DC, 1999.

91. Vukovich, J. M.; Pierce, T. In *The Implementation of BEIS3 within the SMOKE modeling framework*, 2002; MCNC-Environmental Modeling Center, Research Triangle Park and National Oceanic and Atmospheric Administration: 2002.

92. Kleeman, M. J.; Schauer, J. J.; Cass, G. R., Size and composition distribution of fine particulate matter emitted from motor vehicles. *Environmental Science & Technology* **2000,** *34*, (7), 1132-1142.

93. Kleeman, M. J.; Schauer, J. J.; Cass, G. R., Size and composition distribution of fine particulate matter emitted from wood burning, meat charbroiling, and cigarettes. *Environmental Science & Technology* **1999,** *33*, (20), 3516-3523.

94. Hays, M. D.; Fine, P. M.; Geron, C. D.; Kleeman, M. J.; Gullett, B. K., Open burning of agricultural biomass: Physical and chemical properties of particle-phase emissions. *Atmospheric Environment* **2005,** *39*, (36), 6747-6764.

95. Sweeten, J. M.; Parnell, C. B.; Shaw, B. W.; Auvermann, B. W., Particle size distribution of cattle feedlot dust emission. *Transactions of the Asae* **1998,** *41*, (5), 1477-1481.

96. Wang, C. F.; Chang, C. Y.; Tsai, S. F.; Chiang, H. L., Characteristics of road dust from different sampling sites in northern Taiwan. *Journal of the Air & Waste Management Association* **2005,** *55*, (8), 1236-1244.

97. Kupiainen, K. J.; Tervahattu, H.; Raisanen, M.; Makela, T.; Aurela, M.; Hillamo, R., Size and composition of airborne particles from pavement wear, tires, and traction sanding. *Environmental Science & Technology* **2005,** *39*, (3), 699-706.

98. Fritz, S. G. *Locomotive Fuel Effects Study: Particulate Size Characterization, Final Report*; Southwest Research Institute: 2000.

99. Taback, H. J.; Brienza, A. R.; Marko, J.; Brunetz, N. *Fine Particulate Emissions from Stationary and Miscellaneous Sources in the South Coast Air Basin.*; California Air Resources Board.: Sacramento, California, 1979.

100. Zhang, K. M.; Knipping, E. M.; Wexler, A. S.; Bhave, P. V.; Tonnesen, G. S., Size distribution of sea-salt emissions as a function of relative humidity. *Atmospheric Environment* **2005,** *39*, (18), 3373-3379.

101. Lewis, E. R.; Schwartz, S. E., Comment on "size distribution of sea-salt emissions as a function of relative humidity". *Atmospheric Environment* **2006,** *40*, (3), 588-590.

102. Boylan, J. W.; Russell, A. G., PM and light extinction model performance metrics, goals, and criteria for three-dimensional air quality models. *Atmospheric Environment* **2006,** *40*, 4946-4959.

103. Wood, E. C.; Canagaratna, M. R.; Herndon, S. C.; Kroll, J. H.; Onasch, T. B.; Kolb, C. E.; Worsnop, D. R.; Knighton, W. B.; Seila, R.; Zavala, M.; Molina, L. T.; DeCarlo, P. F.; Jimenez, J. L.; Weinheimer, A. J.; Knapp, D. J.; Jobson, B. T.; Stutz, J.; Kuster, W. C.; Williams, E. J., Investigation of the correlation between odd oxygen and secondary organic aerosol in Mexico City and Houston. *Atmospheric Chemistry and Physics Discussions* **2010,** *10*, 3547-3606.

104. Zhang, Q.; Alfarra, M. R.; Worsnop, D. R.; Allan, J. D.; Coe, H.; Canagaratna, M. R.; Jimenez, J. L., Deconvolution and quantification of hydrocarbon-like and oxygenated organic aerosols based on aerosol mass spectrometry. *Environmental Science & Technology* **2005,** *39*, (13), 4938-4952.

105. De Gouw, J. A.; Hekkert, S. T. L.; Mellqvist, J.; Warneke, C.; Atlas, E. L.; Fehsenfeld, F. C.; Fried, A.; Frost, G. J.; Harren, F. J. M.; Holloway, J. S.; Lefer, B.; Lueb, R.; Meagher, J. F.; Parrish, D. D.; Patel, M.; Pope, L.; Richter, D.; Rivera, C.; Ryerson, T. B.; Samuelsson, J.; Walega, J.; Washenfelder, R. A.; Weibring, P.; Zhu, X., Airborne Measurements of Ethene from Industrial Sources Using Laser Photo-Acoustic Spectroscopy. *Environmental Science & Technology* **2009,** *43*, (7), 2437-2442.

106. Wert, B. P.; Trainer, M.; Fried, A.; Ryerson, T. B.; Henry, B.; Potter, W.; Angevine, W. M.; Atlas, E.; Donnelly, S. G.; Fehsenfeld, F. C.; Frost, G. J.; Goldan, P. D.; Hansel, A.; Holloway, J. S.; Hubler, G.; Kuster, W. C.; Nicks, D. K.; Neuman, J. A.; Parrish, D. D.; Schauffler, S.; Stutz, J.; Sueper, D. T.; Wiedinmyer, C.; Wisthaler, A., Signatures of terminal alkene oxidation in airborne formaldehyde measurements during TexAQS 2000. *Journal of Geophysical Research-Atmospheres* **2003,** *108*, (D3).

107. Kean, A. J.; Littlejohn, D.; Ban-Weiss, G. A.; Harley, R. A.; Kirchstetter, T. W.; Lunden, M. M., Trends in on-road vehicle emissions of ammonia. *Atmspheric Environment* **2008,** *43*, (8), 1565-1570.

108. Helmig, D.; Ortega, J.; Guenther, A.; Herrick, J. D.; Geron, C., Sesquiterpene emissions from loblolly pine and their potential contribution to biogenic aerosol formation in the Southeastern US. *Atmospheric Environment* **2006,** *40*, (22), 4150-4157.

109. Kleinman, L. I.; Daum, P. H.; Lee, Y. N.; Nunnermacker, L. J.; Springston, S. R.; Weinstein-Lloyd, J.; Rudolph, J., A comparative study of ozone production in five U.S. metropolitan areas. *Journal of Geophysical Research-Atmospheres* **2005,** *110*, (D2), 20.

110. Sakulyanontvittaya, T.; Guenther, A.; Helmig, D.; Milford, J.; Wiedinmyer, C., Secondary Organic Aerosol from Sesquiterpene and Monoterpene Emissions in the United States. *Environmental Science & Technology* **2008,** *42*, (23), 8784-8790.

111. Chen, J. J.; Ying, Q.; Kleeman, M. J., Source apportionment of wintertime secondary organic aerosol during the California regional PM10/PM2.5 air quality study. *Atmospheric Environment* **2010,** *44*, (10), 1331-1340.

112. Murphy, C. F.; Allen, D. T., Hydrocarbon emissions from industrial release events in the Houston- Galveston area and their impact on ozone formation. *Atmospheric Environment* **2005,** *39*, (21), 3785-3798.

113. Li, G. H.; Zhang, R. Y.; Fan, J. W.; Tie, X. X., Impacts of biogenic emissions on photochemical ozone production in Houston, Texas. *Journal of Geophysical Research-Atmospheres* **2007,** *112*, (D10).

114. Vizuete, W.; Junquera, V.; Allen, D. T., Sesquiterpene emissions and secondary organic aerosol formation potentials for Southeast Texas. *Aerosol Science and Technology* **2004,** *38*, 167-181.

115. Russell, M.; Allen, D. T., Predicting secondary organic aerosol formation rates in southeast Texas. *Journal of Geophysical Research-Atmospheres* **2005,** *110*, (D7).

116. Bahreini, R.; Ervens, B.; Middlebrook, A. M.; Warneke, C.; de Gouw, J. A.; DeCarlo, P. F.; Jimenez, J. L.; Brock, C. A.; Neuman, J. A.; Ryerson, T. B.; Stark, H.; Atlas, E.; Brioude, J.; Fried, A.; Holloway, J. S.; Peischl, J.; Richter, D.; Walega, J.; Weibring, P.; Wollny, A. G.; Fehsenfeld, F. C., Organic aerosol formation in urban and industrial plumes near Houston and Dallas, Texas. *Journal of Geophysical Research-Atmospheres* **2009,** *114*.

117. Strader, R.; Lurmann, F.; Pandis, S. N., Evaluation of secondary organic aerosol formation in winter. *Atmospheric Environment* **1999,** *33*, (29), 4849-4863.

118. Pankow, J. F., An Absorption-model of the gas aerosol partitioning involved in the formation of secondary organic aerosol. *Atmospheric Environment* **1994,** *28*, (2), 189-193.

119. Helmig, D.; Ortega, J.; Duhl, T.; Tanner, D.; Guenther, A.; Harley, P.; Wiedinmyer, C.; Milford, J.; Sakulyanontvittaya, T., Sesquiterpene emissions from pine trees - Identifications, emission rates and flux estimates for the contiguous United States. *Environmental Science & Technology* **2007,** *41*, (5), 1545-1553.

120.surratt, J.; Lewandowski, M.; Offenberg, J. H.; Jaoui, M.; Kleindienst, T. E.; Edney, E. D.; Seinfeld, J. H., Effect of acidity on secondary organic aerosol formation from isoprene. *Environmental Science and Technology* **2007,** *38*, 167-181.

121. Mysliwiec, M. J.; Kleeman, M. J., Source apportionment of secondary airborne particulate matter in a polluted atmosphere. *Environmental Science & Technology* **2002,** *36*, (24), 5376-5384.

122. Carlton, A. G.; Pinder, R. W.; Bhave, P. V.; Pouliot, G. A., To what extent can biogenic SOA be controlled? *Environmental Science and Technology* **2010,** *44*, 3376-3380.

123. Carter, W. P. L. In *Development of a Chemical Speciation Database and Software for Processing VOC Emissions for Air Quality Models*, Proceedings of the 13th International Emission Inventory Conference "Working for Clean Air in Clearwater", Clearwater, Florida, USA, 2004; Clearwater, Florida, USA, 2004.

124. Volkamer, R.; Jimenez, J. L.; San Martini, F.; Dzepina, K.; Zhang, Q.; Salcedo, D.; Molina, L. T.; Worsnop, D. R.; Molina, M. J., Secondary organic aerosol formation from anthropogenic air pollution: Rapid and higher than expected. *Geophysical Research Letters* **2006,** *33*, (17).

125. Chen, J. J.; Mao, H. T.; Talbot, R. W.; Griffin, R. J., Application of the CACM and MPMPO modules using the CMAQ model for the eastern United States. *Journal of Geophysical Research-Atmospheres* **2006,** *111*, (D23).

126. Kalberer, M.; Yu, J.; Cocker, D. R.; Flagan, R. C.; Seinfeld, J. H., Aerosol formation in the cyclohexene-ozone system. *Environmental Science & Technology* **2000,** *34*, (23), 4894-4901.

127.Brown, S. G.; Reid, S. B.; Roberts, P. T.; Buhr, M. P.; Funk, T. H.; Kim, E.; Hopke, P. K. In *Reconciliation of the VOC and NOx Emission Inventory with Ambient Data in the Houston, Texas Region*, 13th International Emission Inventory Conference "Working for Clean Air in Clearwater", Clearwater, FL, 2004; Clearwater, FL, 2004.

128.Herndon, S. C.; Onasch, T. B.; Wood, E. C.; Kroll, J. H.; Canagaratna, M. R.; Jayne, J. T.; Zavala, M. A.; Knighton, W. B.; Mazzoleni, C.; Dubey, M. K.; Ulbrich, I. M.; Jimenez, J. L.; Seila, R.; de Gouw, J. A.; de Foy, B.; Fast, J.; Molina, L. T.; Kolb, C. E.; Worsnop, D. R., Correlation of secondary organic aerosol with odd oxygen in Mexico City. *Geophysical Research Letters* **2008,** *35*, (15).

129. Seinfeld, J. H.; Pankow, J. F., Organic atmospheric particulate material. *Annual Review of Physical Chemistry* **2003,** *54*, 121-140.

130. Li, G. H.; Zavala, M.; Lei, W.; Tsimpidi, A. P.; Karydis, V. A.; Pandis, S. N.; Canagaratna, M. R.; Molina, L. T., Simulations of organic aerosol concentrations in Mexico City using the WRF-CHEM model during the MCMA-2006/MILAGRO campaign. *Atmospheric Chemistry and Physics* **2011,** *11*, 3789-3809.

131. Zhang, H.; Ying, Q., Secondary Organic Aerosol Formation and Source Attribution in Southeast Texas. *Atmos. Environ.* **2011,** *45*, (19), 3217-3227.

132. Ravindra, K.; Sokhi, R.; Grieken, R. V., Atmospheric polycyclic aromatic hydrocarbons: Source attribution, emission factors and regulation. *Atmospheric Environment* **2008,** *42*, 2895-2921.

133. Marchand, N.; Besombes, J. L.; Chevron, N.; Masclet, P.; Aymoz, G.; Jaffrezo, J. L., Polycyclic aromatic hydrocarbons (PAHs) in the atmospheres of two French alpine valleys: sources and temporal patterns. *Atmospheric Chemistry and Physics* **2004,** *4*, 1167-1181.

134. Griffin, R. J.; Dabdub, D.; Seinfeld, J. H., Secondary organic aerosol 1. Atmospheric chemical mechanism for production of molecular constituents. *J. Geophys. Res.* **2002,** *107*, (D17), 4332.

135. Pun, B. K.; Griffin, R. J.; Seigneur, C.; Seinfeld, J. H., Secondary organic aerosol: II. Thermodynamic model for gas/particle partitioning of molecular constituents. *Journal of Geophysical Research* **2002,** *107*, 4333.

136. Mastral, A. M.; Callén, M. S., A Review on Polycyclic Aromatic Hydrocarbon (PAH) Emissions from Energy Generation. *Environ. Sci. Technol.* **2000,** *34*, (15), 3051-3057.

137. Chen, Y.; Ho, K. F.; Ho, S. S. H.; Ho, W. K.; Lee, S. C.; Yu, J. Z.; Sit, E. H. L., Gaseous and particulate polycyclic aromatic hydrocarbons (PAHs) emissions from commercial restaurants in Hong Kong. *Journal of Environmental Monitoring* **2007,** *9*, (12), 1402-1409.

138. Ho, K. F.; Ho, S. S. H.; Lee, S. C.; Cheng, Y.; Chow, J. C.; Watson, J. G.; Louie, P. K. K.; Tian, L., Emissions of gas- and particle-phase polycyclic aromatic hydrocarbons (PAHs) in the Shing Mun Tunnel, Hong Kong. *Atmos. Environ.* **2009,** *43*, (40), 6343-6351.

139. Gilman, J. B.; Kuster, W. C.; Goldan, P. D.; Herndon, S. C.; Zahniser, M. S.; Tucker, S. C.; Brewer, W. A.; Lerner, B. M.; Williams, E. J.; Harley, R. A.; Fehsenfeld, F. C.; Warneke, C.; de Gouw, J. A., Measurements of volatile organic compounds during the 2006 TexAQS/GoMACCS campaign: Industrial influences,

regional characteristics, and diurnal dependencies of the OH reactivity. *Journal of Geophysical Research-Atmospheres* **2009,** *114*.

140. Zhang, Y.; Tao, S., Global atmospheric emission inventory of polycyclic aromatic hydrocarbons (PAHs) for 2004. *Atmospheric Environment* **2009,** *43*, 812-819.

141. Larsen, R. K., III; Baker, J. E., Source Apportionment of Polycyclic Aromatic Hydrocarbons in the Urban Atmosphere: A Comparison of Three Methods. *Environmental Science and Technology* **2003,** *37*, 1873-1881.

142. Harrison, R. M.; Smith, D. J. T.; Luhana, L., Source Apportionment of Atmospheric Polycyclic Aromatic Hydrocarbons Collected from an Urban Location in Birmingham, U.K. *Environmental Science and Technology* **1996,** *30*, 825-832.

143. Yang, H.; Chen, C., Emission inventory and sources of polycyclic aromatic hydrocarbons in the atmosphere at a suburban area in Taiwan. *Chemosphere* **2004,** *56*, 879-887.

144. Carter, W. P. L., Development of a condensed SAPRC-07 chemical mechanism. *Atmos. Environ.* **2010,** *40*, (44), 5336-5345.

145. Li, J.; Zhang, H.; Ying, Q., Comparison of the SAPRC07 and SARPC99 Photochemical Mechanisms during a High Ozone Episode in Texas: Differences in Concentrations, OH Budget and Relative Response Factors. *Atmos. Environ.* **2011,** *Submitted for Review*.

146. Carter, W. P. L., Development of the SAPRC-07 chemical mechanism. *Atmos. Environ.* **2010,** *44*, (3), 5324-5335.

147. Atkinson, R., Kinetics and mechanisms of the gas-phase reactions of the hydroxyl radical with organic compounds. *Journal of physical and Chemical Reference Data Monograph* **1989,** *1*, 1-246.

148. Atkinson, R.; Arey, J., Mechanisms of the gas-phase reactions of aromatic hydrocarbons and PAHs with OH and NO3 radicals. *Polycyclic Aromatic Compounds* **2007,** *27*, 15-40.

149. Phousongphouang, P. T.; Arey, J., Rate Constants for the Gas-Phase Reactions of a Series of Alkylnaphthalenes with the OH Radical. *Environmental Science and Technology* **2002,** *36*, 1947-1952.

150. Allen, J. O. Atmospheric Partitioning of Polycyclic Aromatic Hydrocarbons (PAH) and Oxygenated PAH. Massachusetts Institute of Technology, 1997.

151. TCEQ *Houston-Galveston-Brazoria Attainment Demonstration and Reasonable Further Progress State Implementation Plan Revisions for the 1997 Eight-Hour Ozone Standard. Appendix B.*; Texas Commission of Environmental Quality: 2010.

152. Wiedinmyer, C.; Akagi, S. K.; Yokelson, R. J.; Emmons, L. K.; Al-Saadi, J. A.; Orlando, J. J.; Soja, A. J., The Fire INventory from NCAR (FINN): a high resolution global model to estimate the emissions from open burning. *Geoscientific Model Development* **2011,** *4*, 625-641.

153. Hays, M. D.; Geron, C. D.; Linna, K. J.; Smith, N. D.; Schauer, J. J., Speciation of Gas-Phase and Fine Particle Emissions from Burning of Foliar Fuels. *Environmental Science and Technology* **2002,** *36*, (11), 2281-2295.

154. U.S.EPA *Compilation of Air Pollutant Emission Fators, Volumn 1: Stationary Point and Area Sources*; 1995.

155. Wood, E. C.; Canagaratna, M. R.; Herndon, S. C.; T.B., O.; Kolb, D. R.; Worsnop, J. H.; Kroll, W. B.; Knighton, W. B.; Seila, R.; Zavala, M.; Molina, L. T.; DeCarlo, P.; Jimenez, J. L.; Weinheimer, A. J.; Knapp, D. J.; Jobson, B. T.; Stutz, J.; Kuster, W. C.; Williams, E. J., Investigation of the correlation between odd oxygen and secondary organic aerosol in Mexico City and Houston. *Atmospheric Chemistry and Physics Discussions* **2010,** *10*, 3547-3606.

156. Turpin, B. J.; Lim, H., Species contributions to PM2.5 mass concentrations: Revisiting common assumptions for estimating orgainc mass. *Aerosol Science and Technology* **2001,** *35*, 602-610.

157. Gilardoni, S.; Russell, L. M.; Sorooshian, A.; Flagan, R. C.; Seinfeld, J. H.; Bates, T. S.; Quinn, P. K.; Allan, J. D.; Williams, B.; Goldstein, A. H.; Onasch, T. B.; Worsnop, D. R., Regional variation of organic functional groups in aerosol particles on four U.S. east coast platforms during the International Consortium for Atmospheric Research on Transport and Transformation 2004 campaign. *Journal of Geophysical Research* **2007,** *112*, D10S27.

158. Russell, L. M., Aerosol Organic-Mass-to-Organic-Carbon Ratio Measurements. *Environmental Science and Technology* **2003,** *27*, 2982-2987.

159. Pöschl, U.; Letzel, T.; Schauer, C.; Niessner, R., Interaction of Ozone and Water Vapor with Spark Discharge Soot Aerosol Particles Coated with Benzo[a]pyrene: O3 and H2O Adsorption, Benzo[a]pyrene Degradation, and Atmospheric Implications. *J Phys Chem A* **2001,** *105*, 4029-4041.

160. Mmereki, B. T.; Donaldson, D. J., Direct observation of the kinetics of an atmospherically important reaction at the air-aqueous interface. *J Phys Chem A* **2003,** *107*, 11038-11042.

161. Nájera, J. J.; Wamsley, R.; Last, D. J.; Leather, K. E.; Percival, C. J.; Horn, A. B., Heterogeneous oxidation reaction of gas-phase ozone with anthracene in thin films and on aerosols by infrared spectroscopic methods. *International Journal of Chemical Kinetics* **2011,** *43*, (12), 694-707.

162. Zhou, S.; Wenger, J. C. *Health Effects Associated with the Atmospheric Degradation of Polycyclic Aromatic Hydrocarbons*; Environmental Protection Agency, Ireland: 2010.

163. Chameides, W. L.; Bergin, M., Soot takes center stage. *Science* **2002,** *297*, 2214-2215.

164. Jacobson, M. Z., Strong radiative heating due to the mixing state of black carbon in atmospheric aerosols. *Nature* **2001,** *409*, 695-697.

165. Ackerman, A. S.; Toon, O. B.; Stevens, D. E.; Heymsfield, A. J.; Ramanathan, V.; Welton, E. J., Reduction of tropical cloudiness by soot. *Science* **2000,** *288*, 1042-1047.

166. Ramanathan, V.; Carmichael, G., Global and regional climate changes due to black carbon. *Nature geoscience* **2008,** *1*, 221-227.

167. Bond, T. C.; Sun, H., Can reducing black carbon emissions counteract global warming? *Environmental Science & Technology* **2005,** *39*, 5921-5926.

168. Bond, T. C.; Bergstrom, R. W., Light absorption by carbonaceous particles: an investigative review *Aerosol Science and Technology* **2006,** *40*, 27-67.

169. Menon, S.; Hansen, J.; Nazarenko, L.; Luo, Y., Climate Effects of Black Carbon Aerosols in China and India. *Science* **2002,** *297*, 2250-2253.

170. Zhang, D.; Zhang, R., Laboratory investigation of heterogeneous interaction of sulfuric acid with soot. *Environmental Science and Technology* **2005,** *39*, 5722-5728.

171. McMeeking, G. R.; Good, N.; Petters, M. D.; McFiggans, G.; Coe, H., Influences on the fraction of hydrophobic and hydrophilic black carbon in the atmosphere. *Atmos. Chem. Phys.* **2011,** *11*, (10), 5099-5112.

172. Cooke, W. F.; Wilson, J. N., A global black carbon aerosol model. *Journal of Geophysical Research* **1996,** *101*, 19395-19408.

173. Wilson, J.; Cuvelier, C.; Raes, F., A modeling study of global mixed aerosol fields. *Journal of Geophysical Research* **2001,** *106*, 34081-34108.

174. Croft, B.; Lohmann, U.; von Salzen, K., Black carbon ageing in the Canadian Centre for Climate modelling and analysis atmospheric general circulation model. *Atmos. Chem. Phys.* **2005,** *5*, (7), 1931-1949.

175. Park, S. H.; Gong, S. L.; Bouchet, V. S.; Gong, W.; Makar, P. A.; Moran, M. D.; Stroud, C. A.; Zhang, J., Effects of black carbon aging on air quality predictions and direct radiative forcing estimation. *Tellus B* **2011,** *63*, (5), 1026-1039.

176. Moffet, R. C.; Prather, K. A., In-situ measurements of the mixing state and optical properties of soot with implications for radiative forcing estimates. *Proceedings of the National Academy of Sciences of the United States of America* **2009,** *106*, (29), 11872-11877.

177. Kleeman, M. J., Cass, G. R., A 3d Eulerian source-oriented model for an externally mixed aerosol. *Environmental Science and Technology* **2001,** *35*, (4834-4867), 4834.

VITA

Name:	Hongliang Zhang
Address:	205 WERC, Zachry Department of Civil Engineering, Texas A&M University, College Station, Texas 77843-3136
Email Address:	ultidream@gmail.com
Education:	B.S., Environmental Engineering, Tsinghua University, China, 2006 M.S., Thermal Engineering, Tsinghua University, China, 2008 Ph.D., Civil Engineering, Texas A&M University, USA, 2012